CHALMERS
UNIVERSITY OF TECHNOLOGY

Measurement of Posture Using Advanced Sensor Technologies

A Literature Study and Trial Experiment of an IMU-Based System

Master's thesis in Biomedical Engineering, MPMED

LOVISA SVENSSON LAABAN

DEPARTMENT OF ELECTRICAL ENGINEERING
CHALMERS UNIVERSITY OF TECHNOLOGY
Gothenburg, Sweden 2025
www.chalmers.se

Master's thesis 2025

Measurement of Posture Using Advanced Sensor Technologies

A Literature Study and Trial Experiment of an IMU-Based System

LOVISA SVENSSON LAABAN

CHALMERS
UNIVERSITY OF TECHNOLOGY

Department of Electrical Engineering
Division of Biomedical Engineering
Chalmers University of Technology
Gothenburg, Sweden 2025

Measurement of Posture Using Advanced Sensor Technologies
A Literature Study and Trial Experiment of an IMU-Based System
LOVISA SVENSSON LAABAN

Supervisor: Xuezhi Zeng, Associate Professor at Department of Signal Processing and Biomedical Engineering, Electrical Engineering, Chalmers & Gunilla Kjellby Wendt, Head of the Department in Occupational Therapy and Physiotherapy at Sahlgrenska University Hospital; Adjunct Professor in Adaptive Physiotherapy at Chalmers

Examiner: Xuezhi Zeng, Associate Professor at Department of Signal Processing and Biomedical Engineering, Electrical Engineering, Chalmers

Master's Thesis 2025
Department of Electrical Engineering
Division of Biomedical Engineering
Chalmers University of Technology
SE-412 96 Gothenburg
Telephone +46 31 772 1000

Cover: An Xsens Movella DOT kit consisting of five IMU sensors and a charging station.

Typeset in LaTeX
Printed by Chalmers Reproservice
Gothenburg, Sweden 2025

Measurement of Posture Using Advanced Sensor Technologies
A Literature Study and Trial Experiment of an IMU-Based System
LOVISA SVENSSON LAABAN
Department of Electrical Engineering
Chalmers University of Technology

Abstract

The purpose of this thesis was to identify a quantitative postural assessment tool for monitoring the progress of rehabilitation therapies, as current visual methods are subjective and prone to errors. The goal was to measure sagittal angles along the entire spine to provide an objective indicator of postural balance.
A literature review was conducted to provide an overview of conventional clinical methods and to explore novel postural assessment tools available on the market. The most promising emerging methods included Kinect, inertial measurement unit (IMU) systems, and smartphone applications. While Kinect and smartphone-based methods offered limited accuracy and seemed more appropriate for estimating gross misalignments, IMU systems demonstrated superior precision, versatility, and applicability to both dynamic and static measurements, though at a higher cost.
Based on these findings, the Movella DOT IMU system was selected for evaluation in a trial experiment. Four sensors were placed along the spine of a test subject, and results were compared with the Qualisys motion capture system during sitting, standing, and walking tasks. The sensor placed at the cervical lordosis showed the strongest agreement, with an overall mean bias of 1.6°. When gait data were excluded, the cervical placement yielded a mean bias of 0.41° and a mean RMSD of 0.64°, which is considered an excellent result. Sensors placed at lower spinal regions exhibited slightly higher deviations.
Further development of dedicated software and validation in larger test groups is necessary for clinical implementation but is considered highly feasible. The Movella DOT system has the potential to serve as an all-in-one solution for multiple needs in rehabilitation therapy, combining accuracy with versatility, and thus is a highly promising tool for clinical postural assessment.

Keywords: body posture; spinal alignment; sagittal spinal tilt; IMU; inertial sensors; wearables; postural assessment; rehabilitation engineering; medical rehabilitation.

Acknowledgements

I want to begin by thanking my examiner and supervisor Dr. Xuezhi Zeng for guiding me throughout this thesis. Your support and ideas have been invaluable throughout this process, and it would not have been possible to complete it without you. Thank you.
I also want to express my gratitude to Dr. Xuezhi Zeng, Dr. Gunilla Kjellby Wendt, Head of the Department in Occupational Therapy and Physiotherapy at Sahlgrenska University Hospital, and Dr. Emma Varkey and Angelica Dahlbäck, physiotherapists at Sahlgrenska, for giving me the opportunity to participate in improving rehabilitation care. I want to thank you all for your enthusiasm and optimism, your knowledge and support, and I hope this thesis can be another stepping stone toward the ultimate goal of helping patients.
I also especially want to thank Xiaoxuan Dong, who graciously assisted with the data collection part of the thesis. I am so grateful that you had the kindness to jump in and help out, and for being so diligent and hard-working. The experiments truly would not have been possible to perform without you. I appreciate it a lot.

Lovisa Svensson Laaban, Gothenburg, June 2025

List of Acronyms

Below is the list of acronyms that have been used throughout this thesis listed in alphabetical order:

AMI	Athletic Movement Index
AROM	Active Range of Motion
BMI	Body Mass Index
CMLBP	Chronic Mechanical Low Back Pain
CNP	Chronic Neck Pain
ENU	East-North-Up
FHP	Forward Head Posture
ICC	Interclass Correlation Coefficient
IMU	Inertial Measurement Units
LBP	Low Back Pain
MAE	Mean Absolute Error
MDC	Minimal Detectable Change
MEMS	Microelectromechanical Systems
MFM	Magnetic Field Mapping
MoCap	Motion Capture
MLBP	Mechanical Low Back Pain
MSD	Musculoskeletal Disorder
NLBP	Non-Specific Low Back Pain
PPE	Personal Protective Equipment
RMSD	Root Mean Square Deviation
RMSE	Root Mean Square Error
ROK	Range of Kinematics
ROM	Range of Motion
SDI	Strap-Down Integration
SDK	Software Development Kit
TBCM	Total Body Centre of Mass
WMSD	Work-Related MSDs

Contents

List of Figures

List of Tables

1

Introduction

Healthcare continues to face new challenges as society and lifestyle patterns evolve. The growing prevalence of unhealthy lifestyle habits in modern society has been linked to rising rates of chronic pain conditions. For instance, many daily tasks today involve sitting down, both at home and at work [1]. This is of concern, as low expenditure postures, such as sitting or lying down, typically negatively affect our health [2]. When an increasing duration of our day consists of sitting down, the muscles responsible for maintaining good posture, which need exposure to gravity forces, are not stimulated and may result in muscle weakness and atrophy, leading to poor posture [3]. An improper sitting posture can lead to complications such as disorders of the musculoskeletal system, including chronic back pain or improper spine alignment [1]. Today, 1.7 billion people are estimated to suffer from musculoskeletal health disorders (MSDs), with low back pain (LBP) and neck pain having the highest prevalence. The severity of this issue is only increasing, and in 2015 MSDs were the fourth most common cause of disability-adjusted life years worldwide, at a grand total of 95 million years [4].

Of great prevalence are musculoskeletal health disorders caused at work, known as work-related MSDs (WMSDs) [4]. They are the most common occupational health problem worldwide [5], and have become a major global health concern that impacts society, the economy, and individuals. Currently, three out of five workers in the EU are affected by WMSDs. The causes are multifactorial, but risk factors include heavy and repetitive handling, awkward postures, and rapid movements primarily of the upper body [4]. It is estimated that half of workers in the EU are exposed to tiring and painful work postures during 25% of their working time and 14% during their entire working time [4]. Meanwhile, the prevalence of WMSDs is expected to continue rising, mainly attributed to increased overload of the musculoskeletal system at work [5]. WMSDs can have a major effect on the ability of a person to work, as they can impair work capacity, lower job satisfaction, and increase the likelihood of short- and long-term absence from work. They can even result in withdrawal from the labour market [4], as a result of decreased functionality and permanent pain-related disability. In addition to limiting people in their work life, WMSDs also greatly impact daily functional activity of sufferers. In particular, they may lead to reduced physical, psychological, and social well-being of workers [5]. Furthermore, in many countries, population demographics have shifted due to the improvement of modern healthcare, and has led to challenges with adapting to an ageing population. Older citizens are more likely to suffer from multiple and complex health conditions [6]. Therefore, the increasing incidence of WMSDs is also believed to be associated with a higher percentage of older workers [5].

The leading cause of disability worldwide is attributed to low back pain. The burden this places on society in terms of costs, both indirect and direct, is estimated to range between 0.4% to 1.7% of GDP, depending on the country and model used. Approximately 1% of LBP cases are diagnosed as being caused by some serious pathology, such as cancer, while 20% of cases are attributed to nerve root irritation caused by [7], for example, acute disc prolapse [8]. The remaining 80% of LBP cases go under the label "non-specific", where a definitive cause of the pain cannot be determined due to uncertainties and difficulties in diagnosis [7][8]. However, a common feature of these non-specific cases is that the non-surgical methods available today are inadequate and only result in short-term, moderate effects. This could be attributed to non-specific LBP (NLBP) patients suffering from different conditions that belong to different subgroups. Thus, there is an incentive to identify the characteristics of each subgroup and develop customized treatments [7]. Among the mechanical risk factors that have been identified for NLBP, poor posture is one of the most consistently reported [9].
Improper posture, often referred to as *non-neutral spinal postures*, is recognized as not only a root cause of pain but also a factor that perpetuates it [10]. For example, people may engage in dysfunctional pain-related movement patterns, including muscle activations or posture patterns, which can result in increased trunk stiffness, postural abnormalities, and altered activation patterns of the abdominal and extensor muscles. That is, pain itself can reinforce maladaptive movement patterns and postures, maintaining or even worsening the condition [7].
It is vital to find solutions to detect, combat, monitor and prevent conditions caused by improper posture [4]. In addition, collecting data and developing reliable ways to monitor posture can give a better picture of the causes of the conditions, which can lead to more effective treatment strategies [11]. Posture measurement is an important tool in this quest [12], and while there already exist conventional methods used clinically, primarily consisting of simple manual tools, there is a growing body of research on prospective measurement methods of higher accuracy and versatility, as well as some already commercialized novel solutions [13].

1.1 Aim and Research Questions

This thesis was conducted in collaboration with physiotherapists at the Sahlgrenska University Hospital, who had identified the need for a more accurate postural assessment tool in rehabilitation therapy of pain disorders. The aim of this thesis is thus to find a new measurement method to assess posture in patients, which is more reliable, from an inter-tester and intra-tester perspective, to the visual assessment that is employed as a standard today. The method should be able to quantitatively measure changes in posture during the rehabilitation treatment of a patient, in order to provide concrete evidence of the effectiveness of the treatment, and to give feedback to the patient. The data should also be recordable and analysable. Furthermore, it is of interest to measure posture in both static and dynamic activities: standing, sitting, and walking. The main anatomical plane of interest is the sagittal plane, with the aim of assessing the alignment of the upper body and pelvis and identifying forward or backward lean postures. Importantly, the device should be

capable of measuring all points along the spine, to provide a more accurate representation of global posture balance. For clinical implementation, it is preferred to select an already existing commercial device or technology that can be applied efficiently, rather than developing a new prototype.
Initially, a literature review will be conducted to gain an overview of existing postural assessment tools, both conventional and novel. Based on this evaluation, one promising postural measurement device will be selected and a trial experiment will be carried out using it to assess its feasibility for clinical implementation in the given context. The aim of the thesis can be summarized through the following research questions:

Research Questions:

- Which conventional postural assessment methods are currently used clinically?
- Which novel postural assessment tools available on the market are suitable for this context?
- What is the most promising device identified in the literature search?
- How accurately does the chosen technology determine postural alignment?
- How feasible is clinical implementation of the tool?

1.1.1 Limitations

It should be noted that the literature study is limited to the information available online at the time of data collection. Subsequent releases of new devices and studies after the publication of this thesis could influence the potential of some of the devices discussed.
Another limitation concerns the difficulty of estimating the costs of postural assessment devices, as pricing is often based on negotiation with companies. Some are based on subscription fees and some on one-off costs. As such, costs will not be of focus in the analysis. A more comprehensive cost analysis would be necessary to enable a fair comparison between devices, but this lies beyond the scope of this thesis.
Finally, the experimental study will be restricted to a preliminary trial of the chosen device, aimed only at making an initial observation of the suitability and performance of the tool. The purpose of this thesis is therefore not to draw any clinical conclusions or develop methodologies for practical application.

2

Theory - Literature Review

In this chapter, the basics of human posture and its relationship to pain will be explained.

2.1 Body Posture

The human spine is comprised of a column of 33 bones called *vertebrae*, most of which are moveable [14]. There are three spinal curvatures that are used to describe posture in an upright position, illustrated in Figure 2.1. They are referred to as the following:

- **Cervical lordosis** (10-30°): curvature of the cervical spine (upper region)
- **Thoracic kyphosis** (20-40°): cuvature of the thoracic spine (middle region)
- **Lumbar lordosis** (34-42°): curvature of the lumbar spine (lower region) [15]

where *lordosis* is the increased curvature towards the front of the body (anterior curve), and *kyphosis* is the rounding of the spine (posterior curve) [3][16].
Based on these curvatures, four common types of non-structural misalignments have been identified: 1) *lordotic posture*, defined by increased lumbar lordosis and pelvic anteversion; 2) *kyphotic posture*, defined for example by increased thoracic kyphosis and head protraction; 3) *flat-back posture*, defined by flattened lumbar lordosis and lower part of thoracic kyphosis; and 4) *sway-back posture*, defined by for example anterior pelvis shift and longer thoracic kyphosis; see Figure 2.2 for illustrations. These abnormalities cause disturbances in the physiological loading of the musculoskeletal system in different manners, leading to pain and disorders [3].
Factors that may affect posture are complex and include minimal perturbations in the psychophysics and socioenvironment. It is a dynamic system, constantly changing [5]. The maintenance of global body balance can be described by the **cone of economy** [17]. The concept was introduced by Jean Dubousset in the 1970s, based on full spine X-rays [18]. In this model, dynamic muscles and static ligaments are continuously counterbalancing each other to maximize energy conservation [17]. When a disturbance occurs in one region, compensatory changes occur in other regions, leading to a change in the overall shape of the spine [19]. Each part of the spine has an influence on the other, and therefore it is considered important to treat the human spine globally, rather than segmentally [11]. For example, in the standing position, pelvic orientation has a great impact on posture. Pelvic orientation has been found to correlate with lumbar lordosis, where pelvic anteversion leads to more lumbar lordosis, and pelvic retroversion leads to less lumbar lordosis [10]. Thus, there is a strong interdependence between the pelvis and lumbar spine in

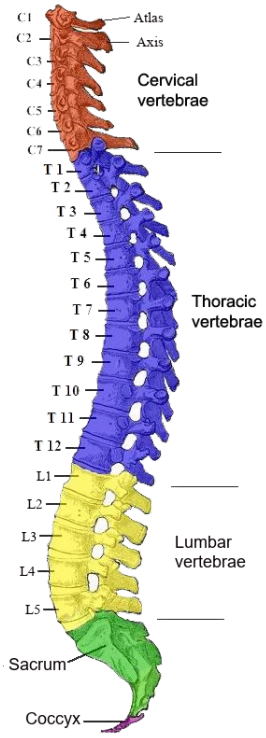

Figure 2.1: Curvatures of the spine. *Note.* Illustration by H. V. Carter, modified by Uwe Gille and delldot. From *Gray's Anatomy* (1918). Retrieved from `https://commons.wikimedia.org/wiki/File:Gray_111_-_Vertebral_column-coloured_labels.png`. Public domain.

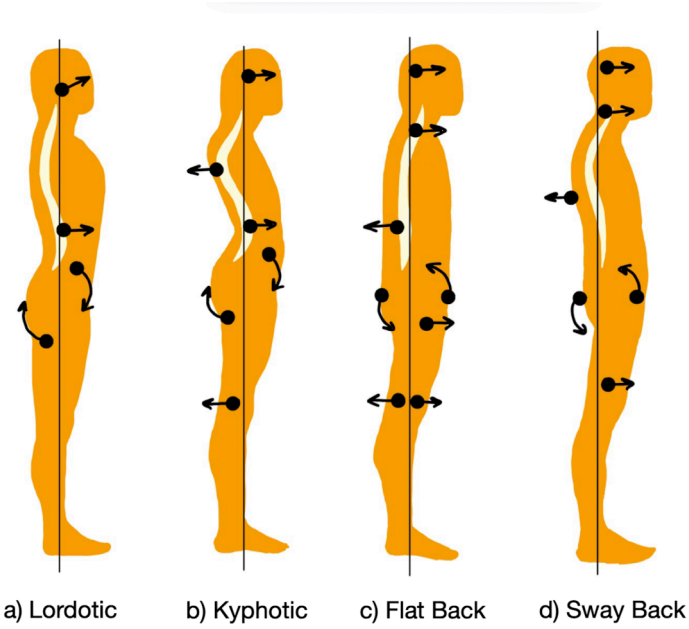

Figure 2.2: Illustrations of lordotic, kyphotic, flat back, and sway back body postures.

maintaining a well-balanced posture [11].

Overloads on the spine, both external and internal, can lead to anatomical changes in the alignment of the spine and subsequently in the three spinal curvatures. When curvatures are shifted, the biomechanics of the body can be altered, which can lead to misalignment of the body posture [15]. The compensatory ability is limited by the inherent flexibility of the spine, and thus an abnormal posture can lead to excessive stress and strain in the spinal structure. This can induce pain [11] and decrease functionality of the spine [20]. In other words, postural-related spinal pain may have roots in *non-neutral spinal postures* [10].

There exists no consensus on a definition of "good posture" [10], but it could be described as a posture that produces the maximal biomechanical efficiency with minimal energy expenditure [15], by keeping the body segments aligned about the line of gravity [5]. More specifically, it could be argued that good posture is described by the alignment of the ear, shoulder, knee, hip, and ankle from the side view, while improper posture implies the postural alignment strays from the centre of gravity. For example, if the head is in front of the centre of gravity, a hunch will be induced in the upper back [21] and the pelvis will tilt anteriorly [11], while if the head is too far behind the line of gravity, excessive arching will occur in the lower back [21]. Thus, it is paramount to obtain a balanced alignment, and importantly one that is comfortable for each specific individual. Harmful effects may arise when body segments are misaligned with the line of gravity [5].

In treating spinal disorders, a key focus is achieving alignment in the sagittal reference plane [20], the vertical plane that divides the body into left and right halves (see Figure 2.3). To achieve sagittal balance, the centre of gravity should be arranged upon the pelvis. Research has also revealed that, at equilibrium, the C7 plumb line should lie posterior to the gravity line [22]. The main cause of misalignment in the sagittal plane is usually increased kyphosis. While the lower extremities and pelvis act in sagittal posture compensation, they are typically biomechanically inefficient, often resulting in strain and pain. This often tilts the head downward, resulting in a loss of horizontal gaze. It is important to note, again, that a local malalignment can cause a disturbance in the overall balance of the spine [23].

The role of the different body parts in maintaining posture varies with activity. For example, depending on whether a person is sitting or standing up, the mechanism of keeping the centre of gravity at equilibrium differs. While standing, the lower limbs may participate in correcting the centre of gravity, whereas in the sitting position this correction is mainly controlled by the pelvis [10]. Although it is important to evaluate the patient in various static positions, such as standing, sitting, and supine, the assessment of standing position has been deemed the most accurate for assessing deformities in both the sagittal and coronal planes [20]. However, certain factors in the lower extremities that can affect posture, such as a discrepancy in leg length, can be avoided if the assessment is performed in a sitting position [24].

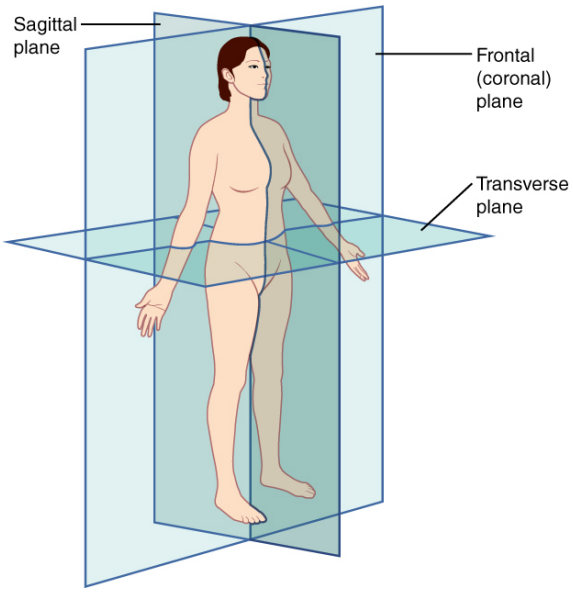

Figure 2.3: Anatomical planes. *Note.* From *Planes of Body* by OpenStax College, 2013, Wikimedia Commons (https://commons.wikimedia.org/wiki/File:Planes_of_Body.jpg). Licensed under CC BY 3.0.

2.2 Pain Disorders Caused by Improper Body Posture

2.2.1 Low Back Pain (LBP)

LBP is one of the leading causes of disability worldwide and the second most common cause of medical consultations [11]. It is estimated to affect 60-80% of the population at some point in their lifetime [8], and 5-10% of sufferers eventually develop chronic LBP [11]. Lower back disorders represent the most significant musculoskeletal condition globally [8].

The causes of LBP are multifactorial and complex. The lumbar spine is of particular interest, as its posture and movement patterns have been found to correlate with lower back injuries. Lumbar spine posture is the most frequently cited cause of LBP [8]. Research has shown that individuals with LBP exhibit a decreased active range of motion (AROM) in the lumbar spine, particularly in the sagittal plane [19]. Furthermore, sagittal postural alignment has been identified as an important risk factor for low back pain in adolescents [12].

Loads placed on the spine are another major risk factor for LBP and are particularly relevant in occupational settings [8]. Mechanical low back pain (MLBP) refers to back pain caused by the placement of abnormal stress and strain on the back [11]. Mechanical risk factors for LBP include lifting, sagittal flexion, rotation or lateral flexion, and prolonged sitting [8]. An example of excessive loading as a risk factor for incident LBP is to use more than 60% lumbar spine flexion for more than 5% of the work day [7]. Poor habits, including poor posture, may also contribute to the development of chronic mechanical low back pain (CMLBP) [11].

2.2.2 Neck Pain

Neck pain is a major public health concern, with high prevalence, incidence, and years lived with disability. It has a high tendency to progress to chronic neck pain (CNP), during which biomechanical issues extend beyond the cervical spine [19].
There is strong evidence that neck pain intensity is associated with greater forward head posture (FHP). Individuals with FHP tend to exhibit lower trunk muscle endurance and control, and walk with a stiffer spine due to reduced trunk rotation, further increasing their risk of developing LBP [19].
Research has also shown that neck pain intensity in individuals with CNP is linked to sagittal spinal posture and mobility while sitting. For instance, in a resting seated position, a higher neck pain intensity has been observed to correlate with a more forward-leaning trunk. One study further reported that women with moderate to severe neck pain display decreased AROM in the spinal sagittal plane, along with greater sacral kyphosis while sitting, compared to women with mild neck pain [19]. During neck movements while sitting down, the intensity of the pain has also been found to be significantly associated with greater lumbar lordosis, suggesting that neck pain may be related to sagittal lumbopelvic posture [19].

3

Methods - Literature Review

In this literature review, articles and studies on postural measurement methods were analysed. The purpose of the analysis was (1) to identify current technologies and tools used to measure body posture, and (2) to find specific devices that met the criteria given by the physiotherapists at Sahlgrenska.
The search began with a set of relevant overview articles supplied with the thesis: [2], [4], [7], [8], and [13]. From there, promising technologies were investigated through screening references and analysing those studies. A broader literature search was then performed to gather additional information on specific topics or technologies. The databases used included Scopus, PubMed, Google Scholar, ScienceDirect, and Web of Science, from which full-text PDFs of the articles were downloaded. The search focused on peer-reviewed journal articles, reviews, theses, and meta-analyses. Articles had to be written in English or have an English abstract, and be accessible through Chalmers institutional login. Search terms included were: *posture monitoring; posture analysis; postural assessment; postural alignment; sagittal alignment; wearables; smartphones; IMU; mobile devices; lumbar; thoracic*; and device names. Articles and devices were included based on the following criteria:

1. Devices had to be applicable and validated for the sagittal spinal plane.
2. Studies had to examine the spine, neck, or pelvis.
3. Tools solely applied in sports were excluded.
4. Devices had to be commercially available.
5. Novel methods could not be based on invasive methods (e.g., radiography).

When a study met these criteria, its references were screened for additional relevant studies, which were also analysed. All qualifying studies were included in the thesis. The names of devices were also used as search inputs in Google to find official websites, brochures, and other information.
To enable comparison between devices, a summary table was created. It included the device components, medical grading, validated spinal regions, suitability for full spine measurement, applicability to static or dynamic measurements, and overall advantages and disadvantages. Images were included for devices where permission was granted.

4

Results - Literature Review

Postural assessment methods are generally categorized into invasive and non-invasive techniques [26]. The targeted angles and movement patterns of the spine are diverse and subtle, posing difficulties in measuring and monitoring them with non-invasive methods. In contrast, invasive methods typically have harmful effects on patients [7].
The key challenges in implementing postural assessment tools include accessibility to clinicians, affordability, complexity of use, and the need for specialist training [13]. Many conventional methods which are valid, simple, and affordable are still used clinically today and will be discussed in Chapter 4.1. However, the need for more accurate, versatile, and patient-safe tools drives the search for novel postural assessment methods, some of which are presented in Chapter 4.2. At the end of the chapter, the novel commercial methods are summarized in a comparison table.

4.1 Conventional Postural Measurement Methods

This chapter presents some conventional postural assessment methods that are used as standard tools in clinics, categorized into invasive and non-invasive approaches.

4.1.1 Invasive Methods

4.1.1.1 Radiography

Radiography has traditionally been considered the gold standard for examining sagittal spinal curvatures. However, it is classified as invasive because it exposes the patient to harmful radiation [15]. X-ray beams that pass through the body have been shown to increase the incidence of cancer in subjects [13]. Thus, the use of radiography for postural examination is limited [27], and is typically implemented only when pathology is suspected [12].
In radiography, spinal curvatures are quantified by analysing X-ray scans. The upper and lower limits of the spine curvature are determined manually [15], and angles are measured via the Cobb method (see Chapter 4.1.1.1.1) [15][26]. Besides the carcinogenic risks associated with radiography, it is also expensive and therefore not recommended for assessing posture variables. Consequently, it is not used routinely for this purpose [13].

4.1.1.1.1 Cobb Angle The Cobb angle, introduced in 1947, was the first parameter used to measure spinal alignment, and remains the most well-known method

to this day. It is considered the standard for curvature estimation, favoured for its simplicity and user-friendliness [18]. The Cobb angle can be used to measure spinal deformities such as scoliosis (from frontal radiographs), as well as kyphosis and lordosis (from sagittal radiographs) [28]. For example, it is considered the gold standard for evaluating the degree of kyphosis, measured at the intersection of two lines drawn from T4 and T12; see Figure 4.1 [29].
At the time of its invention, the Cobb angle was introduced to improve scoliosis evaluation. By the 1990s, advances in imaging technologies led to rapid growth in research on the relationship between the spine and pelvis, giving rise to many new postural evaluation methods. While the Cobb angle is used to this day, the radiation risks associated with radiography have made other non-invasive methods more attractive options for routine postural assessments [18].

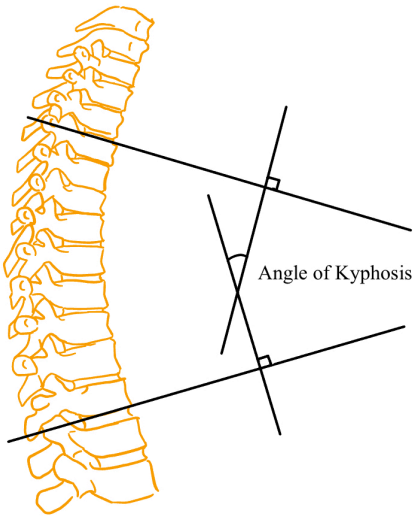

Figure 4.1: Cobb angle method for measuring kyphosis.

4.1.2 Non-Invasive Methods

4.1.2.1 Photogrammetric Methods

In photogrammetry, body measurements are obtained using photographic images. Compared to radiography, photogrammetric methods are associated with lower costs and a lack of harmful health effects. Therefore, they are considered feasible postural assessment methods for clinical practice [13]. Photogrammetric images can be analysed in various ways by combining them with software [26] that calculates the lengths of body segments and the angles between them [15].
However, these methods are largely limited to laboratory use and are unsuitable for continuous posture monitoring [5]. They also suffer from inconsistencies in the data acquisition procedure, where a varying distance between the camera and the patient can introduce errors. In addition, there is a possibility that muscle mass can obstruct the visibility of the spine in the sagittal plane [13].

4.1.2.2 Visual Inspection

Visual observation is one of the most widely used postural assessment methods used in clinics today [15], and is generally used as an initial assessment of the spine [12]. However, due to being highly subjective and user-dependent, it has low reliability and reproducibility, making it unsuitable as a scientific measure [15].
An example is the *plumb line method*, which is an affordable and simple approach where standing posture is examined using body landmarks to imagine a vertical plumb line through the midline of the body [27][30]. While it demonstrates high intra-rater reliability, it is prone to movement errors [13]. As it is a purely visual method, it also provides no quantitative data [30].

4.1.2.3 Flexiruler

The flexiruler is another common method for static posture evaluation in the sagittal plane [8][13]. It is a simple method, where a flexible ruler, a so-called *flexiruler*, is positioned along the back to trace the thoracic and lumbar contours (see Figure 4.2). These contours are subsequently drawn onto paper, where angles and the kyphosis index can be calculated [15].
It is considered an objective method [13] and has shown intra-tester reliability [8]. However, no inter-tester reliability was found in one study [31]. There are also issues with inaccurate estimates due to manual errors, and the process is laborious and time-consuming [8]. Nevertheless, a strong correlation has been reported between flexiruler measurements and surface and radiographic measurements to measure the curvature of the lumbar spine [13].

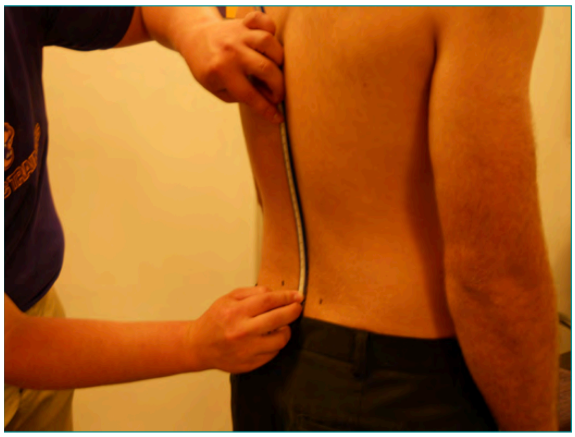

Figure 4.2: Measurement of lumbar spinal curvature using a flexiruler.
Note. Reproduced with permission from Hecimovich & Reid (2015). Source: https://doi.org/10.13140/RG.2.1.4539.1844.

4.1.2.4 Goniometry

Digital goniometers are considered one of the gold standards for kinematic assessment [5] and for measuring joint range of motion (ROM) [13]. They enable measurement of the angle of movement of a body segment and consist of two rods, rotatable

by 360°, which can be placed at the centre of a joint [15] (see Figure 4.3) . They are easy to access and use, but their accuracy depends largely on the expertise of the assessor [5]. Although goniometers can be used to determine 3D coordinates and spinal curvatures, and have previously been used clinically, their area of use is also limited due to bulkiness [32].

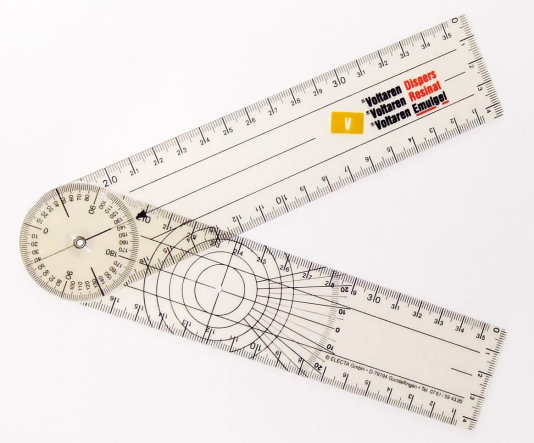

Figure 4.3: Goniometer. *Note.* From *Goniometer* by Jooja, 2020, Wikimedia Commons (`https://commons.wikimedia.org/wiki/File:Goniometer-en.svg`). Licensed under CC BY-SA 4.0.

4.1.2.5 Inclinometer

The inclinometer is a pendulum-based device that measures the angle of inclination and vertebral elevation [15], providing an estimate of the angle between the body and the gravity line. For example, to assess lumbar spine motion, the *double inclinometer (DI)* technique can be used, where one inclinometer is placed at the upper lumbar spine (T12/L1), and a second one is placed at the lower lumbar spine (S1). The difference between these angular measurements relative to gravity indicates the angular position of the lumbar spine [8].

Inclinometer results can be directly compared with X-ray scans. They are affordable, widely available, and have shown proof of inter- and intra-tester reliability. However, like other non-invasive methods, they are time-consuming and prone to human error [8].

4.1.2.6 Kyphometer

A kyphometer is used to measure thoracic kyphosis [33]. It consists of a protractor with two parallel arms that are placed over spinal landmarks; see Figure 4.4. It is simple to use, affordable, and has shown good correlation with the goniometer and the flexiruler methods. However, it is less readily available and unsuitable for real-time measurements [8].

Figure 4.4: Measurement of Cobbs angle of kyphosis using a kyphometer. *Note.* Reproduced with permission from Katzman *et al.* (2016). Source: https://www.researchgate.net/figure/295939358

4.2 Novel Approaches for Postural Assessment

This chapter presents novel approaches for the assessment of human body posture, which can be categorized into camera- and sensor-based methods.

4.2.1 Camera-Based Methods

Camera-based postural assessment methods use imaging devices or cameras to capture photos or videos, which are then processed by computer vision or machine learning algorithms to extract clinically relevant information. These approaches are classified as non-invasive methods [34].
However, camera-based methods place specific demands on the test environment. For example, light must be adequate, the background must not be too complex, and the image quality must be high [34]. Some primary limitations include occlusion and spatial constraints [35]. Another issue to consider is the privacy of the subject, as there are confidentiality issues associated with using cameras to collect images or videos of a patient [2].

4.2.1.1 Optical Motion Capture Systems

Optical motion capture (MoCap) systems use 4 to 32 cameras to record images or videos that can be used to determine body movement or posture. The cameras feed image data to a computer, where it is processed and analysed [36]. Typically, reference markers are placed on the body, and the cameras capture their motion and

orientation in 3D space to determine joint centres and anatomical landmarks [27]. At least two cameras per marker are required to get an accurate determination of its 3D position [36].
Although highly accurate, MoCap systems have several limitations that restrict their clinical use. Marker placement can be time-consuming [36], and a recurring issue has been the creation of reliable models for skin marker placement [27], partly due to the presence of soft tissue artifacts [37]. Moreover, marker-based technologies require controlled environments to collect accurate data [36], limiting them to laboratory settings [5]. Exposure of body areas where markers are attached can also potentially cause discomfort to the test subject [37]. In addition, MoCap systems are substantially more expensive than other alternatives, as they require multiple cameras and involve high computational demands [2].
Despite these drawbacks, motion analysis systems are frequently used to investigate walking, but rarely for posture assessment [27]. Still, optical motion capture is considered a gold standard and is commonly used as a ground truth in research. However, due to impracticality and high costs, MoCap systems are considered unsuitable for routine use in medical clinics [36].

4.2.1.2 Kinect

Kinect® was launched by Microsoft Xbox in 2010 as a video game device, using two PrimeSense cameras [36]: one RGB camera for colour and one infrared (IR) camera for depth [13], seen in Figure 4.5a. It is a three-dimensional, markerless MoCap system, which generates a 25-joint skeleton (Kinect v2) (see Figure 4.5b) [38] picturing the user in real time [36]. This is achieved by projecting a speckle pattern with a laser light source and analysing its deformations [13]. The data are subsequently processed using a randomized decision forest algorithm for feature extraction to determine anatomical landmarks [37]. To function as a MoCap system, Kinect must be paired with dedicated software [36].
The main advantages of Kinect are its simplicity and low price point, as no additional equipment is required apart from the system itself. While the absence of markers makes it easier to use, it results in reduced tracking accuracy compared to marker-based methods. It is therefore most suitable for tasks where high accuracy is not essential [36]. Nevertheless, Kinect has already been used in clinical applications to measure back surface and posture. In scoliosis research, it has demonstrated excellent validity and reliability compared to an optical MoCap system [13], and has been deemed acceptable for clinically diagnosing gait and postural disorders [39].
The second generation of Kinect (v2) includes several improvements compared to its predecessor (v1), such as a wider field of view and enhanced image resolution and recognition through an increased number of pixels [39]. Despite this, there has been no substantial improvement of joint centre identification. It should be noted that the Kinect system was originally designed for game play, and that daily postural tasks of interest in postural assessment, such as sitting or standing, may not be tracked as accurately by the algorithm. Joint centre recognition accuracy can also be affected by loose clothing, and may be less reliable in individuals with higher body mass index (BMI) [38].

(a) Xbox 360 Kinect system.

(b) The 25 anatomical landmarks (joints) detected by Kinect v2.

Figure 4.5: Kinect system and joint skeleton. *Note.* Subfigure (a) from *KinectSensor* by Alphathon, modified from a photo by James Pfaff (litheon), 2010, Wikimedia Commons (`https://commons.wikimedia.org/wiki/File:KinectSensor.png`). Licensed under CC BY-SA 3.0.

Several studies have evaluated the feasibility of using Kinect for clinical postural assessment. Yeung *et al.* [40] investigated its feasibility to measure body sway, specifically the total body centre of mass (TBCM), but reported offsets in the Kinect measurements that they hypothesized could be due to the system's limited resolution, accuracy, and sensitivity. The study also recognized the comparable accuracy Kinect has shown to MoCap systems such as Vicon in previous studies, but concluded that the accuracy and sensitivity of the Kinect system would need to be improved for clinical use.

Su *et al.* [41] deduced that Kinect's depth information was inadequate and suffered from inaccuracy and instability in rotation angle measurements which caused large errors, though they suggested it may be acceptable for clinical measurements where a mean absolute error of 1.1-1.5° is tolerable.

Koda *et al.* [42] compared Kinect with the Spinal Mouse (see Chapter 4.2.2.2.1) and found a poor correlation in the lumbar spine ($r = 0.25$), but a moderate positive correlation in the thoracic spine ($r = 0.56$), leading them to consider Kinect a valid measurement tool for the thoracic spine, but not for the lumbar spine.

Wiedemann *et al.* [43] compared Kinect with Vicon and observed a median difference of less than 7.2° in upper joint angles and body inclinations, and up to 24.0° for neck tilt.

Clark *et al.* [44] also reported deviations of the trunk flexion angle of 0.4-4° in reaching tasks and standing balance tests compared to Vicon, yet deemed it useful for clinical tests of postural control. In another study [45], Clark *et al.* used

Kinect to measure trunk lean in subjects trained to have a 10° lateral lean, finding errors of high magnitude (> 2°), which improved to 0.8° following an individualized calibration procedure.
It is important to note that in these studies, the trunk was modelled as the entire spine in a single rigid segment. Additionally, other studies have explored ways to increase Kinect's precision and reliability, for example by combining it with sensor technologies [46][47].

4.2.2 Wearable Sensor Systems

Common sensor-based technologies include pressure sensors, distance sensors, deformation sensors [2], accelerometers, gyroscopes, and magnetometers [34]. The development of wearable sensors has been made possible by the recent miniaturization of sensors and electronic circuits, particularly by the advancement of *microelectromechanical systems* (MEMS). In the past, sensor systems were too large and bulky to be used for rehabilitation purposes [6]. Today, sensor technology can be made wearable by integrating them into clothing or accessories that sit comfortably on the body, which simplifies measurements of the human body [5].
Sensor-based devices are highly accurate and sensitive to small changes in angle. The technology itself is not new and has previously been utilized in rehabilitation, sports, and ergonomics, both for the lower and upper body [4]. Their widespread use allows the cost of sensors to remain low, due to the availability of commercial sensors produced through batch manufacturing [6]. The main design objectives for wearable sensor-based systems are generally to make them cost-effective, reduce their power consumption, and maximize user convenience [48].
The choice of sensor is highly dependent on the specific application [2], but wearable systems usually follow a similar architectural structure:

1. **Physiological data sensing:** the sensors that collect physiological and movement data.
2. **End-to-end data transmission:** the communication hardware and software that transmit data to a host device.
3. **Processing, analytics, and visualization:** the data analysis techniques (signal processing and pattern recognition algorithms) used to extract body movement and posture information from physiological and movement data [6] [34][48].

Back-end support is usually provided by cloud environments, where data can be stored long-term in a secure manner, and to reduced operating costs. They also support big data analytics and data visualization, as well as the implementation of machine learning toolboxes, which are useful in health monitoring applications [48].

4.2.2.1 Biofeedback

The ability to record and analyse the movement patterns of the spine provides valuable insights into what may be considered abnormal. The information can be used to provide informed guidance on how movement patterns should be altered. To facilitate this guidance, **biofeedback** is an attractive strategy to restrict certain

movements or enforce desired movement patterns. Sensor systems utilizing augmented feedback can provide real-time corrective sensory stimuli, which can alert the wearer when it adopts postures that exceed angular thresholds that are predetermined as harmful [4][5].
Feedback is usually conveyed through three main modalities: *audio feedback*, such as beep noises, *haptic feedback*, such as vibratory stimulus, or *visual feedback* [4], such as blinking LEDs or pop-up windows on a computer screen [4][7]. Among these, haptic feedback is generally the most popular choice due to its discreetness and flexibility [5]. In contrast, auditory feedback can be muffled by outside noise, and visual feedback can obstruct user view, which is undesirable and could potentially compromise safety in occupational settings [49].
Feedback can also differ in timing. When delivered when a task has been completed, it is defined as *terminal feedback*, and if it is given simultaneously to the task, it is known as *concurrent feedback*. Concurrent feedback is considered the most ideal, as it encourages immediate change, increases postural awareness, and induces instant reduction in musculoskeletal overload.
Currently, sensor systems used for this purpose are often in the prototype stage, as commercially available devices typically do not combine postural monitoring with feedback [5]. Still, research has proven biofeedback to be effective in increasing awareness of movement pattern aberrations and voluntarily controlling posture [7]. Although this feature is not directly within the scope of this thesis, it remains an important and advantageous characteristic of wearable sensor systems.

4.2.2.2 Deformation Sensors and Smart Textiles

Advances in the field of material science have led to the invention of e-textile-based systems, where sensors are integrated into the fabric of garments [6]. The deformation or stretching of the material can be detected and used to determine the movement patterns of the body [1]. For example, movement data can be collected by printing conductive elastomer-based components onto fabric, so that during body movements, the component will stretch, leading to a change in resistance which can be recorded [6]. Other approaches, such as weaving electrodes into the fabric, have also been explored.
Deformation sensors are generally easily accessible and inexpensive. However, some key challenges that arise when designing clothing with integrated sensors are how to adapt the garment to different body sizes, ensuring wearer comfort, and maintaining accurate calibration [2].

4.2.2.2.1 Epionics SPINE The Epionics SPINE system consists of two flexible circuit board strips with 12 embedded strain gauge sensors each, which are placed along the back according to Figure 4.6. The embedded sensors measure electrical resistance at 50 Hz, providing the bending angle of each segment [50][51] and enabling an assessment of the sagittal curvature of the thoraco-lumbar spine [52]. The data can be used to calculate the range of motion (RoM) and range of kinematics (RoK), thereby assessing spinal mobility. In a test group of healthy subjects, the system has demonstrated high accuracy, with an average interclass correlation coefficient

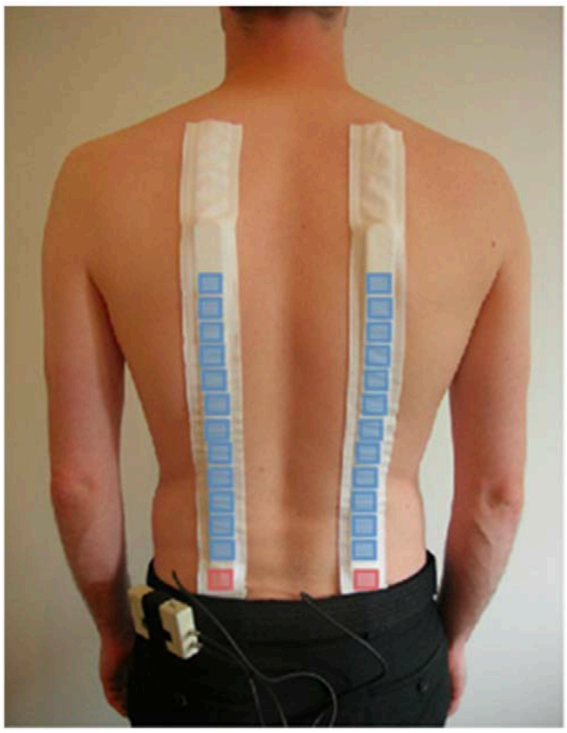

Figure 4.6: Epionics SPINE applied on back. *Note.* Reproduced from Consmüller *et al.* (2012) under CC BY 4.0. Source: `https://doi.org/10.1371/journal.pone.0050135`

(ICC) of > 0.98 [50], and produced results similar of the Vicon MoCap system when measuring lumbar lordosis angles during functional activities. However, the minimal detectable change (MDC) recorded for standing, sitting, and walking ranged from 6° to 12°, indicating that angle changes smaller than this cannot be reliably detected. Additionally, Epionics SPINE reports the overall curvature of the spine, rather than segmental curvatures [51].

4.2.2.3 Mechanical Encoder Sensors

4.2.2.3.1 SpinalMouse (Idiag M360) The SpinalMouse® (Idiag M360) measures the shape and mobility of the spine in both the sagittal and coronal planes [53]. The device is handheld and designed to roll, similar to a computer mouse, along the spinous processes of the vertebral column, sampling data every 1.3 mm [54]. It uses mechanical encoder sensors that convert motion into digital signals [55], which are transmitted via Bluetooth to a computer where the measured curvatures are displayed. The accompanying software calculates the relative positions and angles between the vertebra and provides the total angle of frontal and sagittal curvatures [54]. When compared to X-ray scans, the SpinalMouse shows an accuracy of ±1.96°, making it a a quick and easy method suitable for rehabilitation practice [56].
Sugino *et al.* [53] evaluated the SpinalMouse in static standing measurements in the sagittal plane using radiography as ground truth. They found that it performed similarly to radiography in the thoracic spine but showed smaller angles for several other spinal segments. Thus, the validity was concluded to be high in the thoracic spine and low in the lumbar spine. Similarly, Amgad *et al.* [57] evaluated the device

against X-ray methods and found it to be valid for measuring spinal deformities of the thoracic and lumbar spine in the sagittal plane. Yousefi *et al.* [58] compared three non-invasive methods to the X-ray Cobb angle and reported mean deviations of 7.88° for thoracic kyphosis and 4.81° for lumbar lordosis when using the SpinalMouse, while a flexible ruler outperformed it.
Mannion *et al.* [59] investigated the reliability of the SpinalMouse and found consistent results for global regions of the spine. However, for smaller segmental angles, reliability was much lower, with ICCs ranging from 0.39-0.83 within examiners and 0.28-0.81 between examiners. Standard errors of measurement ranged from 2-3°, giving a smallest detectable change of 6-8° (95% Cl). They concluded that interpreting "real change" on an individual level for segmental motion is questionable. Likewise, Post *et al.* [60] also advised that the SpinalMouse is not reliable for measuring intersegmental ROM.

4.2.2.4 Inertial Measurement Units (IMUs)

Most wearable systems utilize **Inertial Measurement Units (IMU)**, which combine accelerometers, magnetometers, and gyroscope technologies [5] to give an estimate of the movement and position of the device [61]. They can be used to continuously capture both static and dynamic postures, for either shorter or longer time-frames, and their results are considered reliable and accurate. IMUs are also lightweight, compact, portable, low-cost, and energy efficient, making them attractive for widespread use [5].
The development of IMU systems is still in its early stages, and several challenges remain. These include technical functionality, usability, battery life, long-term comfort, setup time, and stability of wireless communication. As with many new technologies, there may also exist a reluctance to adopt them. Therefore, improving user-friendliness is a primary objective [5], as many IMUs nowadays are already highly accurate [1].
In occupational settings, IMUs are particularly relevant, as they provide reliable and trustworthy assessments of human movement in real and dynamic situations [5]. Their reliability and accuracy are also of interest in the fields of health and rehabilitation [1]. IMU sensors are typically attached to body joints and could, in theory, be placed on all 17 major joints of the body to capture whole-body motion. More commonly, they are placed on only a few joints, such as the wrists, spine, or arms [34]. They may be secured using adhesive tape or elastic straps, or they can be integrated into smartwatches [5], placed in pockets on garments [62], or attached to personal protective equipment (PPE) such as helmets [5]. However, placement on the body is believed to introduce discrepancies in the results due to soft tissue artifacts, but these effects have not yet been fully understood [62]. Some of these effects can be reduced through signal filtering [63], but it is also vital to carefully select where and in which manner to attach the sensors to mitigate these disturbances [2]. Additionally, it is important to be mindful not to attach them too close to the centre of rotation, as the amplitude of the signal may be attenuated [63].
In order to combine the separate data flows from the accelerometer, gyroscope, and magnetometer and compute a single estimate of orientation, an **orientation filter**

is employed. This filter fuses the data in an optimal way, that considers the high levels of noise the data is subjected to. Today, the operation filter algorithm most often used is the **Kalman filter**, due to its accuracy and effectiveness [64].
The kinematic variables that can be collected with an IMU module include *displacement* and *angular velocity*, *linear* and *angular acceleration*, and *linear position*, either in a separate or combined manner. IMUs are typically classified according to their degrees of freedom: three-axis, six-axis, or nine-axis (nonaxial) IMUs. Nonaxial IMUs, which consist of a triaxial accelerometer, a triaxial magnetometer, and a triaxial gyroscope, are the most common. They provide a greater robustness and reliability of the received data compared to simpler systems. However, all configurations have been shown to be highly valid for measuring joint position and may be the only alternative to the gold standard in occupational contexts [5].

4.2.2.4.1 Accelerometer The role of an accelerometer is to measure the Earth's gravitational field in order to provide an absolute reference of orientation [64] through measurements of linear acceleration [65]. Due to the gravity vector, this can also give an estimate of the inclination. The accelerometer is based on a mass-spring system within a vacuum, which records the displacement of mass during acceleration [61].
If the acceleration (a) obtained from the accelerometer is double-integrated over time (t) and the gravity vector is removed, an estimate of the change of position ($p(t)$) can be obtained. That is,

$$v(t) = \int_0^t a\, dt + v_0 \tag{4.1}$$

$$p(t) = \int_0^t v\, dt + p_0 \tag{4.2}$$

where v represents velocity [61].
There are three types of accelerometers: uni- bi-, and triaxial. Uniaxial accelerometers only measure acceleration in a single direction, whereas orthogonal axes are added for the biaxial and triaxial accelerometers, enabling them to measure accelerations in two dimensions (x, y) and three dimensions (x, y, z), respectively [63]. Accelerometers can measure both static acceleration forces, such as gravity, and dynamic acceleration forces, such as movement and vibration [66]. They can thus detect a variety of human activities, such as tilt and rotation, and are one of the cheapest and most reliable sensors. A triaxial accelerometer can also detect the difference between walking, sleeping, and sitting. Generally, accelerometers are inexpensive, small in size, give high quality measurements and can record data up to several months due to their relatively low current draw [63]. However, accelerometers are temperature sensitive and their accuracy degrades with time [66].
According to the scoping review carried out by Figueira *et al.* [5] a majority of studies on IMUs use only the accelerometer. Results were however made more robust if a gyroscope and magnetometer were used in addition to the accelerometer [5].

4.2.2.4.2 Gyroscope The gyroscope component of an IMU device measures the angular velocity, or the rotation rate of the sensor relative to the local coordinate system [67]. Thereby, it tracks shorter changes in orientation and provides stability to the reference directions. A gyroscope measures the rate of turn using a tiny oscillating mass within a spring system that reacts to the forces applied to it when rotations occur [61].
Integrating the rate of turn (ω) obtained from the gyrosc
ope over time (t) gives an estimate of the change in orientation ($q(t)$) [61]

$$q(t) = \int_0^t \omega \, dt + \omega_0. \tag{4.3}$$

Gyroscopes can detect whether a patient is sitting, standing, walking, or lying down [7]. Gyroscopes are also the main source of errors for IMUs, as they suffer from drift errors during prolonged usage [67]. The information from the accelerometer and magnetometer has a stabilizing effect in preventing drift over time [61].

4.2.2.4.3 Magnetometer Magnetometers measure the direction and strength of the magnetic field of the Earth in order to provide an absolute reference of orientation [64], acting as a sort of compass needle [61]. Their measurements are sensitive to errors produced by disturbances from nearby magnetic fields or ferrous materials [68]. However, magnetometers do not experience drift, and are often implemented in IMU sensors to correct for gyroscope drift, which otherwise causes offsets in the heading angle [67].

4.2.2.5 Commercial IMU Systems

Commercial IMU sensor systems that have shown validity in measuring sagittal spinal curvatures are listed in this chapter.

4.2.2.5.1 Xsens Movella DOT Xsens Movella DOT® is an industry-leading 9-axial IMU sensor system, embedded with the highest accuracy sensor fusion algorithm on the market. The sensors connect to a smartphone application, the *Movella DOT app*, which enables logging of orientation data (Euler angles and quaternions) and free acceleration. Euler angles can also be live-streamed for easy visualization. The system supports the development of custom applications via the Movella Software Development Kit (SDK) [69]< and has the flexibility to connect up to 11 sensors. Extensive online documentation guides users on how to correctly place sensors on different parts of the body [61].
According to the user manual, the accuracy of inclination is within 0.5° for static measurements and 1.0° for dynamic measurements [70]. A 2024 study that evaluated the spine range of motion (ROM) using the Movella DOT system reported high validity for tracking multiplanar spine movement when compared to a MoCap system. The study found an overall absolute mean absolute error (MAE) of 0.74° and intersegmental MAE of 1.10°, with ICCs of 0.953 and 0.950, respectively. These results support the use of Movella DOT for the evaluation of spinal movement in clinics [71]. Additionally, the Movella DOT sensors have been used to study lumbar sitting behaviour in individuals with LBP [72].

Figure 4.7: Xsens Movella DOT IMU sensor kit. *Note.* Reproduced with permission from Movella/Xsens. Source: Movella/Xsens.

4.2.2.5.2 Noraxon myoMOTION The Noraxon Ulltium Motion 3D Capture System/myoMOTION uses state-of-the-art IMU modules for kinematic measurements, giving orientation and joint angles, along with linear acceleration. The system provides accurate and reliable data that is visualized both with graphs and a skeletal avatar. The full-body avatar is generated by placing sensors on pre-defined locations on the body. However, the sensors can be used stand-alone as well. The system outputs raw data from the sensor components (e.g., acceleration), orientation data (quaternions), and user-defined angles [73][74][75].
The Noraxon system aims primarily to assess changes in movement patterns [73][74][75]. Several validation studies have demonstrated strong agreement with MoCap systems. One study reported maximum root mean square error (RMSE) values of 0.2° for static movements and 0.5° for dynamic movements, with a correlation coefficient of 0.99 [76]. Another study compared the joint angles of the pelvis and lower extremities between Noraxon and MoCap and found the highest agreement in the sagittal plane, with maximum differences of 5° across most movements [77]. It has also shown excellent agreement in measurements of sagittal joint movement for change-of-direction and jump-landing tasks, with cross-correlation values above 0.88 [78].

4.2.2.5.3 dorsaVi ViMove dorsaVi® ViMove™ is a CE-marked medical grade wireless 9-axis IMU system that combines an accelerometer, a gyroscope and a magnetometer. Although most ViMove products are targeted at athletes, to track athletic movement index (AMI), running performance, and to collect kinematic data, it is also used clinically to diagnose, treat, and rehabilitate musculoskeletal conditions. The system focuses on being versatile, user-friendly, and accessible to professionals with different technological proficiency [79].
One of their latest products is the ViMove v6 system, which consists of two movement sensors and two muscle activity sensors, along with a specially designed program of a series of sitting and standing positions to report ROM and muscle activity in the sagittal and coronal planes of the lumbar spine. The ViMove software can be downloaded to an iPad via the Apple App Store, where data can be visualized,

Figure 4.8: Noraxon myoMOTION inertial sensor system, including sensors and wireless modules. *Note.* Reproduced with permission from Noraxon USA Inc. (n.d.). Source: https://www.noraxon.com/download/myomotion-system-user-manual/?wpdmdl=18194

recorded, and stored in folders for separate patients and grouped into sessions so progress can be monitored [80].
Multiple studies have assessed dorsaVi systems during dynamic movements, showing clinically acceptable agreement with gold-standard MoCap systems [81][82]. In one study using dorsaVi v6 on 12 participants, lumbar flexion during lifting activities was measured and compared to Vicon. The results were below clinically acceptable thresholds ($r > 0.90$) with RMSE values below 2° [81]. Another study measured the inclination motion of the lumbar region in the sagittal and coronal planes of 34 participants and found clinically acceptable concurrent validity compared to the Vicon system, with RMSE values of $1.82° \pm 1.00°$ for flexion (forward bend) and $0.71° \pm 0.34°$ for extension (backward bend) [82]. However, these studies were limited to evaluating gait and dynamic activities in the region of the lumbar spine [81][82].

4.2.3 Smartphone-Based Systems

There is growing interest in utilizing sensors already integrated into the technology used in daily life, such as smartphones, smart watches, or wristbands, to improve accessibility and promote postural awareness. Smartphones have already-embedded MEMS accelerometers which can be used to perform accurate angle measurements. Previous studies have, for example, deemed the iPhone an equivalent tool to the manual protractor [7]. However, their main drawbacks are their weight and bulkiness, which can make them uncomfortable to wear, and have previously posed obstacles in postural assessment studies [21].

4.2.3.1 PostureScreen Mobile

PostureScreen Mobile® is a smartphone app that uses AI-assisted computer vision to accurately measure angles and linear distances. It is marketed as an inexpensive,

user-friendly, quick, valid, and accurate tool for postural assessment [83]. The app collects 2-4 pictures of the patient in the coronal and sagittal planes using the device camera, which are then analysed to calculate posture variables from digitized anatomical landmarks. Landmarks are determined by overlaying a grid on the body, with physical markers improving localization accuracy [84]. See Figure 4.9 for an example of the app interface. When taking photographs, it is also advised that the patient wear minimal or tight-fitting clothing [83].
Rehabilitation progress can be easily tracked through comparative PDF reports within the app, called *Posture Trend Analysis*, and can be directly uploaded to electronic health records. In addition, virtual assessments are possible through the RemoteScreen application. Recently, a module was released that takes advantage of the built-in gyroscope of the Apple iPhone or iPad to measure ROM of the cervical and thoraco-lumbar spine. However, no validity studies have been published on this feature to date. It should be noted that the full version of the PostureScreen Mobile app is only available for iOS, while only a "Lite" version, which does not use AI Computer Vision, is available for Android [83].
Several studies have evaluated the reliability of the PostureScreen Mobile. A 2014 master's thesis [85] involving 50 participants assessed its validity and reliability for head, shoulder, hip, and knee tilt measurements in the frontal and sagittal planes in a static standing position, using Vicon as a reference. For sagittal measurements, the app tended to underestimate tilt and showed variances that exceeded the MoCap system. ICC values also indicated substantial trial-to-trial variation. These findings suggested that the app is generally not suitable for high-accuracy postural assessments or applications that require high repeatability. Yet, the sagittal tilt measurements had clinically acceptable levels of bias at $< 5°$. The app was still recommended mainly as an initial screening method and not as a diagnostic instrument [85].
These findings are supported by a 2018 study by Boland *et al.* [86], which concluded that the app is not appropriate for tasks that require high precision. Nonetheless, they found that PostureScreen Mobile was most reliable for sagittal head tilt and could be used as a quantitative diagnostic tool for forward head posture. In contrast, Szucs *et al.* [84] evaluated the same body segments in the same anatomical planes and recommended the app for clinical and research settings based on good to excellent intra- and inter-rater reliability. Test-retest reliability was, however, not investigated.

4.2.3.2 Scoliometer 1.1 App

The Scoliometer 1.1 app uses the built-in accelerometer of smartphones and is compatible with both iOS and Android. It aims to replace the role the scoliometer (a type of inclinometer) has in clinics, by offering a quicker, more convenient, and easier way to measure spinal curvature. In addition, the app can measure angles up to 50°, compared to the 30° limit of a traditional scoliometer. The app displays an animated scoliometer that changes angle based on the tilt of the phone [87].
Although originally designed to measure the degree of scoliosis, studies have utilized the Scoliometer 1.1 app to measure sagittal spine parameters. Waś *et al.* [88] used the app to measure sacral slope, lumbar lordosis, thoracic kyphosis, upper thoracic

Figure 4.9: Screenshot of the PostureScreen mobile app showing postural assessment results. *Note.* Reproduced with permission from PostureCo, Inc. (2025). Source: `https://www.postureanalysis.com/wp-content/uploads/2025/05/PostureScreen_results__iPhone-14-Pro-Max-Space-Black-Portrait-copy-scaled.png`

kyphosis, and lower thoracic kyphosis in static standing and sitting postures for 40 healthy subjects, and compared the results with a Saunders digital inclinometer, which is a standard diagnostic tool. Measurement errors ranged from 9.8° to 12° for the different curvatures, but the app was considered suitable for more basic clinical use, as it had results comparable to those of the traditional scoliometer.

4.2.3.3 iHandy Level App

The iHandy Level is a free Android application that utilizes the smartphone's embedded accelerometer to measure angles, which are displayed in real time on the screen. It has previously been validated for measuring spinal ROM and posture [89].
Koumantakis *et al.* [89] evaluated the reliability of the iHandy Level app for measuring the sagittal lumbosacral posture in a static standing posture among 183 subjects. For the lumbar curve (T12-L1), they found an ICC of 0.96 and an MDC of 5.9°, and for the sacral slope (S1-S2), an ICC of 0.96 and an MDC of 4.46°. They concluded that the app was a reliable and valid tool in this context. However, since no ground truth was implemented, the accuracy of the app could not be determined.
In a separate study, Kolber *et al.* [90] used a gravity-based bubble inclinometer as ground truth to examine the reliability and concurrent validity of the iHandy Level app to quantify lumbar spine mobility. They observed good concurrent validity (ICC $\geq$ 0.86) but reported disagreements between devices of up to 18° and interrater MDCs of 4-9°. Similarly, Salamh *et al.* [91] reported an MDC of 7° for standing lumbar lordosis, with iHandy Level readings ranging from 9° higher to 8° lower than those obtained with the inclinometer.

4.2.3.4 Summary of Postural Assessment Methods

Tables 4.1 and 4.2 summarize the postural assessment methods introduced in this chapter. Table 4.2 lists all IMU-based systems, while Table 4.1 presents all the non-IMU devices. Each system is compared in terms of its components, medical certification, validated spinal segments, measurement type (static or dynamic), and main advantages and limitations.

System	Company	Components	Medical Grade	Spinal Segment Validity	Full Spine	Static or Dynamic	Advantages	Disadvantages
Camera-Based Systems								
Kinect	Microsoft Corp. (USA)	RGB and IR camera, laser source (3 DoF) [13]	No [40][92]	Thoracic [42]	No [42]	Both [40][44]	Easily accessible, easy to use, low-cost, portable, no skin markers [38][36][13]	Not posture-validated, reportedly not accurate enough for clinical use, lack of accuracy and sensitivity to environment [40][43]
Deformation Sensors								
Epionics SPINE	Epionics Medical Gmbh (Germany)	Strain gauge sensor array (1-2 DoF) [50][51]	No (no certification found)	Lumbar region [52][51]	No [52][51]	Both [51]	Comfortable, captures lumbar curve [52][50][51]	Limited to thoracolumbar region, less common on the market, high errors (~6-12°) [51]
Mechanical Encoder								
Spinal Mouse (Idiag M360)	Idiag AG (Switzerland)	Mechanical encoder (1-2 DoF) [57][54]	Yes (CE-marked) [93]	Thoracic and lumbar [53][57]	No [53]	Static [57][54][56][94]	Cost-effective, quick, easy to use, validated [57][54]	Only static measurements, no real-time data [57][54], only high validity in thoracic spine [53], deviations from X-ray of 7.88° for thoracic kyphosis and 4.81° for lumbar lordosis [58]
Smartphone Apps								
PostureScreen Mobile	PostureCo, Inc. (USA)	Camera (2D) and software [83]	No (no certification found)	Whole spine [84]	Yes [84]	Static [84]	Easy, valid, tailored for clinical use [84][83]	No precise angles, user-dependent, recommended as screening tool [85][86]
Scoliometer 1.1	ScolioLife (Singapore)	Built-in accelerometer (3 DoF) [88]	No (no certification found)	Sacral, lumbar, thoracic [88]	No [88]	Static [88]	Low-cost, accessible, validated against clinical scoliometer [88]	Only static measurements, high errors (~9-12°) [88]
iHandy Level	iHandySoft Inc. (Hong Kong/China)	Built-in accelerometer (3 DoF) [89]	No (no certification found)	Lumbar (T12-L1), Sacral (S1-S2) [89]	No [89]	Static [89]	Easy to use, free, valid [89]	Only static tracking, limited to lumbosacral spine [89], readings reported to be 9° higher or 8° lower than the inclinometer [91], up to 18° disagreements between devices [90]

Table 4.1: Summary of commercially available non-IMU postural assessment systems.

System	Company	Components	Medical Grade	Spinal Segment Validity	Full Spine	Static or Dynamic	Advantages	Disadvantages
IMU Systems								
Xsens Movella DOT	Movella Inc. /Xsens (Netherlands/USA)	Accelerometer, Gyroscope, Magnetometer (9 DoF) [69]	No [95]	Customizable [61]	Yes [61]	Both [70]	High precision, flexible setup [61][70]	Not medically graded, requires software skills to develop custom app [69][71][70]
Noraxon MyoMotion	Noraxon USA Inc. (USA)	Accelerometer, Gyroscope, Magnetometer (9 DoF) [75]	Yes (CE-marked) [75]	Customizable [73][74]	Yes [73][75]	Both [76][75]	Can be combined with EMG, validated protocols, accurate [76][78]	Only studied for dynamic postures, less flexible [76][77][78]
dorsaVi ViMove	dorsaVi Ltd. (Australia)	Accelerometer, Gyroscope, Magnetometer (9 DoF) [79]	Yes (CE-marked, FDA-cleared) [79][80]	Typically lumbar (T12-L5) [80][81][82]	No [80][81]	Both[80][82] [82]	User-friendly, accurate results and clinically acceptable for lumbar region [80][81][82]	Focus on dynamic movement, less flexible and limited points of use (often only 2 sensors) [80][81][82][80]

Table 4.2: Summary of commercially available IMU-based postural assessment systems.

5

Discussion - Literature Review

The results indicate that numerous promising devices are available for postural assessment. However, the suitability of each device depends on the intended application, and many can be excluded based on the specific use case.

5.1 Discussion of Research Process and Limitations

It should first be noted that only a few studies have used device to measure the entire spine. Whole-spine measurements are largely supported only by prototypes and not commercial models. Most available research focuses on some segment of the spine, and although it is possible that the device could be applied to other regions, this has not yet been validated for most systems. The column *"Spinal Segment Validity"* in Tables 4.1 and 4.2 shows the specific parts of the spine for which each device has be en validated.
Most validation studies have been small in scale, and for most systems a very limited number of studies have been done. It should be noted that all studies meeting the inclusion criteria were included in the analysis of each device. For instance, only one eligible study was identified for the Scoliometer 1.1 app. Furthermore, many devices are intended for use primarily in the sports industry and therefore only consider kinematic measurements of, for example, gait or running. Consequently, there remains an evident lack of research investigating static postures.
Postural assessments can be more challenging to perform accurately in individuals with higher BMIs due to soft tissue artifact. Most existing studies include only participants with a normal ranged BMI, and several have highlighted the need for further studies on people with higher BMI values (e.g., [38][51][52]). However, such studies have not yet been carried out for most devices. Regardless of which solution is chosen, it is vital to perform studies on a diverse range of body types before clinical implementation, to ensure that the method is accurate and reliable for all users.
The inclusion criteria used in this review proved restrictive, as many devices were excluded because they were not applicable or validated for the whole back. Full-spine measurement capability was emphasized as a particularly important feature of the device by the team at Sahlgrenska, as the purpose of the new tool is to give a comprehensive diagnosis of overall posture. Several devices have yet to be studied for the whole spine, but could be considered potential candidates as soon as they are. Thus, it is important to recognize that this study is limited to the information

available at the time of the analysis.
If dialogue was established with the respective companies, perhaps more information could be collected and costs for the different devices could be estimated. However, the matter of cost was not considered a major determinant of which system was selected, as it was established that IMU systems, which were the most costly alternative, were considered a reasonable choice for implementation at Sahlgrenska.

5.2 Discussion of Devices

5.2.1 Kinect

The Kinect has become a prominent topic in postural assessment and recognition research due to its accessibility and affordability. It offers low-cost MoCap technology without the need for time-consuming marker placement [13][36][38]. In this context, it is necessary to measure small angles precisely during static positions, such as standing or sitting, which makes the inaccuracy of the Kinect problematic. Several studies have advised against its use for tasks that require high precision or have questioned its overall measurement accuracy [40][43][45]. A median deviation of approximately 7.2° has been reported for upper body angles [43], which is relatively high compared to the other investigated solutions.
Reported accuracies of the Kinect vary substantially between studies [40][41][42][43] [44][45]. The system has also not been validated for posture assessment, and its reliability for estimating sagittal spinal curvatures remains uncertain. Previous studies have, for example, found that it is invalid for the lumbar spine [42] and neck tilt [43], suggesting that it may not be suitable for full-spine assessment. Additionally, many studies have simply modelled the trunk as a single rigid segment and have not considered segmental angles [43][44][45], making their findings less relevant for this thesis.
While it is a convenient system and there are new approaches to using software and hardware to increase the Kinect system's accuracy and reliability [46][47], it is currently not considered suitable or feasible for clinical use in this application due to its insufficient precision. Perhaps, it would be better suited to screen for global posture.

5.2.2 Epionics SPINE and SpinalMouse

The Epionics SPINE and SpinalMouse were developed as convenient and quick posture evaluation tools. SpinalMouse is an intuitive product that rolls along the patient's back and is highly user-dependent, but is still realistic to use for a quick and easy profiling of the shape of the thoracic and lumbar back [54]. However, its reliability for segmental measurements has been questioned [59][60], with studies reporting relatively large angular deviations of up to 7.88° for thoracic kyphosis and 4.81° for lumbar lordosis when compared with X-ray scans [58]. On the other hand, Epionics SPINE uses strain gauge sensors placed along the lower back and is anatomically limited to the lumbar spine [52]. During standing, sitting, and walking, Epionics SPINE was found to give unreliable readings below 6°-12° [51], which would be of

concern when measuring subtle changes in the tilt of the spinal curvatures. Although both systems are feasible options to use clinically for posture evaluation, they lack the versatility and accuracy necessary for the requirements of this study.

5.2.3 Smartphone Applications

The investigated smartphone apps were Scoliometer 1.1, iHandy Level, and PostureScreen Mobile. They all represent simple and cost-effective posture evaluation methods that suffer from a relative lack of accuracy. The Scoliometer 1.1 has been validated against a traditional inclinometer, but showed high error margins of 10-12° [88]. iHandy Level had MDCs of 4-9° [89][90][91], but high disagreements of up to 18° were observed between devices [90] and discrepancies from the inclinometer of up to 9° [91]. In contrast, the PostureScreen Mobile app does not use the embedded sensors of the smartphone, but instead relies on visual data [83]. It demonstrated a clinically acceptable bias of less than 5° [85], and has been described as a feasible clinical tool for forward head diagnosis [86]. While it was the only smartphone app validated for use on the full spine, it does not actually give the true angles of the spine, as it is based on a 2D visualization of the spine and manually placed markers. Several studies have therefore advised against its use as a diagnostic tool or for contexts where repeatability or high precision is necessary [85][86]. Overall, these three smartphone apps do not have the capacity to make precise estimates of spinal tilts at the same level as dedicated devices and are generally better suited for more basic screenings or to estimate gross misalignments.

5.2.4 IMU Systems

Wearable IMU systems are accurate, practical, modular, can be used for both static and dynamic measurements, and have been validated for measuring spinal tilts [1][5]. Importantly, they avoid privacy concerns that may arise in a clinical setting, where photography of patients can be sensitive and potentially violate the GDPR. Unlike Kinect, IMU sensor systems also do not suffer from issues with occlusion and vulnerability to the background environment, other than influences of magnetic fields for IMUs containing magnetometers [68]. IMU systems also have many exciting features that would allow them to be used for more purposes than solely a diagnostic tool. Augmented biofeedback facilitates the use of IMUs directly as part of rehabilitation therapy, since it can reinforce changes in habituated movement patterns in the daily life of the patient [4][5]. IMU systems are modular and can be placed anywhere on the body, which gives the physician flexibility to monitor any point of the body. Additionally, they can be used to measure the range of motion of the spine [5][34][71]. This flexibility is unique to IMU sensor systems. The main drawback is their high cost compared to Kinect or smartphone apps. In this analysis, they are nevertheless considered the most suitable devices for monitoring small changes in postural tilt throughout rehabilitation therapy.
While dorsaVi ViMove is user-friendly and medically certified [79][80], it is not suitable for full-spine tracking, since it is only valid for the lumbar region (T12-L5) and is generally limited to two IMU sensor modules [80][81][82]. In contrast, Movella

DOT and Noraxon myoMOTION are considered more suitable choices, as their customizability allows for full spinal measurements of high accuracy [61][73][74]. Noraxon myoMOTION is already medically certified [74] and has pre-developed protocols, facilitating implementation [73][74]. Although the Movella DOT system lacks clinical certification [95], it offers excellent accuracy at 0.5° for static and 1.0° for dynamic performances [70], and additionally has excellent validity for studying ROM, with a MAE of 0.74° [71]. Furthermore, the Movella DOT system has been more extensively validated for sagittal spinal posture than Noraxon myoMOTION. However, it should be noted that Movella DOT requires the development of new software to enable integration into clinical practices [69][71][70].
To conclude, while Noraxon myoMOTION is medically graded and has a straightforward path for clinical implementation, it lacks the flexibility and validated precision of the Movella DOT system. During communication with Movella, the company also expressed interest in developing medically graded solutions. Consequently, moving forward with a trial posture assessment experiment, the Movella DOT sensor system will be implemented.

6
Theory - Sensor Experiment

This chapter details the theory behind the experimental part of the thesis.

6.1 Movella DOT

Movella DOT is a wearable IMU-based sensor system developed by Movella/Xsens Inc. for tracking human body motions. The sensor modules are 9-axial and consist of a three-axis accelerometer, a three-axis gyroscope, and a three-axis magnetometer, with an already embedded processor [70] using state-of-the-art signal processing [96]. They are described as durable, lightweight, and IP68 water-proof, making them applicable in many contexts and activities. Previously, they have been implemented in health and rehabilitation, sports and exercise science, and ergonomics. The Movella DOT system utilizes the data from its individual sensor components, including linear acceleration, angular velocity, and magnetic field data, to compute three-dimensional orientation and free acceleration through sensor fusion algorithms. Data can be streamed and recorded in real time by connecting the sensors with Bluetooth 5.0 to the Movella DOT smartphone application, which is available for both Android and iOS. Movella also offer the possibility to build custom apps using their Software-Development-Kit (SDK) [70].
The Movella DOT v2 kit includes 5 sensor modules which may be combined in any configuration. The maximum number of sensor modules that can be connected simultaneously is dependent on the hardware and OS used. Android, MacOS and Windows have a ceiling of 7 sensors, while iOS, Linux PC and Raspberry Pi have a ceiling of 11 sensors. In addition to the sensors, the kit also includes a charging station with a power cable; see Figure 6.1a. The sensor modules have a power button on the sensor face, an LED light at the top of the sensor, and a micro-USB charging port at the bottom of the sensor, illustrated in Figure 6.1b. They measure 36.30 x 30.35 x 10.80 mm and weigh 11.2 g, making them small and lightweight. The battery life of a sensor is up to 8 hours and it has a full recharging time of about 1 hour [97].
Movella DOT uses strap-down integration (SDI) and sensor fusion algorithms (XKFCore) in the signal processing architecture. The **SDI algorithm** is used to obtain the orientation and velocity increments. It integrates the angular velocity measured by the gyroscope and the acceleration measured by the accelerometer, sampled at 800 Hz, which is generally suitable for recording dynamic human motions. To convert the data to a lower frequency, which will reduce the transmission load put on the receiving device and make Bluetooth transmission possible, the SDI processes

(a) Movella DOT sensor kit with included charger docking station and cover.

(b) Parts of the Movella DOT sensor.

Figure 6.1: Movella DOT sensor kit and individual sensor.

the data into a 60 Hz signal, while keeping the accuracy of the data intact. To estimate the free acceleration and orientation of the sensors in three-dimensional space, sensor fusion is performed by the **Kalman filter core algorithm (XKFCore)** developed by Movella/Xsens Inc. The output from the SDI process is fed into the XKFCore which computes the statistically optimal 3D orientation. Errors in this computation are compensated for through measurements of gravitational acceleration and the Earth magnetic north. There are two different filter profiles for the XKFCore, the *general*, suited for moderate dynamics, and the *dynamic*, suited for rapid and fast motions [70].
Data can be collected through two modes in the Movella DOT app: Real-time streaming, or Recording. During **Real-Time streaming**, data are transmitted to a central device via Bluetooth connection. Data can be stored in a log file on the device either as *Euler angles* or *Quaternions* (see Chapters 6.1.3 and 6.1.4). In **Recording** mode, data are stored within the internal storage of each sensor, which has a total storage capacity of 64MB (v2). The data can then be exported from the sensor via USB or Bluetooth [70].

6.1.1 Coordinate Systems

Two coordinate systems are used in this thesis. The *local Earth coordinate system*, or **L**, is denoted by uppercase letters X, Y, Z, and remains fixed in space, allowing it to be used as a reference frame for other measurements. It uses an East-North-Up (ENU) coordinate system, where

- the X-axis is positive toward the east,
- the Y-axis is positive toward the north,
- the Z-axis is positive upward.

Meanwhile, the *sensor coordinate system*, or **S**, is denoted by lowercase letters x, y, z, and represents the coordinate system that moves with each sensor. The Movella DOT sensors use a right-handed Cartesian coordinate system, with axes oriented as presented in Figure 6.2, where

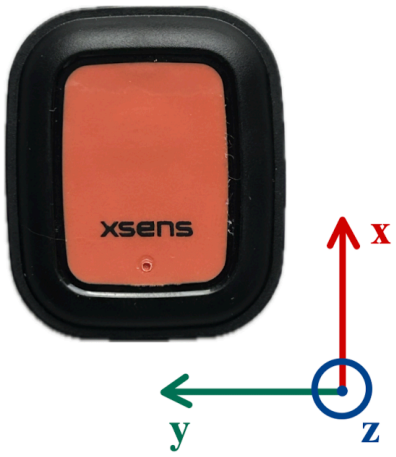

Figure 6.2: Coordinate system of Movella DOT sensor.

- the x-axis points along the long side of the sensor,
- the y-axis points along the short side of the sensor,
- the z-axis points outward from the sensor face.

The relationship between these two coordinate systems can be used to determine the orientation of the sensors in space. It is commonly described using three rotation angles: *yaw, pitch,* and *roll*. The **yaw** output represents the angle between the X-axis (east) and the x-axis of the sensor, positive about the Z-axis, and is defined within [-180°, 180°] [70]. Similarly, **pitch** (tilt) corresponds to the rotation about the Y-axis (defined within [-90°, 90°]), and **roll** the rotation about the X-axis (defined within [-180°, 180°]) [98][99].

6.1.2 Using the Movella DOT Sensors

Sensor synchronization operates by assigning one of the sensors as root node and the others as scanners, which adjust their timestamps according to the root. The start of measurement may have a different delay for the sensors; however, any excess data points can be removed during post-processing. During synchronization, the phone and sensors should not be kept further than 50 cm apart to ensure a successful connection, and synchronization should ideally be performed before the sensors are placed on the body [100].

The main source of error for Movella DOT sensors is the magnetometer, which is used as a compass to decide the direction of the Earth true north. It should be noted that the local magnetic field may be distorted by ferromagnetic materials, magnets, or strong electrical currents in the close vicinity of the sensors and are thus advised to be avoided. The magnitude of the magnetic distortion can be examined with the *Magnetic Norm* feature in the Movella DOT app, which computes the norm of all three magnetic axis vectors. An area is deemed magnetically homogeneous when the norm equals 1 and the maximum variation is ± 0.2; under these conditions, measurements are optimal. Performing measurements remains acceptable even if the initial norm is 2 or 3. However, large fluctuations in the magnetic norm are seen as

unideal. In addition, the sensors have a built-in XKFCore algorithm to compensate for any magnetic disturbances [70].
It is important to place the sensors carefully, in order to avoid distortions caused by soft tissue artifacts or other unwanted movements. Thus, it is recommended to place the sensors where they are less likely to wiggle or move. Ideally, the sensors should be placed on flat surfaces and not on top of muscle or soft tissue. Movella recommends two methods for attaching the sensors to the body. The first method is to use adjustable body straps, such as those offered by Movella, which are made of Fabrifoam® X-treme™, allowing the sensors to be snapped in place in a pocket or holder. The second method is to attach the sensor directly to the skin using kinesiotape [101].

6.1.3 Euler Angles

Euler angles are expressed in degrees and constitute one of the two orientation formats available for Movella DOT data. They describe any rotation through a series of three angles along three axes, often in the form (X, Y, Z) [99].
The notation that will be used in this thesis is:

$$\mathbf{u} = (X, Y, Z) \tag{6.1}$$

where

- X represents
- ch**pit**
- **ch, rotation about the global X-axis,**
- Y **represents roll, rotation about the global Y-axis,**
- Z **represents yaw, rotation about the global Z-axis.**

Figure 6.3 gives a visualization of Euler angles, where a fixed coordinate system, x, y, z, is shown in relation to a rotated coordinate system, X, Y, Z. Here, the γ-angle corresponds to yaw, the β-angle corresponds to pitch, and the α-angle corresponds to roll.

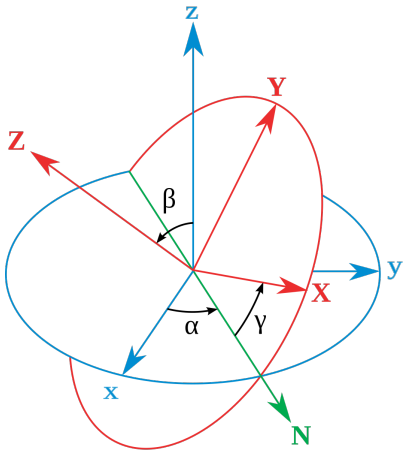

Figure 6.3: Visualization of Euler angles showing three sequential rotations: yaw (γ), pitch (β), and roll (α). *Note.* Image adapted from *Eulerangles* by David W., Wikimedia Commons (`https://commons.wikimedia.org/wiki/File:Eulerangles.svg`). Licensed under CC BY-SA 3.0.

The main downside of Euler angles is that they suffer from singularities, or a loss of degree of freedom, whenever two axes are in parallel. This is known as *gimbal lock* [61].

6.1.4 Quaternions

An efficient way to represent 3D orientation is through quaternions [99]. They are used to increase accuracy and avoid issues with gimbal lock associated with Euler angles as they lack singularities [102]. A quaternion, q, can be represented as a vector $\mathbf{q}$,

$$\mathbf{q} = [q_0, q_1, q_2, q_3]^T, \tag{6.2}$$

or alternatively as the sum of a scalar part, q_0, and a vector part, $\mathbf{q}$,

$$q = q_0 + \mathbf{i}q_1 + \mathbf{j}q_2 + \mathbf{k}q_3. \tag{6.3}$$

The unit quaternion $\boldsymbol{q}_{\mathrm{LS}}$ obtained from the Movella DOT system rotates a vector in the reference coordinate system L to the sensor coordinate system S. The quaternion data is reported in the format (W, X, Y, Z), where W represents the scalar part and X, Y, and Z constitute the vector component of the quaternion [99]. However, in this thesis, quaternions will be expressed in lowercase letters (w, x, y, z) to remain consistent with mathematical conventions:

$$\mathbf{q} = (w, x, y, z). \tag{6.4}$$

6.1.5 Rotation Matrix

A quaternion can be converted into a rotation matrix to give a representation of its direction. The purpose of a rotation matrix is to rotate a vector, either as a frame or a point. It is defined as:

$$R = [\mathbf{r}_1, \mathbf{r}_2, \mathbf{r}_3] = \begin{bmatrix} r_{11} & r_{12} & r_{13} \\ r_{21} & r_{22} & r_{23} \\ r_{31} & r_{32} & r_{33} \end{bmatrix}. \tag{6.5}$$

For instance, if a vector $\mathbf{z} \in \mathbb{R}^3$ exists in the fixed global coordinate system, it can be multiplied by the rotation matrix to yield the same vector expressed in the sensor coordinate system, $\mathbf{z}' \in \mathbb{R}^3$:

$$\mathbf{z}' = R\mathbf{z}. \tag{6.6}$$

Conversely, the original vector can be retrieved by:

$$\mathbf{z} = R^{\mathsf{T}}\mathbf{z}'. \tag{6.7}$$

7

Methods - Sensor Experiment

The Movella DOT sensors were selected to be evaluated as a potential clinical postural assessment device. An experiment was carried out with measurements from the sensors compared to the Qualisys MoCap system as ground truth. The methodology of the experiments will be described below.

7.1 Setup of Movella DOT System

A standard kit containing five Movella DOT IMU sensors was used. To collect data from the sensors, the **Movella DOT app** was used on a smartphone (iPhone 14, iOS 18.4.1); see Figure 7.1a for an example of the app interface. Prior to measurement, a **Magnetic Field Mapping (MFM)** was performed by slowly rotating the sensors in the space where measurements were to be made. During **synchronization**, the sensors were kept within approximately 10 cm of the smartphone. The general filter profile in 60 Hz was used, giving an interval time between samples of 16667 μs. After these steps, the sensors were ready to be attached to surfaces and data could be logged.

For ease of interpretation, the vertical axis was defined as the 0° line, with backward tilts represented by negative angles and forward tilts by positive angles (see Figure 7.2 for a schematic drawing). The *pitch angle* is what defines the sagittal backward or forward tilt.

When **Real-time Streaming** is active in the app, plots showing the Euler (X, Y, Z) angles are displayed (see Figure 7.1b). Using this feature, it was observed that when the sensor was facing down, the Y-angle was 0°, when upright $-90°$, and lying backward 0°. Within this range, the Y-angle remained negative. To determine whether the tilt leaned forward or backward, the Z-angle component was utilized, as it showed negative values when tilting backward and positive values when tilting forward. However, the direction of positive versus negative values changed depending on the orientation of the sensor.

Two approaches were implemented to obtain spinal tilt: (1) an Euler angle-based approach and (2) a quaternion-based approach. The codes for these methods were created in MATLAB. Static and dynamic tilt measurements were made by attaching sensors to various surfaces to estimate the accuracy of the codes.

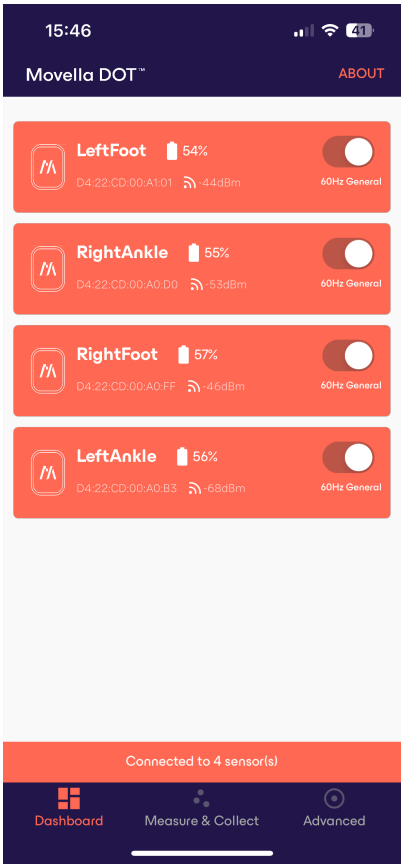

(a) Movella DOT app interface: sensor connection.

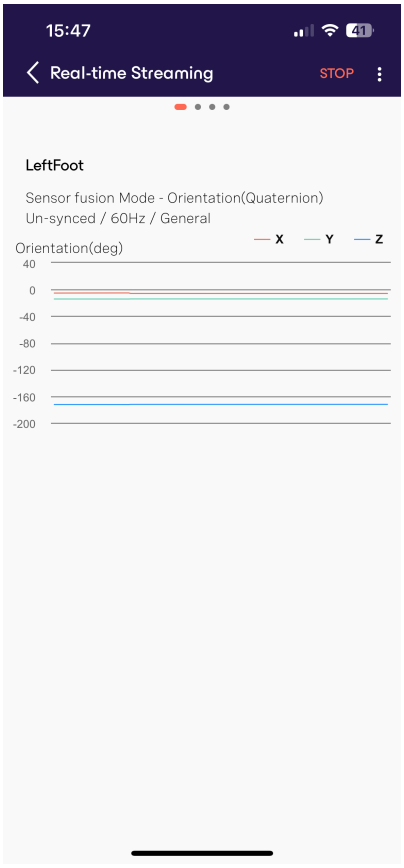

(b) Movella DOT app: Real-time Streaming-mode.

Figure 7.1: Movella DOT app interface.

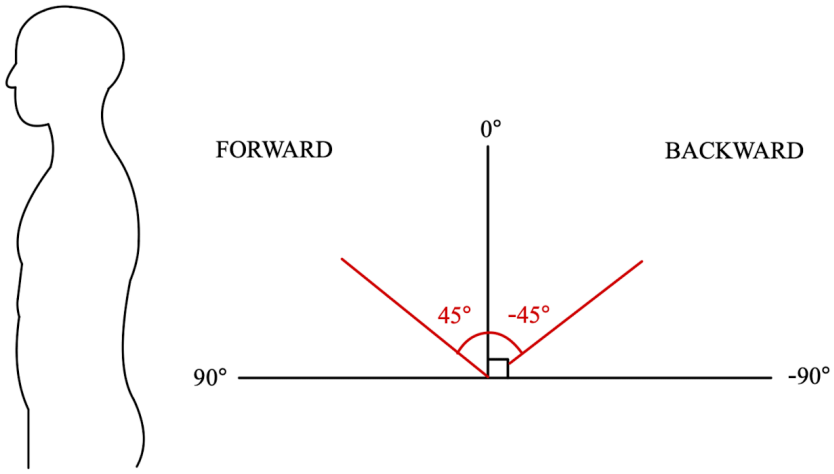

Figure 7.2: Schematic diagram of angle definitions in spinal tilt system.

7.1.1 Approach I: Euler-Based Computation

In the first approach, sagittal tilt was estimated using the Euler angles provided directly by the Movella DOT app. The Euler angles, in an (X, Y, Z) format, were logged as a `.csv` file and imported into MATLAB. The Y- and Z-components (pitch and yaw, respectively) were extracted and the desired angle, θ_{Euler}, was obtained by multiplying the absolute value of the Y-component with the sign of the Z-value and subtracting it from 90° to conform to the tilt definition (see Figure 7.2). Thus,

$$\theta_{Euler} = 90° - |Y| \cdot \text{sign}(Z). \tag{7.1}$$

The resulting angles, θ_{Euler}, were then plotted against time in MATLAB. See Appendix A for the associated MATLAB code.

7.1.2 Approach II: Quaternion-Based Computation

In the second approach, quaternion data were logged in the Movella DOT application, giving the quaternion coordinates in a (w, x, y, z) format. The analysis was performed in MATLAB using the *Sensor Fusion and Tracking Toolbox*. The `quaternion` MATLAB function was used to transform the `.csv` data into a quaternion array for each sensor, and the `normalize` function was applied to produce unit quaternions.
Then, the `rotmat` MATLAB function was used to convert the quaternions into 3x3 rotation matrix representations, denoted $\mathbf{R}$, using the standard textbook-defined algorithm, as shown in Equation 7.2 [103]:

$$\mathbf{R} = \begin{bmatrix} 1 - 2(y^2 + z^2) & 2(xy - wz) & 2(xz + wy) \\ 2(xy + wz) & 1 - 2(x^2 + z^2) & 2(yz - wx) \\ 2(xz - wy) & 2(yz + wx) & 1 - 2(x^2 + y^2) \end{bmatrix}. \tag{7.2}$$

The resulting rotation matrix represents the orientation of the sensor in the global coordinate system, expressed by the sensor axes $\mathbf{X}_{\text{sensor}}$, $\mathbf{Y}_{\text{sensor}}$, and $\mathbf{Z}_{\text{sensor}}$:

$$\mathbf{R} = (\mathbf{X}_{\text{sensor}}, \mathbf{Y}_{\text{sensor}}, \mathbf{Z}_{\text{sensor}}). \tag{7.3}$$

To represent the orientation of the sensor frame relative to the fixed global frame and to calculate the pitch angle, the $\mathbf{Z}_{\text{sensor}}$-column of the rotation matrix $\mathbf{R}$ was extracted and compared with the fixed global vertical axis:

$$\boldsymbol{Z}_{\text{global}} = [0, 0, 1]^T, \tag{7.4}$$

as illustrated in Figure 7.3. The angle ϕ between the sensor's z-axis, $\mathbf{Z}_{\text{sensor}}$, and the global vertical, $\mathbf{Z}_{\text{global}}$, is given by their dot product:

$$\cos(\phi) = \mathbf{Z}_{sensor} \cdot \mathbf{Z}_{global}. \tag{7.5}$$

Figure 7.3: Illustration of quaternion based tilt, $\phi_{quaternion}$, defined as the angle between the sensor Z-axis and the global Z-axis.

For reference, the sensor z-axis points out of the sensor (see Figure 6.2), while the global Z-axis points upwards (see Figure 7.3). To align with the tilt definition in Figure 7.2, the calculated cosine angle was adjusted by subtracting it from 90°

$$\phi_{quaternion} = 90° - \phi. \tag{7.6}$$

The resulting angles, $\phi_{quaternion}$, were plotted against time in MATLAB. See Appendix B for the associated MATLAB code.

7.2 Experimental Setup

The experiments were conducted at the Physiology and Sports Lab at the FUSE department of Chalmers University of Technology. Body movements were tracked using the **Qualisys MoCap system**, consisting of 14 cameras placed around the room (see Figure 7.4). The tracking with the MoCap system was performed simultaneously as data collection from the sensors.
The placement of the sensors was chosen as four segments:

- Neck (N)
- Upper back (U)
- Lower back (L)
- Pelvis (P)

As no medical personnel was present, the location of the vertebrae could not be determined exactly, and the sensors were placed roughly in the areas of interest; *cervical lordosis* (N), *thoracic kyphosis* (U), *lumbar lordosis* (L), and *sacrum* (P).
The pelvic and lower back sensors were attached using adjustable straps, while the neck and upper back sensors were attached using a piece of double-sided tape applied to the back of the sensor. The strap used for the pelvic sensor was the 5.08 x 128 cm strap from Movella Xsens. As the Xsens strap kit only included one strap long enough to stretch around the torso, a second one was created by connecting two 5.08 x 55 cm straps to each other to wrap around the lower back.
To enable tracking with the Qualisys MoCap system, markers had to be placed on the body. Each sensor was assigned two pairs of markers, with one pair vertically

a) FUSE motion lab

b) Qualisys motion capture camera

Figure 7.4: Motion capture setup: a) lab environment; b) Qualisys motion capture camera.

attached on top of the sensor and another pair positioned directly above and below the sensor. The marker pairs formed two diagonals per sensor, **D1** between the markers adjacent to the sensor, and **D2** between the markers on top of the sensor, as seen in Figure 7.5b.

In total, sixteen markers were placed along the spine. Figures 7.5a and 7.6 illustrate how the sensors and markers were arranged on the back. Measurements were made while standing, sitting and walking straight back and forth in the motion laboratory, taking approximately 6 steps in each direction. Each measurement was repeated three times for both angle formats, since the Euler angles and quaternion measurements could not be carried out simultaneously in the Movella DOT app. The static postures (standing and sitting) were measured for 20 seconds and the dynamic movement (walking) was measured for 40 seconds.

The Qualisys data were exported as a `.mat` file and unpacked in MATLAB. The positions of the 16 markers in the global coordinate system over time were stored as 3D position vectors for each marker i at time frame t:

$$\mathbf{p}_i(t) = \begin{bmatrix} x_i(t) \\ y_i(t) \\ z_i(t) \end{bmatrix}. \tag{7.7}$$

For each experiment, the direction vectors between the marker pairs, eight in total, were calculated by subtracting the bottom marker position, $\mathbf{p}_b(t)$, from the top marker position, $\mathbf{p}_t(t)$:

$$\mathbf{v}(t) = \mathbf{p}_t(t) - \mathbf{p}_b(t).$$

By discarding the y-component, $v_y(t)$, which corresponds to lateral movement, the

direction vector was projected onto the sagittal xz-plane as

$$\mathbf{v}_{xz}(t) = \begin{bmatrix} v_x(t) \\ v_z(t) \end{bmatrix}, \tag{7.8}$$

which was subsequently normalized to

$$\hat{\mathbf{v}}_{xz}(t) = \frac{\mathbf{v}_{xz}(t)}{\|\mathbf{v}_{xz}(t)\|}. \tag{7.9}$$

The sagittal tilt in degrees, denoted $\alpha_{MoCap}(t)$, was defined as the angle of the projected segment vectors $\hat{\mathbf{v}}_{xz}(t)$, measured from the positive z-axis toward the x-axis (see Equation 7.10). The two-argument arctangent, atan2(y, x), was used to ensure that forward tilts corresponded to positive angles:

$$\alpha_{MoCap}(t) = \text{atan2}\Big((\hat{\mathbf{v}}_{xz}(t))_x,\, (\hat{\mathbf{v}}_{xz}(t))_z\Big) \tag{7.10}$$

Since the MoCap data were sampled at 300 Hz and the sensor data at 60 Hz, the MoCap data was also downsampled to align with the sensor data sampling rate.
The tilt angles obtained from the four sensors were then plotted in MATLAB together with the MoCap data for the diagonals D1 and D2 corresponding to each sensor. The final MATLAB code for the Euler-angle calculations is provided in Appendix A, and the code for the quaternion-based calculations is included in Appendix B.
To evaluate the accuracy and agreement between the sensor and MoCap data, the two parameters **root-mean-square deviation (RMSD)** and **bias** were computed for each experiment, as defined in Equations 7.11 and 7.12. The overall mean angle was also calculated.

$$RMSD = \sqrt{\frac{\sum(\theta_{sensor} - \theta_{MoCap})^2}{N}} \tag{7.11}$$

$$Bias = \frac{1}{N}\sum(\theta_{sensor} - \theta_{MoCap}) \tag{7.12}$$

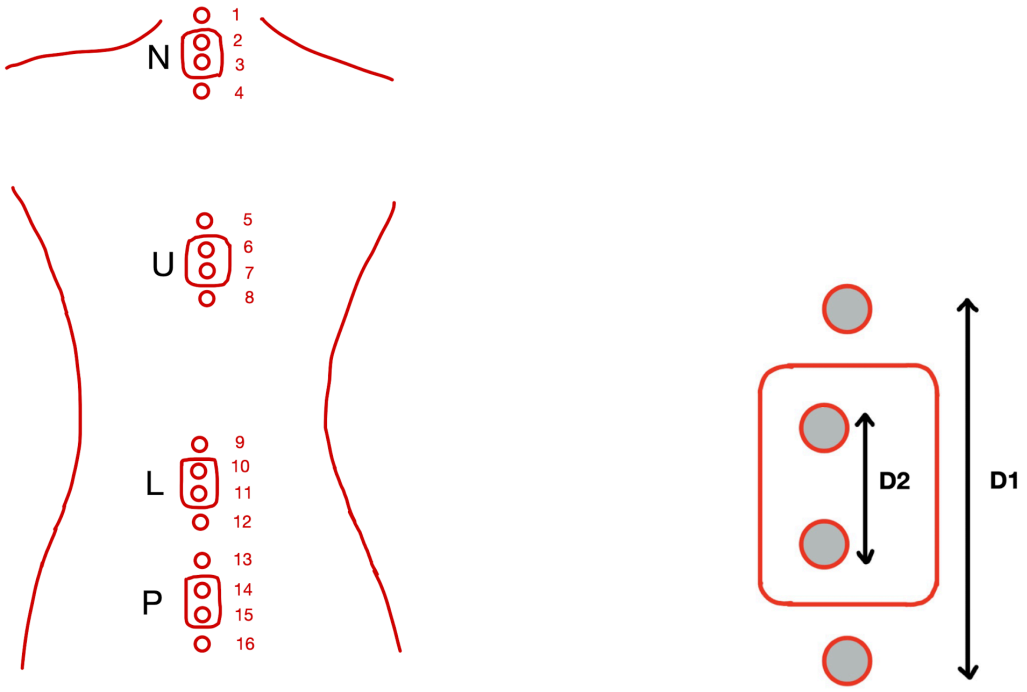

(a) Schematic illustration of arrangement of sensors and markers on back.

(b) Definition of D1 and D2.

Figure 7.5: Schematics of experimental marker and sensor placements: a) arrangement on back; b) definition of D1 and D2 diagonals between markers.

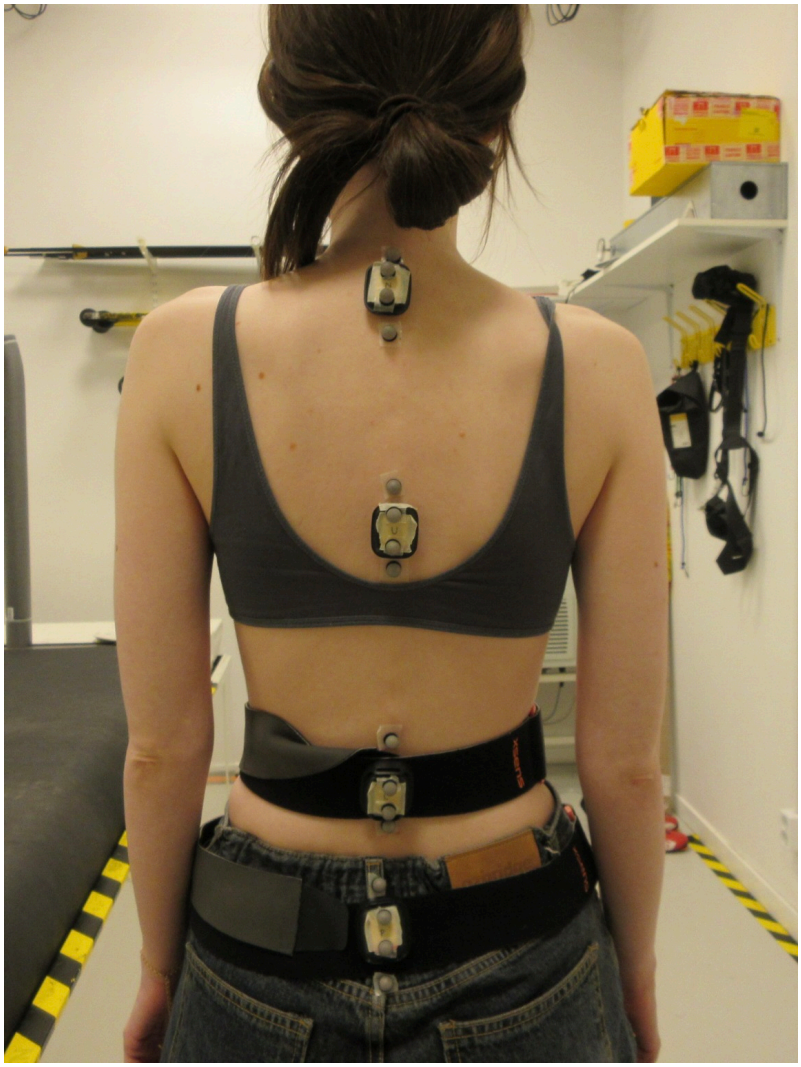

Figure 7.6: Sensor and marker arrangement on back.

8

Results - Sensor Experiment

This chapter presents the results of the sensor experiment. The collected data are displayed in graphs showing the sensor measurements alongside the D1 and D2 data for each segment. Additionally, comparisons were made between the RMSD and bias values. The remaining graphs not included in this chapter are provided in Appendix C, along with the tables of mean angles, RMSD, and bias values.

8.1 Comparison Between Body Segments

Visual inspection of the plots indicates that the neck and pelvis data exhibited more stable trends, while the upper back and lower back measurements were comparatively noisier. Figure 8.1 illustrates two example results from the quaternion and Euler based sitting experiments (Q1 and E1). This observation is supported by the higher average RMSD values of the lower back and pelvis, as presented in Table 8.1. Among all body segments, the neck showed the lowest RMSD and bias values, followed by the upper back, lower back, and pelvis. The neck sensor consistently demonstrated the best agreement with the D1 and D2 marker data in all plots, which agrees with the calculated average bias of 1.60° and the average RMSD of 2.88°, the lowest of all segments. Compared to D1, the neck sensor data showed an average deviation of the overall mean angle of 2.00°, a mean bias of 1.98° and mean RMSD of 3.43°. When compared to D2, deviations were slightly smaller, with a mean deviation of 1.26°, mean bias of 1.22° and mean RMSD° of 2.34°.
Among the average absolute mean RMSD and bias values, the pelvic data showed the lowest fit to the MoCap data in all experiments except the standing quaternion experiments, where the lower back exhibited the lowest fit. The neck sensor yielded the best fit to MoCap data in all experiments except the walking quaternion and sitting Euler experiments, where the upper back provided the best fit. In general, the lower back and pelvis were found to have a lower fit, while the neck and upper back had a higher fit.
Furthermore, a breathing pattern can be observed in both the sensor and D2 data across all standing and sitting lower back tilt plots.

8.2 Comparison Between Marker Pairs

The bias and RMSD values were consistently higher for the D1 data, that is, the diagonal between the markers above and below the sensor, than for the data for D2, the diagonal between the markers on top of the sensor. This was observed across

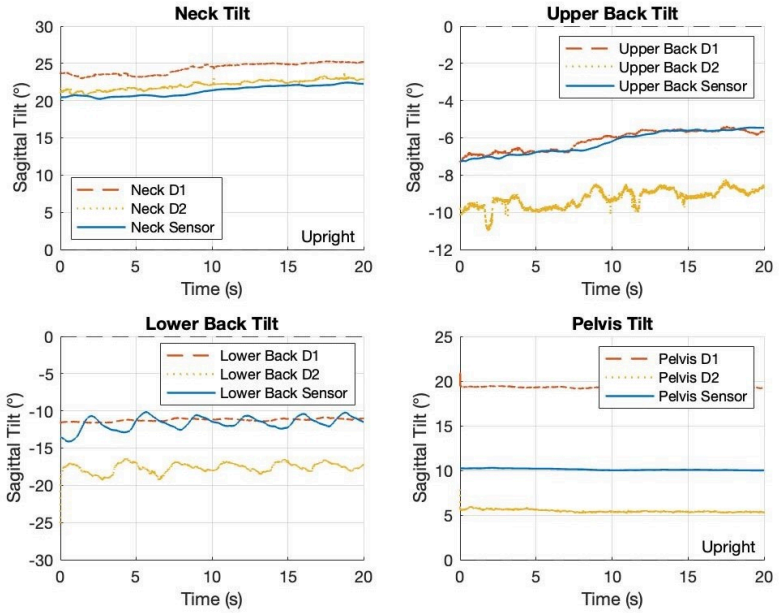

(a) Quaternion based tilt, sitting experiment one (Q1).

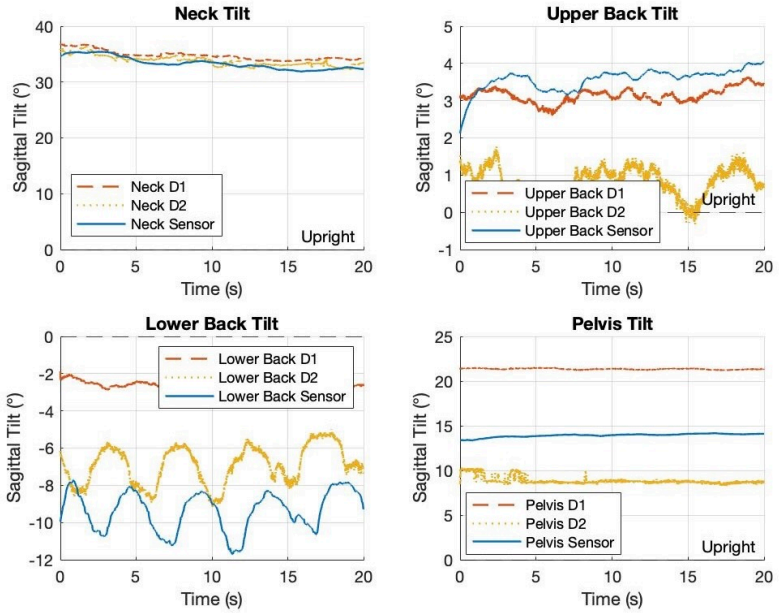

(b) Euler based tilt, sitting experiment one (E1).

Figure 8.1: Sensor and marker (D1 and D2) tilt plots for quaternion and Euler based data, sitting.

Table 8.1: Average absolute bias and RMSD values for the sensor segments.

Condition	Segment	Mean Absolute Bias [°]	Mean RMSD [°]
With walking	Neck (N)	1,6004	2,8843
	Upper Back (U)	2,6740	3,1506
	Lower Back (L)	4,1512	4,6870
	Pelvis (P)	5,8951	6,4644
Without walking	Neck (N)	1,3572	1,4854
	Upper Back (U)	2,5498	2,6684
	Lower Back (L)	3,8611	4,1622
	Pelvis (P)	5,5290	5,5440

all postures, sitting, standing, and walking. See Table 8.2 for the mean bias and RMSD values for D1 and D2 across all experiments.
D2 had both a 1.27° lower average bias (1.11° lower without walking) and a 1.28° lower average RMSD (1.02° without walking) compared to D1. No clear trends in terms of overestimation or underestimation were found. However, for the pelvic tilt, the general trend was that D1 overestimates the angle, while D2 underestimates the angle.

Table 8.2: Mean absolute bias and RMSD for D1 and D2, with and without walking.

Condition	Marker Pair	Mean Absolute Bias [°]	Mean RMSD [°]
With walking	D1	4,2146	4,9372
	D2	2,9457	3,6560
Without walking	D1	3,8817	3,9758
	D2	2,7669	2,9542

Data for D1 and D2 data compared to the neck sensor, the segment with the best fit to the marker data, is provided in Table 8.3.

Table 8.3: Mean absolute bias and RMSD for neck D1 and D2, with and without walking.

Condition	Marker Pair	Mean Absolute Bias [°]	Mean RMSD [°]
With walking	D1 (neck)	1,9800	3,4251
	D2 (neck)	1,2207	2,3434
Without walking	D1 (neck)	2,3000	2,3302
	D2 (neck)	0,4145	0,6406

8.3 Comparison Between Postures

While sitting and standing, the sensor and MoCap data showed smoother and more stable trends, attributed to the positions being stationary. On the contrary, the walking data had more rapid variations in tilt angles both for the sensor and MoCap data, reflecting the dynamic nature of the movements.
Furthermore, the average RMSD and bias were generally similar in value for sitting and standing, while the RMSD values for walking experiments were higher than the bias values, indicating higher noise. Figures 8.2 and 8.3 show representative plots from the first standing and walking experiments for both Euler- and quaternion-based angles. Notice that the walking experiments contain data cut-offs. In the standing and sitting experiments, there is no missing data.
To give a fair comparison, the signs of the sensor and marker data were adjusted, as they often did not match. Consequently, the sign does not necessarily indicate a forward or backward lean in these plots. In the walking plots, the magnitude of the Euler angles had to be used. Thus, the angles appear similar to the quaternions in the plots, but they do not have any valid indication of backward or forward tilt as the quaternions do. The sign of the Euler Z-value can flip unexpectedly depending on the rotation of the body. Therefore, it is especially unreliable when walking, as the sign will switch when changing direction of walking (see Figure 8.4). For the case of quaternions, they consistently, over all plots, showed the correct signage of the tilts. Figure 8.5 shows the plots for the sensor data from the first sitting experiment, where the neck Euler angle has the opposite sign to tilt based on quaternions.

8.4 Euler Angles Compared to Quaternions

In Table 8.4, the RMSD and bias values averaged over all Euler angle-based and quaternion-based experiments are presented. The quaternion-based data yielded lower values in all cases.

Table 8.4: Average RMSD and bias for Euler and quaternion data.

Condition	**Format**	**Bias** [°]	**RMSD** [°]
With walking	Euler	3,6848	4,5285
	Quaternion	3,4756	4,0647
Without walking	Euler	3,4182	3,5877
	Quaternion	3,2988	3,3423
Without walking (D2 only)	Euler	2,9784	3,2209
	Quaternion	2,5553	2,6875

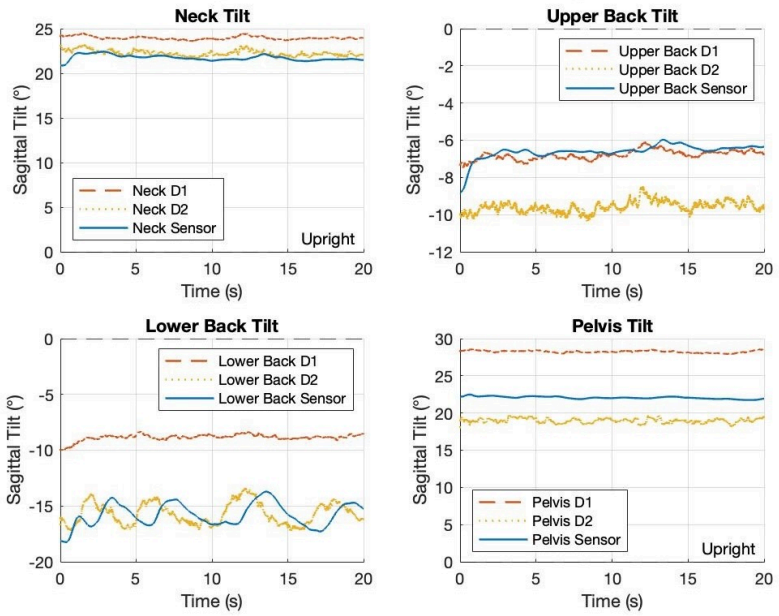

(a) Plots for quaternion based standing data (Q1).

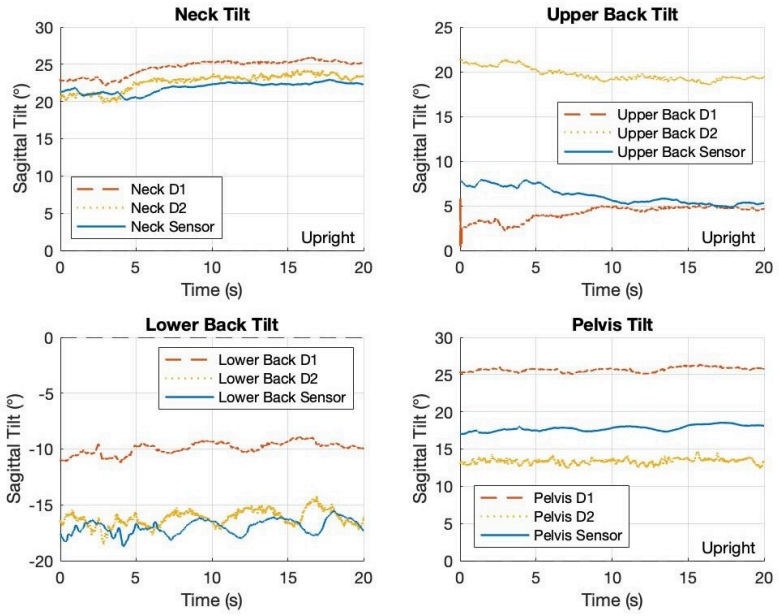

(b) Plots for Euler based standing data (E1).

Figure 8.2: Example plots for standing data.

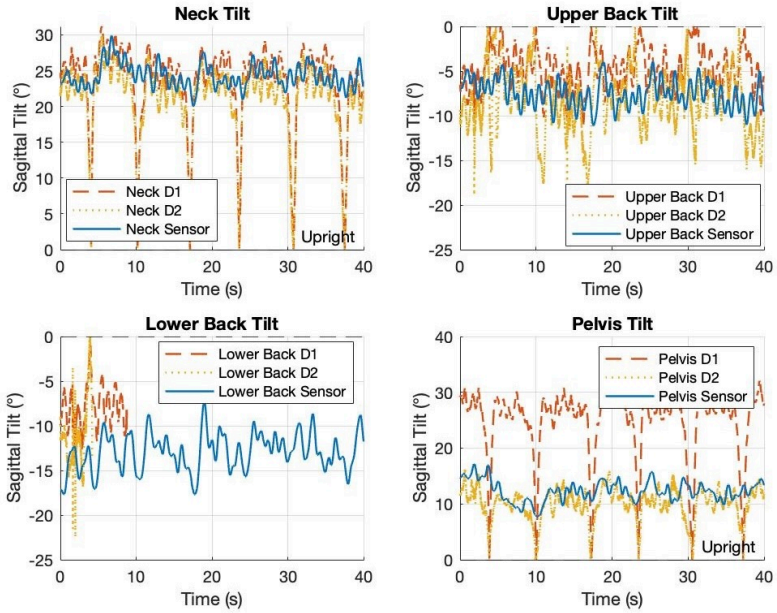

(a) Plots for quaternion based walking data (Q1).

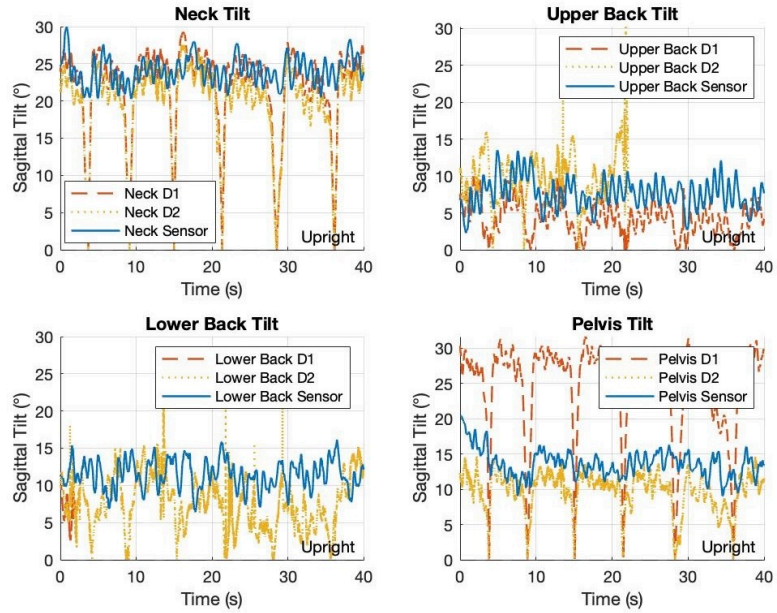

(b) Plots for Euler based walking data (E1).

Figure 8.3: Example plots for walking data.

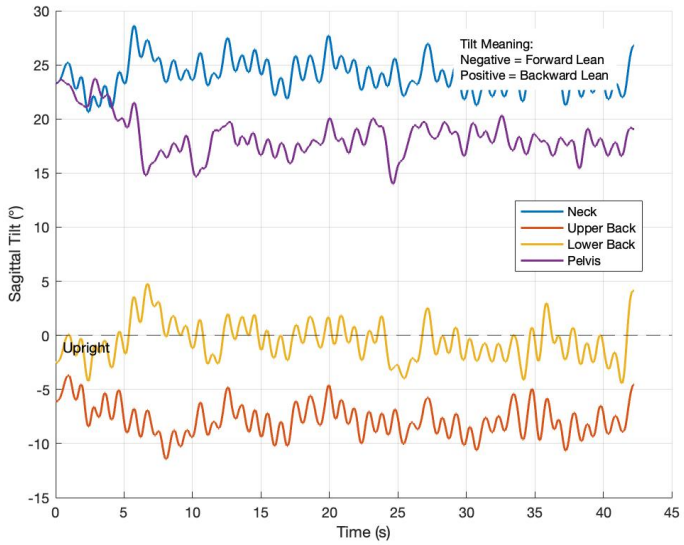

(a) Quaternion based tilt, walking experiment three (Q3).

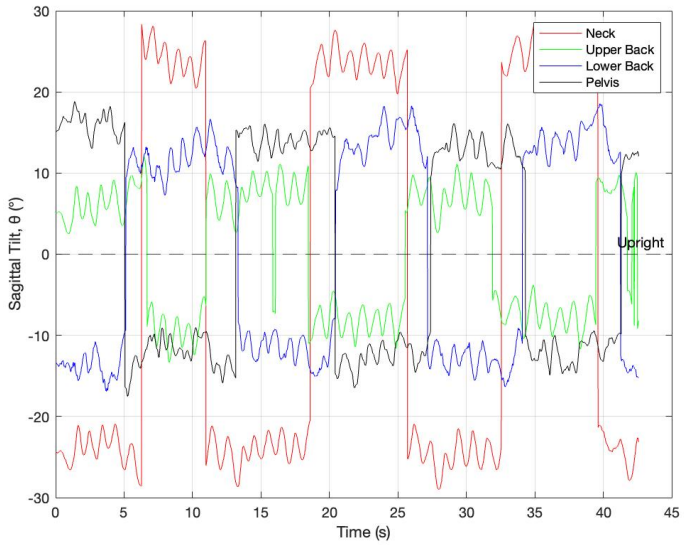

(b) Euler based tilt, walking experiment three (E3).

Figure 8.4: Comparison of direction of tilt between quaternion and Euler based data, walking.

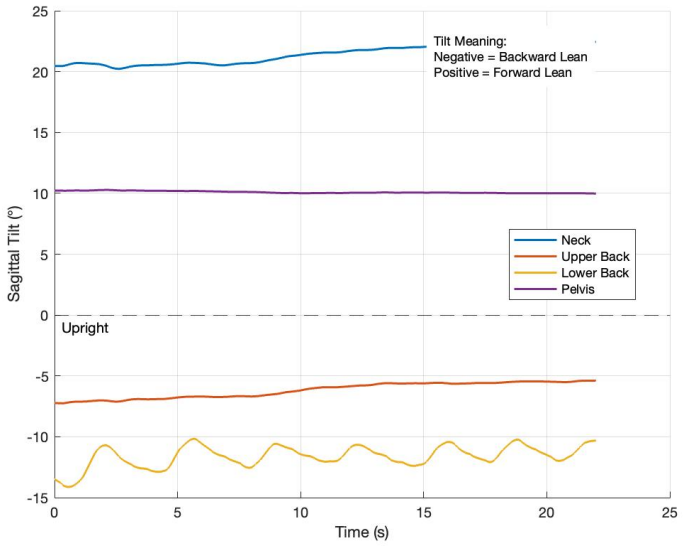

(a) Quaternion based tilt, sitting experiment one (Q1).

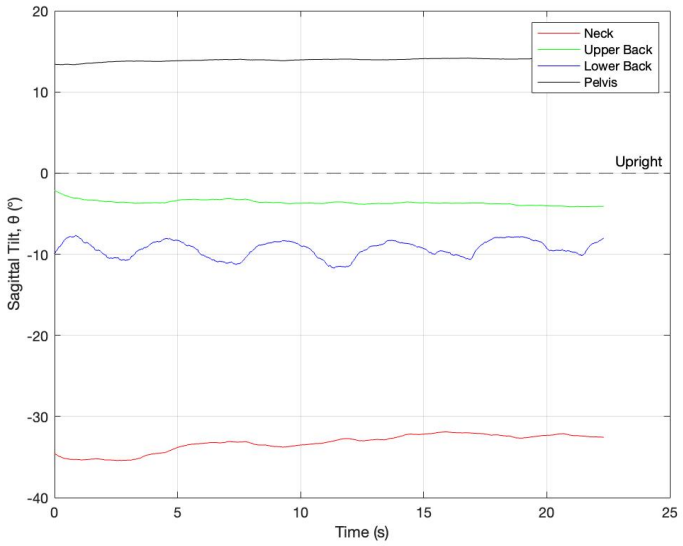

(b) Euler based tilt, sitting experiment one (E1).

Figure 8.5: Comparison of direction of tilt between quaternion and Euler based data.

9

Discussion - Sensor Experiment

9.1 Overview of Main Findings

It was observed that, across all plots, the neck sensor estimated angles similar to both the neck D1 and neck D2 data, suggesting that any major discrepancy between the sensor and MoCap data may be due to poor positioning of markers rather than sensor inaccuracy. However, it could also be the case that the neck is a particularly easy segment to measure, due to minimal movement of skin and lack of soft tissue. The close fit of the neck sensor data with the MoCap data indicates that Movella DOT sensors possess the capability to accurately estimate spinal tilt angles. Overall, the neck sensor demonstrated a mean bias of only 1.60° and an RMSD of 2.88° (see Table 8.1). Table 8.1 shows a consistent trend of the neck sensor exhibiting the best fit, followed by the upper back, lower back, and lastly the pelvis. The difference between these segments was roughly 1°. The pelvis had the worst fit with a bias of approximately 6° and an RMSD of 6.5°. This is thought to be mainly attributed to poor attachment of the sensor and markers to the body.
However, it has also been identified in the literature that there is some extra difficulty in measuring pelvic tilt with IMU sensors. Whether there is a difference in how well different parts of the spine can be represented by the angles provided by the sensors is hard to interpret, since it could depend on soft tissue artifacts, stretching of skin, or perhaps movement of adjacent limbs. Assessing the sensors on different bodies, with different dispositions of body fat, would be essential to establish if the sensors produce reliable results between different people and body parts.

9.2 Sources of Measurement Error and Influencing Factors

Several factors had an influence on the quality of the measurements obtained in this study. In the plots of lower back tilt, where a breathing pattern is visible, a delay can be observed in the sensor data compared to the MoCap data. This likely occurred because the measurements were initialized in the MoCap system, after which streaming in the Movella DOT app was started as quickly as possible. Consequently, all experiments contained an unavoidable temporal offset, which may have influenced the comparison between MoCap and sensor data. In future experiments, this issue could be mitigated by having two operators initializing the MoCap and sensor streaming simultaneously.

Interestingly, the sensitivity of the sensors was high enough to capture breathing patterns in the lower back data. This indicates that they could be suitable for detecting irregular breathing, which can be associated with pain and is of interest in rehabilitation therapy. The prospect of using the same device for multiple types of clinical measurements is appealing, as it could reduce the cost and effort involved in finding additional measurement tools.

The arrangement of sensors and markers was not considered ideal in the experiment. In particular, while walking, the belts shifted due to not being fastened tightly enough. Thus, both the lower back and pelvic sensor measurements have low reliability, although more so the pelvic sensor as it was fastened on top of clothing and noticeably moved around during experiments. This is supported by the data, as the RMSD values and biases of the pelvic sensor during walking were noticeably higher than those of other sensors (see Table 8.1). It could be beneficial to reevaluate the sensors attached with more suitable belts that produce no gaps against the body to give fair readings.

It is vital that the straps are tightly secured when collecting data, which can be challenging, especially in a clinical setting, as the straps must fit all patients. Using straps may simply be unrealistic, which perhaps would have been even more apparent if the experiments had been carried out on several test subjects. The neck and upper back sensors, which were attached by tape, exhibited lower mean absolute bias and RMSD values than the lower back and pelvic sensors. This could indicate that attachment by tape is superior to the strap approach. In this experiment, normal double-sided tape was used to attach the sensors to the body. This leaves some irritation on the skin, and in a clinical application it would be advisable to use kinesiotape instead for the comfort of the patient.

No particular points on the spine that may be more important in characterizing posture or the overall balance of the body were determined or tested in this experiment. This was in part because no physician with knowledge of spinal landmarks was present during the experiments. In the future, it may be of interest to investigate important locations on the spine or body in collaboration with a physician. It would also be essential to determine how accurate the sensors would be on different parts of the body. For example, if the legs are a point of interest, soft tissue artifacts may potentially be an issue.

Missing data occurred only in the walking experiments, where markers went untracked, likely due to loss of visibility during the rapid movements of walking. The walking experiments were repeated several times, but data was consistently missing, rendering the walking experiment results unreliable and in need of being re-evaluated in the future. Furthermore, all average RMSD and bias values were reduced when walking data was removed, suggesting that the fit of sensor data to MoCap data was poorer while walking (see Table 8.1). This is hypothesized to be partly due to the obvious challenge of measuring tilts while moving, as the angles will rapidly fluctuate and expose any delay or lack of sensitivity of sensor and MoCap data. In this case, the MoCap data were insufficient, while the sensor data consistently streamed normal data. Since the sensors, which constitute the main subject of the experiments, had no issue in collecting data while walking, the results do not necessarily have to indicate that the sensors are less accurate while walking but that a more

suitable ground truth should be chosen or that a troubleshooting of the Qualisys system should be done.

9.3 Comparison Between Marker Placements (D1 vs D2)

The marker pair placed on top of the sensor, D2, consistently produced lower bias and RMSD values compared to the marker pair placed above and below the sensors, D1 (see Table 8.2). This indicates that the sensor estimates the D2 tilt better than the D1 tilt, perhaps due to poor placement of the markers, but also due to skin movement.
Considering only D2, which showed the best fit to sensor data, and ignoring walking trials, the lowest mean bias and RMSD values were observed for the neck measurements (0.41° and 0.64°, respectively; see Table 8.3), representing an excellent result. Notably, the 0.41° bias aligns with the official documentation provided by Movella, of accuracies below 0.5° for static measurements [70].

9.4 Comparison of Orientation Formats

The 3D orientation formats analysed were Euler angles and quaternion-based angles. Figures 8.4 and 8.5 display the superiority quaternions have over Euler angles in this context, as beyond the magnitude of the angle, they also properly show the direction of tilt.
In these experiments, the lower back sensor can be observed to shift between tilting backward and forward around the upright 0° line, but in Euler format this would be impossible to distinguish. Moreover, the quaternion angles consistently show the correct direction of tilt because they do not suffer from singularities. Meanwhile, the gimbal lock that Euler angles suffers from leads to inconsistency in the tilt direction. The Euler angles are harder to represent visually especially when walking, since the sign of the angle changes when the direction of walking changes. Using Euler angles clinically would entail only logging the absolute value for each angle, which may be bothersome, as determining backward or forward tilt would have to be assessed visually. With quaternions, the tilt data would automatically be complete, including the magnitude and direction of the tilt.
Observing only the D2 data, which seemed to have the overall best fit to the sensor data, the quaternions on average had a 1.33° lower bias and a 1.42° lower RMSD compared to Euler angles while sitting (calculated from Tables C.6 and C.8). However, Euler angles showed a better fit while standing, although not substantial with about a 0.49° lower bias and 0.35° lower RMSD than quaternions for the D2 data (calculated from Tables C.2 and C.4). The quaternions had a 0.31° lower bias and 0.71° lower RMSD than the Euler angles while walking (calculated from Tables C.10 and C.12), however, these data may be unreliable since a large portion of the MoCap data was missing from the walking experiment. Thus, it is hard to determine whether Euler angles or quaternions are the most accurate for measuring spinal tilt,

as the results seem relatively similar. Ideally, an experiment where Euler angles and quaternions can be recorded simultaneously, for example by creating an app with the Movella SDK, could allow for a more fair comparison. However, it is not hypothesized that there would be a significant difference in Euler angles and quaternions; the intention of the implementation of quaternions was simply to avoid singularities so that forward and backward tilt could consistently be reported correctly. If it is not of importance to register the direction of tilt, the Euler angles could be used instead of quaternions. Still, the elegance and robustness of quaternions give them an obvious edge compared to Euler angles.

9.5 Limitations and Future Work

The experiments carried out in this thesis were merely on a trial level and primarily served as a proof of concept. More thorough experiments are required to properly validate the Movella DOT sensor system for this use context. As stated above, more stable attachment methods, multiple test subjects, more test iterations, and various spinal curvatures and body parts would, for example, need to be applied in future validation experiments. Still, this trial experiment points towards a satisfactory performance of the sensor system.

9.6 Clinical Applicability

The application of Movella DOT sensors as a postural assessment tool in clinical practices is predicted to be relatively smooth. A custom-made app could be easily developed by implementing the logic proposed in this thesis along with the SDK kit supplied by Movella. This could facilitate easy access to spinal tilt data for clinicians, where angle data can be stored and monitored throughout the rehabilitation process. It could also be helpful to provide real-time streaming of the processed angle data within the smartphone app. The format the dorsaVi software uses in which data can be stored in different patient folders and sessions [80] could also be a practical layout to adopt in a future app.
Another advantage is that the system is highly modular and allows for patient-specific tailoring of postural assessment. The physician can choose which locations on the spine, or even legs or neck, or any other part of the body that may be of interest to monitor in each patient. Furthermore, the code could be easily adjusted to accommodate a different number of sensors.
To conclude, this study demonstrates that the use of an IMU-based wearable sensor system appears to be the most promising method to measure postural spinal tilt in this context. The Movella DOT system is intuitive, flexible, patient-customizable, and accurately measures spinal tilt. Further validation testing and development of a suitable app need to be done before the system is ready to be applied in a clinical context, but is considered highly feasible.

10
Conclusion

In conclusion, the literature study identified IMU sensor systems as the most promising postural assessment tool for application in rehabilitation therapy. The Movella DOT IMU sensor system was therefore selected and evaluated in a trial experiment against the Qualisys MoCap system, using four sensors placed along the spine.
During walking experiments, the MoCap suffered data loss, indicating that further investigation is needed to determine the sensors' accuracy in dynamic situations. Sensors attached with tape showed a better fit to the MoCap data than those attached with straps, suggesting that tape attachment might be more stable and would potentially also be more clinically practical. Quaternion-based angle representations outperformed Euler-based angles, due to their consistency in reporting the direction of tilt. This indicates that quaternions are preferable for clinic application where accurate reporting of tilt direction is essential.
The neck data, in particular, showed the best agreement with the MoCap data across all plots. When walking data were excluded, it achieved a bias of 0.41° and RMSD of 0.64°. The sensors thus have the potential to measure spinal tilt with excellent accuracy.
These findings indicate that Movella DOT sensors could be an all-in-one solution to several rehabilitation therapy needs. Beyond measuring spinal tilt, the system may also be useful for range of motion analysis, as well as possibly breathing pattern analysis.
Using the logic developed in this thesis, a smartphone application could easily be developed with the Movella SDK Kit, that is customized to a clinical setting and provides easily accessible, real-time data to the physician.
Further experiments are required to validate the reliability of the sensors across different body types and to develop protocols before they are ready to be implemented clinically. Considering their flexibility, precision, customizability, and ease of use, the Movella DOT sensors closely meet the identified need and is an exciting tool for improving posture assessment and pain management.

Bibliography

[1] Petropoulos, A., Sikeridis, D., & Antonakopoulos, T. (2017). Spomo: IMU-based real-time sitting posture monitoring. *2017 IEEE 7th International Conference on Consumer Electronics - Berlin (ICCE-Berlin),* 59. https://doi.org/10.1109/icce-berlin.2017.8210574

[2] Krauter, C., Angerbauer, K., Sousa Calepso, A., Achberger, A., Mayer, S., & Sedlmair, M. (2024). Sitting posture recognition and feedback: A literature review. *Proceedings of the CHI Conference on Human Factors in Computing Systems,* 120. https://doi.org/10.1145/3613904.3642657

[3] Czaprowski, D., Stoliński, Ł., Tyrakowski, M., Kozinoga, M., & Kotwicki, T. (2018). Non-structural misalignments of body posture in the sagittal plane. *Scoliosis and Spinal Disorders, 13*(1). https://doi.org/10.1186/s13013-018-0151-5

[4] Lind, C. M. (2024). A rapid review on the effectiveness and use of Wearable biofeedback motion capture systems in ergonomics to mitigate adverse postures and movements of the upper body. *Sensors, 24*(11), 3345. https://doi.org/10.3390/s24113345

[5] Figueira, V., Silva, S., Costa, I., Campos, B., Salgado, J., Pinho, L., Freitas, M., Carvalho, P., Marques, J., & Pinho, F. (2024). Wearables for monitoring and postural feedback in the work context: A scoping review. *Sensors, 24*(4), 1341. https://doi.org/10.3390/s24041341

[6] Patel, S., Park, H., Bonato, P., Chan, L.,& Rodgers, M. (2012). A review of wearable sensors and systems with application in rehabilitation. *Journal of NeuroEngineering and Rehabilitation, 9*(1). https://doi.org/10.1186/1743-0003-9-21

[7] Kent, P., Laird, R., & Haines, T. (2015). The effect of changing movement and posture using motion-sensor biofeedback, Versus Guidelines-based care, on the clinical outcomes of people with sub-acute or chronic low back pain-a multicentre, cluster-randomised, placebo-controlled, pilot trial. *BMC Musculoskeletal Disorders, 16*(1). https://doi.org/10.1186/s12891-015-0591-5

[8] Ronchi, A. J., Lech, M., Taylor, N. F., & Cosic, I. (2008). A reliability study of the new back strain monitor based on clinical trials. *2008 30th Annual International Conference of the IEEE Engineering in Medicine and Biology Society,* 693696. https://doi.org/10.1109/iembs.2008.4649247

[9] Ribeiro, D. C., Sole, G., Abbott, J. H., & Milosavljevic, S. (2014). The effectiveness of a lumbopelvic monitor and feedback device to change postural behavior: A feasibility randomized controlled trial. *Journal of Orthopaedic & amp; Sports Physical Therapy, 44*(9), 702711. https://doi.org/10.2519/jospt.2014.5009

[10] Claeys, K., Brumagne, S., Deklerck, J., Vanderhaeghen, J., & Dankaerts, W. (2016). Sagittal evaluation of usual standing and sitting spinal posture. *Journal of Bodywork and Movement Therapies, 20*(2), 326333. https://doi.org/10.1016/j.jbmt.2015.10.002

[11] Elabd, A. M., & Elabd, O. M. (2021). Relationships between forward head posture and lumbopelvic sagittal alignment in older adults with chronic low back pain. *Journal of Bodywork and Movement Therapies, 28,* 150156. https://doi.org/10.1016/j.jbmt.2021.07.036

[12] Ludwig, O., Dindorf, C., Kelm, J., Simon, S., Nimmrichter, F., & Fröhlich, M. (2023). Reference values for sagittal clinical posture assessment in people aged 10 to 69 years. *International Journal of Environmental Research and Public Health, 20*(5), 4131. https://doi.org/10.3390/ijerph20054131

[13] Kandasamy, G., Bettany-Saltikov, J., & van Schaik, P. (2021). Posture and back shape measurement tools: A narrative literature review. *Spinal Deformities in Adolescents, Adults and Older Adults.* https://doi.org/10.5772/intechopen.91803

[14] *Spine Structure and Function.* Cleveland Clinic. (2023, October 18). `https://my.clevelandclinic.org/health/body/10040-spine-structure-and-function`

[15] Moreira, R., Teles, A., Fialho, R., Baluz, R., Santos, T. C., Goulart-Filho, R., Rocha, L., Silva, F. J., Gupta, N., Bastos, V. H., & Teixeira, S. (2020). Mobile applications for assessing human posture: A systematic literature review. *Electronics, 9*(8), 1196. https://doi.org/10.3390/electronics9081196

[16] *Spinal Curvatures (Scoliosis, Kyphosis and Lordosis).* Ohio State Medical University Wexner Medical Center. (n.d.). `https://wexnermedical.osu.edu/brain-spine-neuro/spine-diseases-conditions/spinal-curvatures`

[17] Hey, H. W., Tan, K.-A., Chin, B. Z., Liu, G., & Wong, H.-K. (2019). Comparison of whole body sagittal alignment during directed vs natural, relaxed standing postures in young, healthy adults. *The Spine Journal, 19*(11), 18321839. https://doi.org/10.1016/j.spinee.2019.06.017

[18] Knebel, A., Daher, M., Singh, M., Fisher, L., Daniels, A. H., & Diebo, B. G. (2024). Sagittal spinal alignment measurements and evaluation: Historical perspective. *North American Spine Society Journal (NASSJ), 19,* 100519. https://doi.org/10.1016/j.xnsj.2024.100519

[19] Unal, N. E., Ucurum, S. G., Kirmizi, M., & Altas, E. U. (2024). More neck pain, less spinal mobility, altered sitting posture: Sagittal spinal alignment and mobility in women with chronic neck pain. *Musculoskeletal Science and Practice, 74,* 103205. https://doi.org/10.1016/j.msksp.2024.103205

[20] Satin, A. M., Chen, Y. H., Silber, J., & Essig, D. (2017). Sagittal Plane Deformity: Evaluation and Management. *Seminars in Spine Surgery, 29*(4), 208214. https://doi.org/10.1053/j.semss.2017.08.006

[21] Estrada, J. E., & Vea, L. A. (2016). Real-time human sitting posture detection using mobile devices. *2016 IEEE Region 10 Symposium (TENSYMP),* 140144. https://doi.org/10.1109/tenconspring.2016.7519393

[22] Le Huec, J. C., Thompson, W., Mohsinaly, Y., Barrey, C., & Faundez, A. (2019). Sagittal balance of the spine. *European Spine Journal, 28*(9), 18891905.

https://doi.org/10.1007/s00586-019-06083-1

[23] Ignasiak, D. (2020). A novel method for prediction of postoperative global sagittal alignment based on full-body musculoskeletal modeling and Posture Optimization. *Journal of Biomechanics, 102,* 109324. https://doi.org/10.1016/j.jbiomech.2019.109324

[24] *Assessing Limb Length Discrepancy.* Lower Extremity Review Magazine. (2018, February). `https://lermagazine.com/cover_story/assessing-limb-length-discrepenacy`

[25] Cardoso, J. R., Pereira, L. M., Iversen, M. D., & Ramos, A. L. (2014). What is gold standard and what is ground truth? *Dental Press Journal of Orthodontics*, *19*(5), 2730. https://doi.org/10.1590/2176-9451.19.5.027-030.ebo

[26] Pivotto, L. R., Navarro, I. J., & Candotti, C. T. (2021). Radiography and photogrammetry-based methods of assessing cervical spine posture in the sagittal plane: A systematic review with meta-analysis. *Gait & amp; Posture, 84,* 357367. https://doi.org/10.1016/j.gaitpost.2020.12.033

[27] Kuo, Y.-L., Tully, E. A., & Galea, M. P. (2009). Video analysis of sagittal spinal posture in healthy young and older adults. *Journal of Manipulative and Physiological Therapeutics, 32*(3), 210215. https://doi.org/10.1016/j.jmpt.2009.02.002

[28] Thuaimer, A., Knipe, H., & Elfeky, M. (2013). Cobb Angle. *Radiopaedia.Org.* https://doi.org/10.53347/rid-23612

[29] Koelé, M. C., Lems, W. F., & Willems, H. C. (2020). The clinical relevance of hyperkyphosis: A narrative review. *Frontiers in Endocrinology*, *11.* https://doi.org/10.3389/fendo.2020.00005

[30] Jha, R. (2024a, October 7). *Posture Analysis.* Pain Free Physiotherapy & Chiropractic Clinic. https://painfreephysiotherapy.com/posture-analysis/

[31] Lovell, F. W., Rothstein, J. M., Person, S., & Cholewicki, J. (1989). Reliability of clinical measurements of lumbar lordosis taken with a flexible rule. *Physical Therapy, 69*(2), 96105. https://doi.org/10.1093/ptj/69.2.96

[32] Wong, W. Y., & Wong, M. S. (2008). Trunk posture monitoring with inertial sensors. *European Spine Journal, 17*(5), 743753. https://doi.org/10.1007/s00586-008-0586-0

[33] Korovessis, P., Petsinis, G., Papazisis, Z., & Baikousis, A. (2001). Prediction of thoracic kyphosis using the debrunner kyphometer. *Journal of Spinal Disorders*, *14*(1), 6772. https://doi.org/10.1097/00002517-200102000-00010

[34] Yan, L., & Du, Y. (2025). Exploring trends and clusters in human posture recognition research: An analysis using CiteSpace. *Sensors, 25*(3), 632. https://doi.org/10.3390/s25030632

[35] Shiao, Y., Chen, G.-Y., & Hoang, T. (2024). Three-dimensional human posture recognition by extremity angle estimation with minimal IMU sensor. *Sensors, 24*(13), 4306. https://doi.org/10.3390/s24134306

[36] Fernandez-Baena, A., Susin, A., & Lligadas, X. (2012). Biomechanical validation of upper-body and lower-body joint movements of Kinect motion capture data for rehabilitation treatments. *2012 Fourth International Conference on Intelligent Networking and Collaborative Systems*, 656661. https://doi.org/10.1109/incos.2012.66

[37] Clark, R. A., Pua, Y.-H., Fortin, K., Ritchie, C., Webster, K. E., Denehy, L., & Bryant, A. L. (2012). Validity of the Microsoft Kinect for assessment of postural control. *Gait & amp; Posture, 36*(3), 372377. https://doi.org/10.1016/j.gaitpost.2012.03.033

[38] Xu, X., & McGorry, R. W. (2015). The validity of the first and second generation Microsoft KinectTM for Identifying Joint Center locations during Static Postures. *Applied Ergonomics, 49,* 4754. https://doi.org/10.1016/j.apergo.2015.01.005

[39] Bawa, A., Banitsas, K., & Abbod, M. (2021). A review on the use of Microsoft Kinect for gait abnormality and postural disorder assessment. *Journal of Healthcare Engineering, 2021*, 119. https://doi.org/10.1155/2021/4360122

[40] Yeung, L. F., Cheng, K. C., Fong, C. H., Lee, W. C. C., & Tong, K.-Y. (2014). Evaluation of the Microsoft Kinect as a clinical assessment tool of Body Sway. *Gait & amp; Posture, 40*(4), 532538. https://doi.org/10.1016/j.gaitpost.2014.06.012

[41] Su, M.-C., Lin, S.-H., Lee, S.-F., Huang, Y.-S., & Chen, H.-R. (2016). The implementation of a Kinect-based Postural Assessment System. *Lecture Notes in Computer Science*, 503513. https://doi.org/10.1007/978-3-319-39601-9_ 45

[42] Koda, H., Kai, Y., Kida, N., & Morihara, T. (2023). Spinal alignment measurement with Kinect sensor is valid for thoracic kyphosis but not for lumbar lordosis. *Journal of Orthopaedic Surgery and Research*, *18*(1). https://doi.org/10.1186/s13018-023-03693-w

[43] Wiedemann, L. G., Kampel, M., Planinc, R., & Nemec, I. (2015). Performance evaluation of joint angles obtained by the Kinect V2. *IET International Conference on Technologies for Active and Assisted Living (TechAAL).* https://doi.org/10.1049/ic.2015.0142

[44] Clark, R. A., Pua, Y.-H., Fortin, K., Ritchie, C., Webster, K. E., Denehy, L., & Bryant, A. L. (2012a). Validity of the Microsoft Kinect for assessment of postural control. *Gait & Posture*, *36*(3), 372377. https://doi.org/10.1016/j.gaitpost.2012.03.033

[45] Clark, R. A., Pua, Y.-H., Bryant, A. L., & Hunt, M. A. (2013). Validity of the Microsoft Kinect for providing lateral trunk lean feedback during gait retraining. *Gait & Posture*, *38*(4), 10641066. https://doi.org/10.1016/j.gaitpost.2013.03.029

[46] Tian, Y., Meng, X., Tao, D., Liu, D., & Feng, C. (2015). Upper limb motion tracking with the integration of IMU and Kinect. *Neurocomputing*, *159*, 207218. https://doi.org/10.1016/j.neucom.2015.01.071

[47] Milosevic, B., Leardini, A., & Farella, E. (2020). Kinect and wearable inertial sensors for motor rehabilitation programs at Home: State of the art and an experimental comparison. *BioMedical Engineering OnLine*, *19*(1). https://doi.org/10.1186/s12938-020-00762-7

[48] Petropoulos, A., Sikeridis, D., & Antonakopoulos, T. (2020). Wearable smart health advisors: An IMU-enabled posture monitor. *IEEE Consumer Electronics Magazine, 9*(5), 2027. https://doi.org/10.1109/mce.2019.2956205

[49] Cerqueira, S. M., Silva, A. F., & Santos, C. P. (2020). Smart vest for real-time postural biofeedback and Ergonomic Risk Assessment. *IEEE Access, 8,*

107583107592. https://doi.org/10.1109/access.2020.3000673

[50] Kiefer, D., Baraliakos, X., Adolf, D., Chatzistefanidi, V., Schwarze, I., Lange, U., Brandt-Jürgens, J., Stemmler, E., Sartingen, S., & Braun, J. (2021). Successful evaluation of spinal mobility measurements with the EPIONICS spine device in patients with axial spondyloarthritis compared to controls. *The Journal of Rheumatology*, *49*(1), 4452. https://doi.org/10.3899/jrheum.201470

[51] Suter, M., Eichelberger, P., Frangi, J., Simonet, E., Baur, H., & Schmid, S. (2020). Measuring lumbar back motion during functional activities using a portable strain gauge sensor-based system: A Comparative Evaluation and Reliability Study. *Journal of Biomechanics*, *100*, 109593. https://doi.org/10.1016/j.jbiomech.2019.109593

[52] Consmüller, T., Rohlmann, A., Weinland, D., Druschel, C., Duda, G. N., & Taylor, W. R. (2012). Velocity of lordosis angle during spinal flexion and extension. *PLoS ONE*, *7*(11). https://doi.org/10.1371/journal.pone.0050135

[53] Sugino, S., Matsuo, R., Hironiwa, M., Yokoyama, S., Sadamatsu, T., & Gamada, K. (2013). Measurement validity of spine alignment in healthy young adults:comparison of sagittal measurements with the spinal mouse and radiographic assessment. *Japanese Journal of Health Promotion and Physical Therapy*, *3*(3), 123127. https://doi.org/10.9759/hppt.3.123

[54] Livanelioglu, A., Kaya, F., Nabiyev, V., Demirkiran, G., & Frat, T. (2015). The validity and reliability of Spinal mouse assessment of spinal curvatures in the frontal plane in pediatric adolescent idiopathic Thoraco-lumbar curves. *European Spine Journal*, *25*(2), 476482. https://doi.org/10.1007/s00586-015-3945-7

[55] Critchley, L. (2019, November 25). *What are encoder sensors?*. AZoSensors. https://www.azosensors.com/article.aspx?ArticleID=1730

[56] Idiag AG. (n.d.). *Idiag M360: Radiation-free back scan simple, fast, precise* [Brochure]. Idiag AG. https://www.idiag.ch/idiag-m360/

[57] Amgad, M. M., Abdelmageed, S. F., & Mohamed, N. A. (2024). Is spinal mouse a valid tool in assessing spinal deviation in patients with lumbar spondylosis? *Egyptian Reviews for Medical and Health Sciences*, *0*(0), 00. https://doi.org/10.21608/ermhs.2024.292504.1003

[58] Yousefi M, Ilbeigi S, Mehrshad N, Afzalpour M, Naghibi SE. Comparing the validity of non-invasive methods in measuring Thoracic kyphosis and Lumbar Lordosis. Zahedan J Res Med Sci (ZJRMS) 2012; 14(4): 37-42.

[59] Mannion, A. F., Knecht, K., Balaban, G., Dvorak, J., & Grob, D. (2004). A new skin-surface device for measuring the curvature and global and segmental ranges of motion of the spine: Reliability of measurements and comparison with data reviewed from the literature. *European Spine Journal*, *13*(2), 122136. https://doi.org/10.1007/s00586-003-0618-8

[60] Post, R. B., & Leferink, V. J. (2004). Spinal mobility: Sagittal range of motion measured with the SpinalMouse, a new non-invasive device. *Archives of Orthopaedic and Trauma Surgery*, *124*(3), 187192. https://doi.org/10.1007/s00402-004-0641-1

[61] Dr Jason Konrath. (2020a). *Wearable Technology in Biomechanics and S.T.E.M. Education*. Movella.

[62] Lind, Carl Mikael, Abtahi, F & Forsman, M. (2023). Wearable motion capture devices for the prevention of work-related musculoskeletal disorders in ergonomicsan overview of current applications, challenges, and future opportunities. *Sensors, 23*(9), 4259. https://doi.org/10.3390/s23094259

[63] Godfrey, A., Conway, R., Meagher, D., & ÓLaighin, G. (2008). Direct measurement of human movement by accelerometry. *Medical Engineering & amp; Physics, 30*(10), 13641386. https://doi.org/10.1016/j.medengphy.2008.09.005

[64] Madgwick, S. O. H. (2010, April 30). An ecient orientation filter for inertial and inertial/magnetic sensor arrays. Washington; University of Washington.

[65] Tlili, F., Haddad, R., Bouallegue, R., & Mezghani, N. (2021). A real-time posture monitoring system towards bad posture detection. *Wireless Personal Communications, 120*(2), 12071227. https://doi.org/10.1007/s11277-021-08511-2

[66] Jamian, S., Gunawan, T. S., Kartiwi, M., Ahmad, R., Abdul Kadir, K., & Nordin, M. N. (2022). Human activity and posture classification using smartphone sensors and MATLAB Mobile. *2022 IEEE International Instrumentation and Measurement Technology Conference (I2MTC)*, 16. https://doi.org/10.1109/i2mtc48687.2022.9806551

[67] Huang, X., Xue, Y., Ren, S., & Wang, F. (2023). Sensor-based wearable systems for monitoring human motion and posture: A Review. *Sensors, 23*(22), 9047. https://doi.org/10.3390/s23229047

[68] Tlili, F., Haddad, R., Bouallegue, R., & Shubair, R. (2022). Design and architecture of Smart Belt for Real Time Posture Monitoring. Internet of Things, 17, 100472. https://doi.org/10.1016/j.iot.2021.100472

[69] Movella/Xsens. (n.d.). *Movella DOT*. Movella. https://www.movella.com/wearables/movella-dot

[70] Movella/Xsens. (2023, July). *Movella DOT user manual* (Document XD0502P, Rev. A). Movella Inc. https://www.movella.com/hubfs/Movella%20DOT%20User%20Manual.pdf

[71] Beange, K. H. E., Chan, A. D. C., & Graham, R. B. (2024). Investigating concurrent validity of inertial sensors to evaluate multiplanar spine movement. *Journal of Biomechanics*, *164*, 111939. https://doi.org/10.1016/j.jbiomech.2024.111939

[72] McClintock, F. A., Callaway, A. J., Clark, C. J., Alqhtani, R. S., & Williams, J. M. (2024). Lumbar sitting behavior of individuals with low back pain: A preliminary study using extended real-world data. *Sensors*, *24*(20), 6751. https://doi.org/10.3390/s24206751

[73] *Noraxon Ultium Motion 3D motion capture/IMU System*. HaB Direct. (2025, March 27). `https://www.habdirect.com/product/noraxon-ultium-motion-3d-motion-capture-imu-system/`

[74] Noraxon U.S.A. Inc. (2024, August). *Ultium motion system brochure*. Noraxon U.S.A. Inc. https://www.noraxon.com/wp-content/uploads/2024/09/2024-Ultium-Motion-Brochure.pdf

[75] Noraxon U.S.A. Inc. (2018). *myoMOTION hardware user manual (Rev. J)*. Noraxon U.S.A. Inc. `https://www.noraxon.com/download/myomotion-system-user-manual/`

[76] Balasubramanian, S. (2013, August 23). *Comparison of angle measurements between Vicon and MyoMotion systems* [Unpublished masters study]. Center for Adaptive Neural Systems, Arizona State University.

[77] Rekant, J., & Chambers, A. (2022). Validation of inertial measurement unit-based motion capture with a single calibration file for assessing gait in Healthy Young Adults. *SSRN Electronic Journal*. https://doi.org/10.2139/ssrn.4002945

[78] Heuvelmans, P., Benjaminse, A., Bolt, R., Baumeister, J., Otten, E., & Gokeler, A. (2022). Concurrent validation of the NORAXON MyoMotion wearable inertial sensors in change-of-direction and jump-landing tasks. *Sports Biomechanics*, 116. https://doi.org/10.1080/14763141.2022.2093264

[79] dorsaVi Ltd. (n.d.). *ViMove+*. dorsaVi. https://dorsavi.com/vimove-plus/

[80] dorsaVi USA, Inc. (2017, February 3). *ViMove v6 user manual* (Rev. 20170203). dorsaVi USA, Inc. https://us.dorsavi.com

[81] Chang, R. P., Smith, A., Kent, P., Saraceni, N., Hancock, M., OSullivan, P. B., & Campbell, A. (2022). Concurrent validity of Dorsavi Wireless Motion Sensor System version 6 and the Vicon Motion Analysis System during lifting. *BMC Musculoskeletal Disorders*, *23*(1). https://doi.org/10.1186/s12891-022-05866-w

[82] Mjøsund, H. L., Boyle, E., Kjaer, P., Mieritz, R. M., Skallgård, T., & Kent, P. (2017). Clinically acceptable agreement between the VIMOVE Wireless Motion Sensor System and the Vicon motion capture system when measuring lumbar region inclination motion in the sagittal and coronal planes. *BMC Musculoskeletal Disorders*, *18*(1). https://doi.org/10.1186/s12891-017-1489-1

[83] *PostureScreen*. PostureAnalysis. (n.d.). `https://www.postureanalysis.com/posturescreen-posture-movement-body-composition-analysis-assessment/`

[84] Szucs, K. A., & Brown, E. V. (2018). Rater reliability and construct validity of a mobile application for posture analysis. *Journal of Physical Therapy Science*, *30*(1), 3136. https://doi.org/10.1589/jpts.30.31

[85] Hopkins, B. C. B. (2014). *Validity of PostureScreen Mobile® in the measurement of standing posture* (Masters thesis, Brigham Young University). BYU ScholarsArchive. https://scholarsarchive.byu.edu/etd/4119

[86] Boland, D. M., Neufeld, E. V., Ruddell, J., Dolezal, B. A., & Cooper, C. B. (2016). Inter- and intra-rater agreement of Static Posture Analysis using a mobile application. *Journal of Physical Therapy Science*, *28*(12), 33983402. https://doi.org/10.1589/jpts.28.3398

[87] ScolioLife. (n.d.). *Scoliometer*. ScolioLife. https://scoliolife.com/scoliometer

[88] Waś, J., Sitarski, D., Ewertowska, P., Bloda, J., & Czaprowski, D. (2016). Using smartphones in the evaluation of spinal curvatures in a sagittal plane. *Advances in Rehabilitation, 30*(4), 2938. https://doi.org/10.1515/rehab-2015-0053

[89] Koumantakis, G. A., Nikoloudaki, M., Thacheth, S., Zagli, K., Bitrou, K., Nigritinos, A., & Botton, L. (2016). Reliability and validity measurement of sagittal lumbosacral quiet standing posture with a smartphone application in a mixed population of 183 college students and personnel. *Advances in Orthopedics, 2016*, 19. https://doi.org/10.1155/2016/3817270

[90] Kolber, M.J., Pizzini, M., Robinson, A., Yanez, D., & Hanney, W.J. (2013). *The reliability and concurrent validity of measurements used to quantify lumbar spine mobility: An analysis of an iPhoneő application and gravitybased inclinometry.* International Journal of Sports Physical Therapy, 8(2), 129137. http://www.ncbi.nlm.nih.gov/pubmed/23593551

[91] Salamh, P. A., & Kolber, M. (2013). The reliability, minimal detectable change and concurrent validity of a gravity-based bubble inclinometer and iphone application for measuring standing lumbar lordosis. *Physiotherapy Theory and Practice*, *30*(1), 6267. https://doi.org/10.3109/09593985.2013.800174

[92] Pöhlmann, S. T., Harkness, E. F., Taylor, C. J., & Astley, S. M. (2016). Evaluation of Kinect 3D sensor for Healthcare Imaging. *Journal of Medical and Biological Engineering*, *36*(6), 857870. https://doi.org/10.1007/s40846-016-0184-2

[93] Idiag AG. (2024, January 24). *Radiation-free back scan | IDIAG M360.* Idiag AG. https://www.idiag.ch/en/idiag-m360-en/

[94] Dreischarf, B., Koch, E., Dreischarf, M., Schmidt, H., Pumberger, M., & Becker, L. (2022). Comparison of three validated systems to analyse spinal shape and motion. *Scientific Reports*, *12*(1). https://doi.org/10.1038/s41598-022-13891-x

[95] Movella/Xsens. (2023, July 12). *Movella DOT v2 Certifications.* Movella Inc. https://base.movella.com/s/article/Movella-DOT-v2-Certifications?language=en_US

[96] Konrath, J. (2023). *Connecting the dots in human motion* [e-Book]. Movella Inc. https://www.movella.com/hubfs/Movella%20DOT%20eBook%20-%20Connecting%20the%20Dots.pdf

[97] Movella/Xsens. (2023, August 4). *Xsens DOT data sheet.* Movella Inc. https://www.xsens.com/hubfs/Xsens%20DOT%20data%20sheet.pdf

[98] Bryan He. (2020, Nov 11). *Xsens DOT Wearable Sensor Introduction and Example Application Demo* [Video]. YouTube. https://www.youtube.com/watch?v=rN7-hQBe_1A

[99] Movella/Xsens. (2022, February 1). *Orientation output specifications.* Movella Inc. `https://base.movella.com/s/article/Orientation-output-specifications?language=en_US`

[100] Movella/Xsens. (2025, April 14). *Movella DOT Synchronization Explained.* Movella Inc. `https://base.movella.com/s/article/Movella-DOT-Synchronization-Explained?language=en_US`

[101] Movella/Xsens. (2023, December 7). *Movella DOT sensor placement.* Movella Inc. https://movella.my.site.com/XsensKnowledgebase/s/article/Movella-DOT-Sensor-placement

[102] Diebel, J. (2006, October 20). *Representing attitude: Euler angles, unit quaternions, and rotation vectors* (PDF). Stanford University. https://www.astro.rug.nl/software/kapteyn-beta/_downloads/attitude.pdf

[103] MathWorks. (n.d.). *rotmat (Convert quaternion to rotation matrix).* MathWorks. https://se.mathworks.com/help/nav/ref/quaternion.rotmat.html

Figure credits in order:

Cover picture: Movella/Xsens. (2023, July). *Movella DOT user manual* (Document XD0502P, Rev. A) [Image]. Movella Inc. https://www.movella.com/hubfs/Movella%20DOT%20User%20Manual.pdf. Reproduced with permission from Movella/Xsens.
Figure 2.1: Carter, H. V. (n.d.). *Gray 111 Vertebral column-coloured labels* [Illustration]. Wikimedia Commons.
`https://commons.wikimedia.org/wiki/File:Gray_111_-_Vertebral_column-coloured.png`
Figure 2.3: OpenStax College. (2013). *Planes of Body* [Diagram]. Wikimedia Commons. https://commons.wikimedia.org/wiki/File:Planes_of_Body.jpg
Figure 4.2: Hecimovich, M. D., & Reid, S. A. (2015). *Lumbar sagittal plane spinal curvature and junior-level cricket players* [PDF]. ResearchGate.
https://www.researchgate.net/figure/Flexiruler-applied_fig1_296367757
Figure 4.3: Jooja. (2020). *Goniometer* [SVG image]. Wikimedia Commons. https://commons.wikimedia.org/wiki/File:Medizinischer_Goniometer.jpg
Figure 4.4: Katzman, W. B., Vittinghoff, E., Kado, D. M., Lane, N. E., Ensrud, K. E., & Schafer, A. L. (2016). Thoracic kyphosis and rate of incident vertebral fractures: The Fracture Intervention Trial. Osteoporosis International, 27(3), 899903. https://www.researchgate.net/figure/Kyphometer-measurement-of-Cobbs-angle-of-kyphosis_fig1_295939358
Figure 4.5.a: Alphathon. (2010). *Kinect sensor* [Image]. Wikimedia Commons. https://commons.wikimedia.org/wiki/File:KinectSensor.png
Figure 4.6: Consmüller, T., Rohlmann, A., Weinland, D., et al. (2012). Velocity of Lordosis Angle during Spinal Flexion and Extension. *PLOS ONE*, 7(11), e50135. https://doi.org/10.1371/journal.pone.0050135
Figure 4.7: Movella/Xsens. (2023, July). *Movella DOT user manual* (Document XD0502P, Rev. A) [Image]. Movella Inc. https://www.movella.com/hubfs/Movella%20DOT%20User%20Manual.pdf. Reproduced with permission from Movella/Xsens.
Figure 4.8: Noraxon USA Inc. (n.d.). *MyoMotion system user manual* [Image]. https://www.noraxon.com/download/myomotion-system-user-manual/?wpdmdl=18194
Figure 4.9: PostureCo, Inc. (2025). PostureScreen mobile app results screenshot [Image]. PostureAnalysis.com. `https://www.postureanalysis.com/wp-content/uploads/2025/05/PostureScreen_results__iPhone-14-Pro-Max-Space-Black-Portrait-copy-scaled.png`
Figure 6.3: David W. (2006). Euler angles. Retrieved from https://commons.wikimedia.org/wiki/File:Eulerangles.svg. Image licensed under CC BY-SA 3.0, via Wikimedia Commons.

A

Appendix A - Full Euler-Based MATLAB Code

```
1
2  clc;
3  clear all;
4
5  %% ====== Load motion capture data (.mat from Qualisys) ======
6  data = load('standing1e.mat');
7  val = data.Measurement6.Trajectories.Labeled.Data;
8  frameRate_mocap = data.Measurement6.FrameRate;
9  numFrames_mocap = size(val, 3);
10 time_mocap_full = (0:numFrames_mocap-1)' / frameRate_mocap;
11
12 % Define the marker pairs, bottom to top
13 segments = {
14     'Neck D1',     4, 1;
15     'Neck D2',     3, 2;
16     'Upper D1',    8, 5;
17     'Upper D2',    7, 6;
18     'Lower D1',   12, 9;
19     'Lower D2',   11,10;
20     'Pelvis D1', 16,13;
21     'Pelvis D2', 15,14;
22 };
23
24 % Compute the direction vectors (tilts) between marker pairs
25 nSeg = size(segments,1);
26 tilts_marker_full = zeros(numFrames_mocap, nSeg);
27
28 for i = 1:nSeg
29     idxBot = segments{i,2};  idxTop = segments{i,3};
30     bot = squeeze(val(idxBot, 1:3, :))';    % coordinates of
           bottom marker over time
31     top = squeeze(val(idxTop, 1:3, :))';    % coordinates of top
           marker over time
32     vec = top - bot;                        % direction vector
33     xz = vec(:, [1 3]);                     % project onto xz
           (sagittal) plane
34     xzNorm = xz ./ vecnorm(xz, 2, 2);       % normalize the vector
35     tilts_marker_full(:,i) = atan2d(xzNorm(:,1), xzNorm(:,2));  %
           compute the angle
36 end
37
38 %% ====== Load sensor (Euler) data (.csv) ======
```

```
neck   = readtable('RightFoot_20250507_134100_980.csv', 'NumHeaderLines', 11);
upper  = readtable('RightAnkle_20250507_134100_990.csv', 'NumHeaderLines', 11);
lower  = readtable('LeftFoot_20250507_134100_986.csv', 'NumHeaderLines', 11);
pelvis = readtable('LeftAnkle_20250507_134100_987.csv', 'NumHeaderLines', 11);

frameRate_sensor = 60;
numFrames_sensor = min([height(neck), height(upper), height(lower), height(pelvis)]);
time_sensor_full = (0:numFrames_sensor-1)' / frameRate_sensor;

% Euler tilt calculation
getTilt = @(Y, Z) (90 - abs(Y(1:numFrames_sensor))) .* sign(Z(1:numFrames_sensor));
tilts_sensor_full = [
    getTilt(neck.Euler_Y, neck.Euler_Z), ...
    getTilt(upper.Euler_Y, upper.Euler_Z), ...
    getTilt(lower.Euler_Y, lower.Euler_Z), ...
    getTilt(pelvis.Euler_Y, pelvis.Euler_Z)
];

% Flip signs
tilts_sensor_full(:,1) = -tilts_sensor_full(:,1);       % Neck
tilts_sensor_full(:,2) = abs(tilts_sensor_full(:,2));   % Upper Back
tilts_marker_full(:,2) = tilts_marker_full(:,2);        % Neck D2
tilts_marker_full(:,4) = -tilts_marker_full(:,4);       % Upper Back D2

%% ====== Interpolate MoCap tilts to sensor timestamps ======
% Downsample MoCap data to align with sensor data
tilts_marker_interp = zeros(numFrames_sensor, nSeg);
for i = 1:nSeg
    tilts_marker_interp(:,i) = interp1(time_mocap_full, tilts_marker_full(:,i), time_sensor_full, 'linear', NaN);
end

% Aligned vectors
tilts_marker = tilts_marker_interp;
tilts_sensor = tilts_sensor_full;
time_sensor = time_sensor_full;

%% ====== Plot sensor tilt vs MoCap D1 & D2 ======
figure;
labels = {'Neck', 'Upper Back', 'Lower Back', 'Pelvis'};
colors = lines(3);

for i = 1:4
    subplot(2,2,i); hold on;
    idxD1 = (i-1)*2 + 1;  idxD2 = idxD1 + 1;

    plot(time_mocap_full, tilts_marker_full(:, idxD1), '--', 'Color', colors(2,:), 'LineWidth', 1.2, 'DisplayName', [labels{i} ' D1']);
```

```
    plot(time_mocap_full, tilts_marker_full(:, idxD2), ':',
        'Color', colors(3,:), 'LineWidth', 1.2, 'DisplayName',
        [labels{i} ' D2']);
    plot(time_sensor_full, tilts_sensor_full(:,i), '-', 'Color',
        colors(1,:), 'LineWidth', 1.2, 'DisplayName', [labels{i} '
        Sensor']);

    yline(0, '--k', 'Upright', 'HandleVisibility', 'off');
    title([labels{i} ' Tilt']);
    xlabel('Time (s)');
    ylabel('Sagittal Tilt (ř)');
    xlim([0 20]);
    legend; grid on;
end

sgtitle('Standing E1: Sensor vs Marker Tilt Comparison');

%% ====== Summary Table ======
means = []; stds = []; mean_diffs = [];

for i = 1:4
    idxD1 = (i-1)*2 + 1;
    idxD2 = idxD1 + 1;
    valid_idx = all(~isnan([tilts_sensor(:,i),
        tilts_marker(:,idxD1), tilts_marker(:,idxD2)]), 2);

    m_sensor = mean(tilts_sensor(valid_idx,i));
    s_sensor = std(tilts_sensor(valid_idx,i));
    m_d1 = mean(tilts_marker(valid_idx, idxD1));
    s_d1 = std(tilts_marker(valid_idx, idxD1));
    m_d2 = mean(tilts_marker(valid_idx, idxD2));
    s_d2 = std(tilts_marker(valid_idx, idxD2));

    means = [means; m_sensor, m_d1, m_d2];
    stds  = [stds;  s_sensor, s_d1, s_d2];
    mean_diffs = [mean_diffs; m_sensor - m_d1, m_sensor - m_d2];
end

summaryTable = table(labels', ...
    means(:,1), stds(:,1), ...
    means(:,2), stds(:,2), ...
    means(:,3), stds(:,3), ...
    mean_diffs(:,1), mean_diffs(:,2), ...
    'VariableNames', {'Segment', ...
                      'Sensor_Mean', 'Sensor_Std', ...
                      'MarkerD1_Mean', 'MarkerD1_Std', ...
                      'MarkerD2_Mean', 'MarkerD2_Std', ...
                      'MarkerDiff_D1', 'MarkerDiff_D2'});
disp('--- Summary Table: Sensor vs MoCap D1 & D2 ---');
disp(summaryTable);

%% ====== Compute Bias and RMSD ======
bias_d1 = zeros(4,1); bias_d2 = zeros(4,1);
rmsd_d1 = zeros(4,1); rmsd_d2 = zeros(4,1);

for i = 1:4
```

```
136     idxD1 = (i-1)*2 + 1;  idxD2 = idxD1 + 1;
137     valid_idx = all(~isnan([tilts_sensor(:,i),
            tilts_marker(:,idxD1), tilts_marker(:,idxD2)]), 2);
138
139     diff_d1 = tilts_sensor(valid_idx,i) - tilts_marker(valid_idx,
            idxD1);
140     diff_d2 = tilts_sensor(valid_idx,i) - tilts_marker(valid_idx,
            idxD2);
141
142     bias_d1(i) = mean(diff_d1);
143     bias_d2(i) = mean(diff_d2);
144     rmsd_d1(i) = sqrt(mean(diff_d1.^2));
145     rmsd_d2(i) = sqrt(mean(diff_d2.^2));
146 end
147
148 comparisonTable = table(labels', bias_d1, rmsd_d1, bias_d2,
        rmsd_d2, ...
149     'VariableNames', {'Segment', 'Bias_D1', 'RMSD_D1', 'Bias_D2',
            'RMSD_D2'});
150 disp('--- Bias and RMSD Comparison: Sensor vs MoCap D1 & D2 ---');
151 disp(comparisonTable);
```

Listing A.1: Euler MATLAB Code for Sensor vs MoCap Tilt Comparison

B

Appendix B - Full Quaternion-Based MATLAB Code

```
1
2  clc;
3  clear all;
4
5  %% ====== Load Motion Capture Data (.mat from Qualisys) ======
6  data = load('standing1q.mat');
7  val = data.Measurement18.Trajectories.Labeled.Data;
8  frameRate_mocap = data.Measurement18.FrameRate;
9  numFrames_mocap = size(val, 3);
10 time_mocap_full = (0:numFrames_mocap-1)' / frameRate_mocap;
11
12 % Define the marker pairs, bottom to top
13 segments = {
14     'Neck D1',     4, 1;
15     'Neck D2',     3, 2;
16     'Upper D1',    8, 5;
17     'Upper D2',    7, 6;
18     'Lower D1',   12, 9;
19     'Lower D2',   11,10;
20     'Pelvis D1', 16,13;
21     'Pelvis D2', 15,14;
22 };
23
24 % Compute the direction vectors (tilts) between marker pairs
25 nSeg = size(segments,1);
26 tilts_marker_full = zeros(numFrames_mocap, nSeg);
27
28 for i = 1:nSeg
29     idxBot = segments{i,2};  idxTop = segments{i,3};
30     bot = squeeze(val(idxBot, 1:3, :))';
31     top = squeeze(val(idxTop, 1:3, :))';
32     vec = top - bot;
33     xz = vec(:, [1 3]);
34     xzNorm = xz ./ vecnorm(xz, 2, 2);
35     tilts_marker_full(:,i) = atan2d(xzNorm(:,1), xzNorm(:,2));
36 end
37
38 %% ====== Load Sensor (Quaternion) Data (.csv) ======
39 neck    = readtable('RightFoot_20250507_143549_708.csv',
       'NumHeaderLines', 11);
40 upper   = readtable('RightAnkle_20250507_143549_718.csv',
       'NumHeaderLines', 11);
```

```
lower  = readtable('LeftFoot_20250507_143549_715.csv', 'NumHeaderLines', 11);
pelvis = readtable('LeftAnkle_20250507_143549_716.csv', 'NumHeaderLines', 11);

frameRate_sensor = 60;
numFrames_sensor = min([height(neck), height(upper), height(lower), height(pelvis)]);
time_sensor_full = (0:numFrames_sensor-1)' / frameRate_sensor;

% Normalized quaternions for each sensor
q_neck  = normalize(quaternion(neck.Quat_W, neck.Quat_X, neck.Quat_Y, neck.Quat_Z));
q_upper  = normalize(quaternion(upper.Quat_W, upper.Quat_X, upper.Quat_Y, upper.Quat_Z));
q_lower  = normalize(quaternion(lower.Quat_W, lower.Quat_X, lower.Quat_Y, lower.Quat_Z));
q_pelvis = normalize(quaternion(pelvis.Quat_W, pelvis.Quat_X, pelvis.Quat_Y, pelvis.Quat_Z));

% Compute sensor sagittal tilt
tilt_neck  = computeSagittalTilt(q_neck);
tilt_upper  = computeSagittalTilt(q_upper);
tilt_lower  = computeSagittalTilt(q_lower);
tilt_pelvis = computeSagittalTilt(q_pelvis);

% Trim sensor data to dataset of shortest length
minLen = min([length(tilt_neck), length(tilt_upper), length(tilt_lower), length(tilt_pelvis)]);
tilt_neck  = tilt_neck(1:minLen);
tilt_upper  = tilt_upper(1:minLen);
tilt_lower  = tilt_lower(1:minLen);
tilt_pelvis = tilt_pelvis(1:minLen);
time_sensor_full = time_sensor_full(1:minLen);

tilts_sensor_full = [tilt_neck, tilt_upper, tilt_lower, tilt_pelvis];

%% ====== Interpolate MoCap Tilts to Sensor Timestamps ======
% Downsample MoCap data to align with sensor data
tilts_marker_interp = zeros(numFrames_sensor, nSeg);
for i = 1:nSeg
    tilts_marker_interp(:,i) = interp1(time_mocap_full, tilts_marker_full(:,i), time_sensor_full, 'linear', NaN);
end

% Trim to valid time overlap
valid_interp_idx = ~any(isnan(tilts_marker_interp), 2);
tilts_marker = tilts_marker_interp(valid_interp_idx, :);
tilts_sensor = tilts_sensor_full(valid_interp_idx, :);
time_sensor = time_sensor_full(valid_interp_idx);

%% ====== Plot Sensor Tilt vs MoCap D1 & D2 ======
figure;
labels = {'Neck', 'Upper Back', 'Lower Back', 'Pelvis'};
colors = lines(3);
```

```
87
88  for i = 1:4
89      subplot(2,2,i); hold on;
90      idxD1 = (i-1)*2 + 1;
91      idxD2 = idxD1 + 1;
92
93      plot(time_sensor, tilts_marker(:, idxD1), '--', 'Color',
            colors(2,:), 'LineWidth', 1.2, 'DisplayName', [labels{i} '
            D1']);
94      plot(time_sensor, tilts_marker(:, idxD2), ':',  'Color',
            colors(3,:), 'LineWidth', 1.2, 'DisplayName', [labels{i} '
            D2']);
95      plot(time_sensor, tilts_sensor(:,i), '-', 'Color',
            colors(1,:), 'LineWidth', 1.2, 'DisplayName', [labels{i} '
            Sensor']);
96
97      yline(0, '--k', 'Upright', 'HandleVisibility', 'off');
98      title([labels{i} ' Tilt']);
99      xlabel('Time (s)');
100     ylabel('Sagittal Tilt (ř)');
101     xlim([0 20]);
102     legend; grid on;
103 end
104
105 sgtitle('Standing Q1: Sensor vs Marker Tilt Comparison');
106
107 %% ====== Summary Table ======
108 means = []; stds = []; mean_diffs = [];
109
110 for i = 1:4
111     idxD1 = (i-1)*2 + 1; idxD2 = idxD1 + 1;
112     valid_idx = all(~isnan([tilts_sensor(:,i),
            tilts_marker(:,idxD1), tilts_marker(:,idxD2)]), 2);
113
114     m_sensor = mean(tilts_sensor(valid_idx,i));
115     s_sensor = std(tilts_sensor(valid_idx,i));
116     m_d1 = mean(tilts_marker(valid_idx, idxD1));
117     s_d1 = std(tilts_marker(valid_idx, idxD1));
118     m_d2 = mean(tilts_marker(valid_idx, idxD2));
119     s_d2 = std(tilts_marker(valid_idx, idxD2));
120
121     means = [means; m_sensor, m_d1, m_d2];
122     stds  = [stds;  s_sensor, s_d1, s_d2];
123     mean_diffs = [mean_diffs; m_sensor - m_d1, m_sensor - m_d2];
124 end
125
126 summaryTable = table(labels', ...
127     means(:,1), stds(:,1), ...
128     means(:,2), stds(:,2), ...
129     means(:,3), stds(:,3), ...
130     mean_diffs(:,1), mean_diffs(:,2), ...
131     'VariableNames', {'Segment', ...
132                       'Sensor_Mean', 'Sensor_Std', ...
133                       'MarkerD1_Mean', 'MarkerD1_Std', ...
134                       'MarkerD2_Mean', 'MarkerD2_Std', ...
135                       'MarkerDiff_D1', 'MarkerDiff_D2'});
```

```
136
137 disp('--- Summary Table: Sensor vs MoCap D1 & D2 ---');
138 disp(summaryTable);
139
140 %% ====== Compute Bias and RMSD ======
141 bias_d1 = zeros(4,1); bias_d2 = zeros(4,1);
142 rmsd_d1 = zeros(4,1); rmsd_d2 = zeros(4,1);
143
144 for i = 1:4
145     idxD1 = (i-1)*2 + 1; idxD2 = idxD1 + 1;
146     valid_idx = all(~isnan([tilts_sensor(:,i),
          tilts_marker(:,idxD1), tilts_marker(:,idxD2)]), 2);
147
148     diff_d1 = tilts_sensor(valid_idx,i) - tilts_marker(valid_idx,
          idxD1);
149     diff_d2 = tilts_sensor(valid_idx,i) - tilts_marker(valid_idx,
          idxD2);
150
151     bias_d1(i) = mean(diff_d1);
152     bias_d2(i) = mean(diff_d2);
153     rmsd_d1(i) = sqrt(mean(diff_d1.^2));
154     rmsd_d2(i) = sqrt(mean(diff_d2.^2));
155 end
156
157 comparisonTable = table(labels', bias_d1, rmsd_d1, bias_d2,
    rmsd_d2, ...
158     'VariableNames', {'Segment', 'Bias_D1', 'RMSD_D1', 'Bias_D2',
          'RMSD_D2'});
159
160 disp('--- Bias and RMSD Comparison: Sensor vs MoCap D1 & D2 ---');
161 disp(comparisonTable);
162
163 %% ====== Helper Function for Computing Sagittal Tilt from
    Quaternions======
164 function signedAngle = computeSagittalTilt(q)
165     R = rotmat(q, 'frame');      % convert quaternion into rotation
          matrix
166     Z = squeeze(R(:,3,:));       % extract Z-column
167     Z = Z ./ vecnorm(Z);         % normalize vector
168     angleFromVertical = acosd(Z(3,:));  % compute angle between
          sensor Z-vector and global Z-vector
169     forwardComponent = Z(1,:);  % extracts X-component, defines
          backward/forward tilt
170     signedAngle = (90 - angleFromVertical) .*
          sign(forwardComponent);   % computes signed tilt
171     signedAngle = signedAngle(:);
172 end
```

Listing B.1: Quaternion MATLAB Code for Sensor vs MoCap Tilt Comparison

C

Appendix C - Plots and Values for Experimental Results

This Appendix presents the mean values, standard deviations, difference in mean angles, RMSD values and bias values, as well as all the remaining plots for all experiments.

C.1 Standing Euler

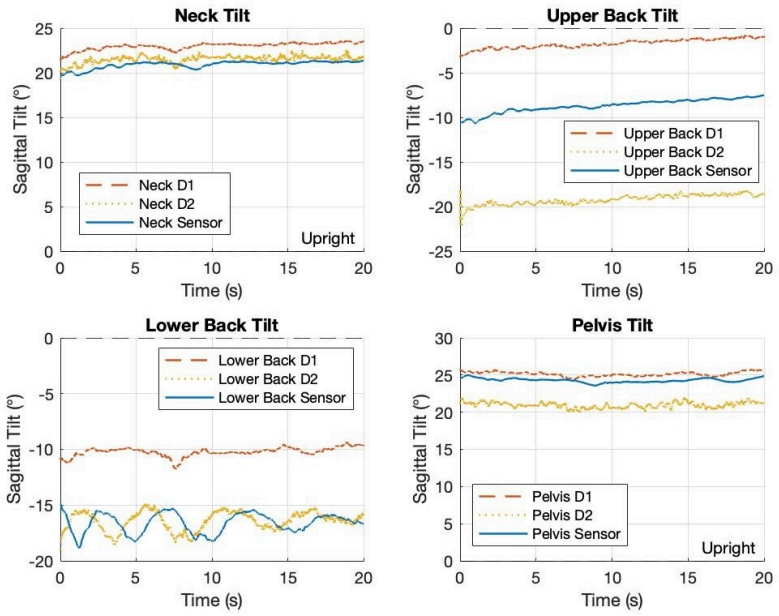

Figure C.1: Plots for Standing E2.

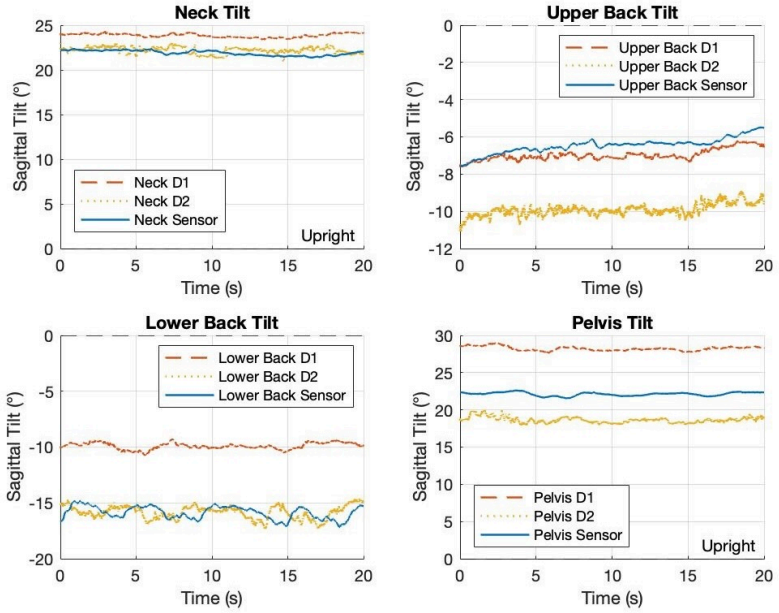

Figure C.2: Plots for Standing E3.

Segment	Bias D1 [°]	RMSD D1 [°]	Bias D2 [°]	RMSD D2 [°]
Experiment 1				
Neck	-2.6963	2.7666	-0.74219	1.0703
Upper Back	1.9741	2.5923	-13.583	13.592
Lower Back	-7.0541	7.0783	-0.78223	1.2556
Pelvis	-7.8786	7.8871	4.4329	4.4573
Experiment 2				
Neck	-1.6005	1.6242	-0.17967	0.40743
Upper Back	-6.1917	6.2173	11.374	11.387
Lower Back	-6.2452	6.3155	0.24901	1.3956
Pelvis	-1.0606	1.117	3.1722	3.2026
Experiment 3				
Neck	-1.954	1.9724	-0.30267	0.56221
Upper Back	0.50201	0.56008	3.448	3.4615
Lower Back	-5.9741	6.0113	-0.02545	0.83119
Pelvis	-6.1124	6.1204	3.4845	3.512

Table C.2: Bias and RMSD values for Standing Euler.

Segment	Sensor Mean [°]	Marker D1 Mean [°]	Marker Difference D1 [°]	Marker D2 Mean [°]	Marker Difference D2 [°]
Experiment 1					
Neck	21.897 ± 0.69211	24.593 ± 1.0292	-2.6963	22.639 ± 1.113	-0.74219
Upper Back	6.1333 ± 0.93881	4.1592 ± 0.81006	1.9741	19.717 ± 0.7279	-13.583
Lower Back	-16.961 ± 0.653	-9.9066 ± 0.53131	-7.0541	-16.178 ± 0.69556	-0.78223
Pelvis	17.789 ± 0.38031	25.668 ± 0.29206	-7.8786	13.356 ± 0.35169	4.4329
Experiment 2					
Neck	20.914 ± 0.41348	22.998 ± 0.38716	-2.0839	21.521 ± 0.41093	-0.60694
Upper Back	-8.6974 ± 0.74378	-1.7429 ± 0.50129	-6.9545	-19.249 ± 0.58169	10.552
Lower Back	-16.616 ± 0.87913	-10.225 ± 0.39839	-6.3908	-16.419 ± 0.84212	-0.19726
Pelvis	24.283 ± 0.26891	25.147 ± 0.28921	-0.86391	20.956 ± 0.38516	3.3274
Experiment 3					
Neck	21.905 ± 0.27971	23.859 ± 0.21413	-1.954	22.207 ± 0.37371	-0.30267
Upper Back	-6.469 ± 0.41226	-6.971 ± 0.29775	0.50201	-9.917 ± 0.32032	3.448
Lower Back	-15.874 ± 0.56439	-9.8995 ± 0.29363	-5.9741	-15.848 ± 0.57753	-0.02545
Pelvis	22.121 ± 0.23769	28.234 ± 0.2783	-6.1124	18.637 ± 0.40049	3.4845

Table C.1: Mean values for Standing Euler.

C.2 Standing Quaternions

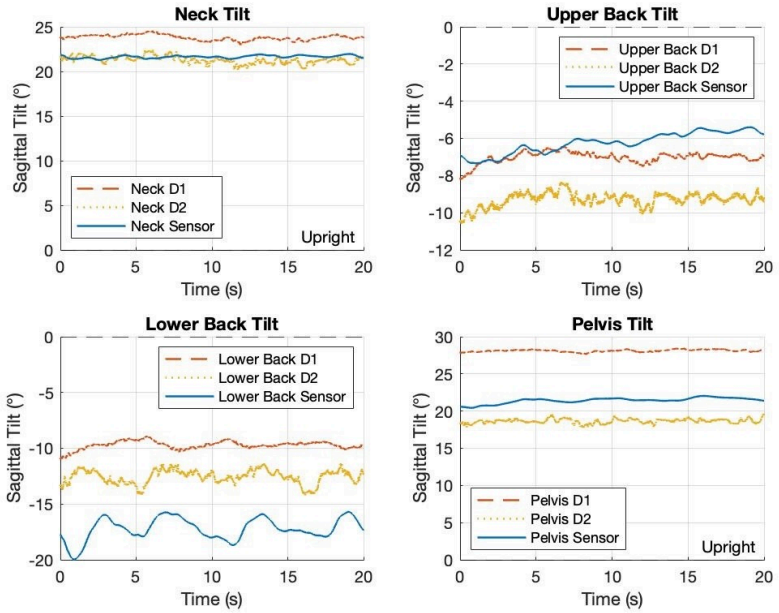

Figure C.3: Plots for Standing Q2.

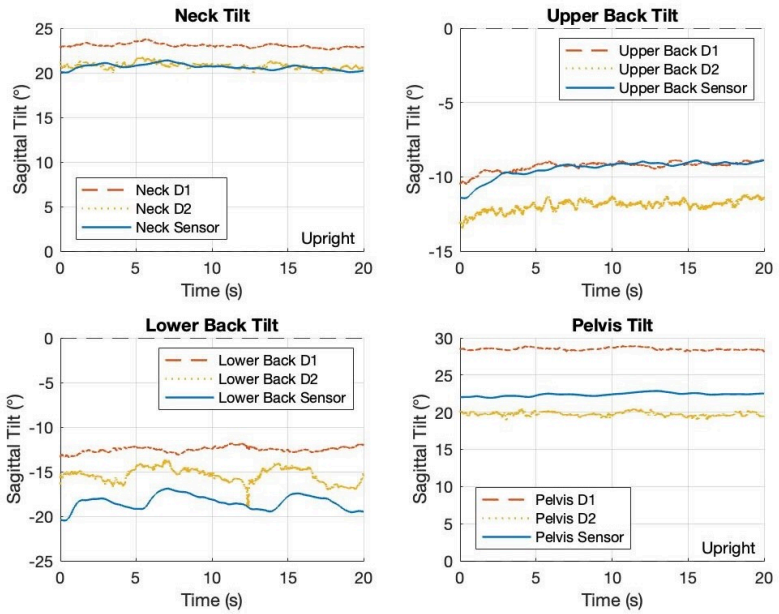

Figure C.4: Plots for Standing Q3.

Segment	Sensor Mean [°]	Marker D1 Mean [°]	Marker Difference D1 [°]	Marker D2 Mean [°]	Marker Difference D2 [°]
Experiment 1					
Neck	21.738 ± 0.31274	23.96 ± 0.18618	-2.2214	22.256 ± 0.32814	-0.51711
Upper Back	-6.6067 ± 0.40178	-6.788 ± 0.24356	0.18127	-9.5733 ± 0.3013	2.9665
Lower Back	-15.779 ± 1.0649	-8.8478 ± 0.27882	-6.931	-15.673 ± 0.98438	-0.10586
Pelvis	22.065 ± 0.16446	28.251 ± 0.14857	-6.1859	18.975 ± 0.30495	3.09
Experiment 2					
Neck	21.642 ± 0.163	23.805 ± 0.29982	-2.163	21.3 ± 0.41847	0.34251
Upper Back	-6.2371 ± 0.56828	-7.0215 ± 0.30124	0.78436	-9.2933 ± 0.37678	3.0562
Lower Back	-17.222 ± 1.0129	-9.7076 ± 0.35129	-7.5147	-12.56 ± 0.62453	-4.6621
Pelvis	21.427 ± 0.37877	28.107 ± 0.15719	-6.6796	18.64 ± 0.30136	2.7869
Experiment 3					
Neck	20.657 ± 0.31567	23.055 ± 0.21973	-2.3978	20.774 ± 0.33156	-0.11716
Upper Back	-9.445 ± 0.58308	-9.2838 ± 0.32588	-0.16115	-11.927 ± 0.38292	2.4825
Lower Back	-18.414 ± 0.80778	-12.519 ± 0.31475	-5.8957	-15.403 ± 0.8337	-3.011
Pelvis	22.381 ± 0.22467	28.511 ± 0.1718	-6.1298	19.759 ± 0.27127	2.6216

Table C.3: Mean values for Standing Quaternions.

Segment	Bias D1 [°]	RMSD D1 [°]	Bias D2 [°]	RMSD D2 [°]
Experiment 1				
Neck	-2.2214	2.2459	-0.51711	0.63998
Upper Back	0.18127	0.38133	2.9665	2.994
Lower Back	-6.931	7.0008	-0.10586	1.4213
Pelvis	-6.1859	6.1885	3.09	3.1094
Experiment 2				
Neck	-2.163	2.1955	0.34251	0.59591
Upper Back	0.78436	0.9568	3.0562	3.106
Lower Back	-7.5147	7.5899	-4.6621	4.7705
Pelvis	-6.6796	6.6883	2.7869	2.8211
Experiment 3				
Neck	-2.3978	2.4164	-0.11716	0.39033
Upper Back	-0.16115	0.37207	2.4825	2.5103
Lower Back	-5.8957	5.9672	-3.011	3.151
Pelvis	-6.1298	6.1358	2.6216	2.6433

Table C.4: Bias and RMSD values for Standing Quaternions.

C.3 Sitting Euler

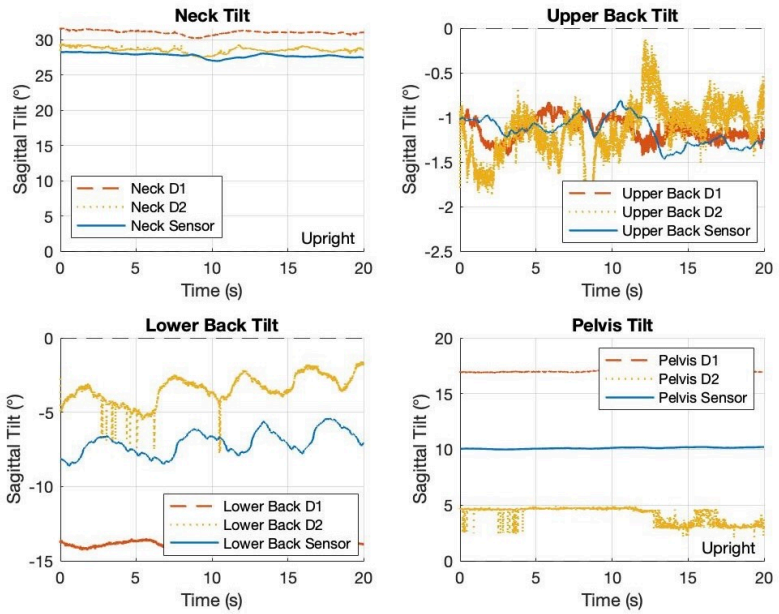

Figure C.5: Plots for Sitting E2.

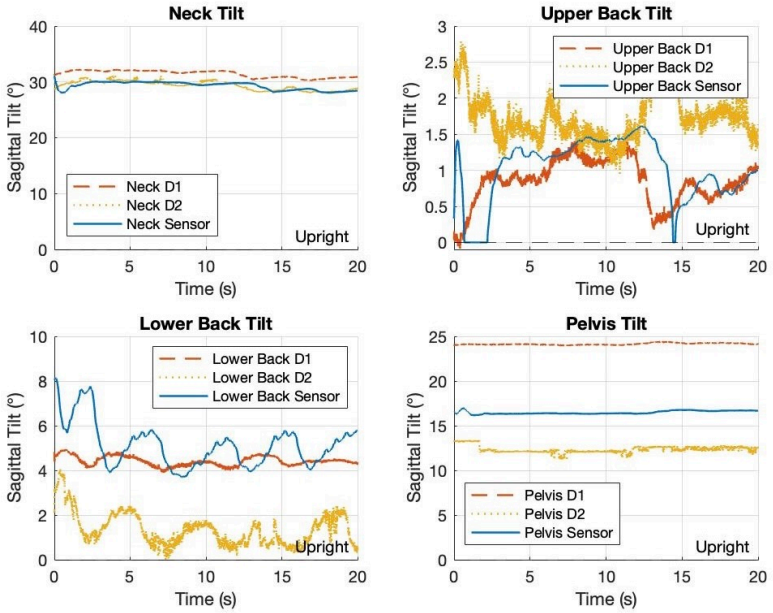

Figure C.6: Plots for Sitting E3.

Segment	Bias D1 [°]	RMSD D1 [°]	Bias D2 [°]	RMSD D2 [°]
Experiment 1				
Neck	-1.3729	1.4578	-0.3932	0.75221
Upper Back	0.42445	0.50072	2.7592	2.7987
Lower Back	-6.6058	6.6834	-2.4397	2.9001
Pelvis	-7.4315	7.4351	5.0831	5.1162
Experiment 2				
Neck	-3.2568	3.2692	-0.77777	0.85586
Upper Back	-0.0076926	0.16688	-0.016316	0.38312
Lower Back	6.6998	6.7403	-3.5983	3.7481
Pelvis	-6.8657	6.866	5.9609	6.0076
Experiment 3				
Neck	-2.145	2.1984	-0.054664	0.56237
Upper Back	0.16348	0.43727	-0.72143	0.97458
Lower Back	0.71041	1.2242	3.7723	3.9227
Pelvis	-7.6636	7.6648	4.1299	4.1454

Table C.6: Bias and RMSD values for Sitting Euler.

Segment	Sensor Mean [°]	Marker D1 Mean [°]	Marker Difference D1 [°]	Marker D2 Mean [°]	Marker Difference D2 [°]
Experiment 1					
Neck	33.382 ± 1.0914	34.755 ± 0.83591	-1.3729	33.775 ± 0.90507	-0.3932
Upper Back	3.5729 ± 0.28509	3.1485 ± 0.19435	0.42445	0.81369 ± 0.39233	2.7592
Lower Back	-9.3525 ± 1.0591	-2.7467 ± 0.25255	-6.6058	-6.9128 ± 1.0264	-2.4397
Pelvis	13.922 ± 0.18776	21.353 ± 0.068771	-7.4315	8.8386 ± 0.42997	5.0831
Experiment 2					
Neck	27.795 ± 0.31188	31.052 ± 0.28652	-3.2568	28.572 ± 0.40724	-0.77777
Upper Back	-1.1494 ± 0.15547	-1.1417 ± 0.12553	-0.0076926	-1.1331 ± 0.30236	-0.016316
Lower Back	-7.0462 ± 0.8067	-13.746 ± 0.22866	6.6998	-3.4478 ± 0.93986	-3.5983
Pelvis	10.112 ± 0.06138	16.978 ± 0.05241	-6.8657	4.1515 ± 0.71469	5.9609
Experiment 3					
Neck	29.292 ± 0.70164	31.437 ± 0.61978	-2.145	29.347 ± 0.79626	-0.054664
Upper Back	1.0152 ± 0.4395	0.85167 ± 0.31234	0.16348	1.7366 ± 0.34184	-0.72143
Lower Back	5.124 ± 0.98184	4.4136 ± 0.21363	0.71041	1.3517 ± 0.72807	3.7723
Pelvis	16.479 ± 0.17387	24.142 ± 0.098493	-7.6636	12.349 ± 0.37821	4.1299

Table C.5: Mean values for Sitting Euler

C.4 Sitting Quaternions

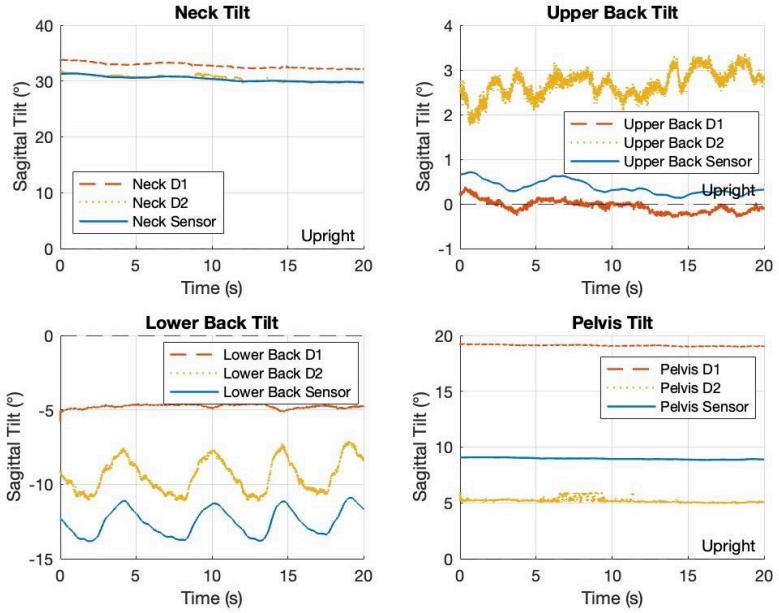

Figure C.7: Plots for Sitting Q2.

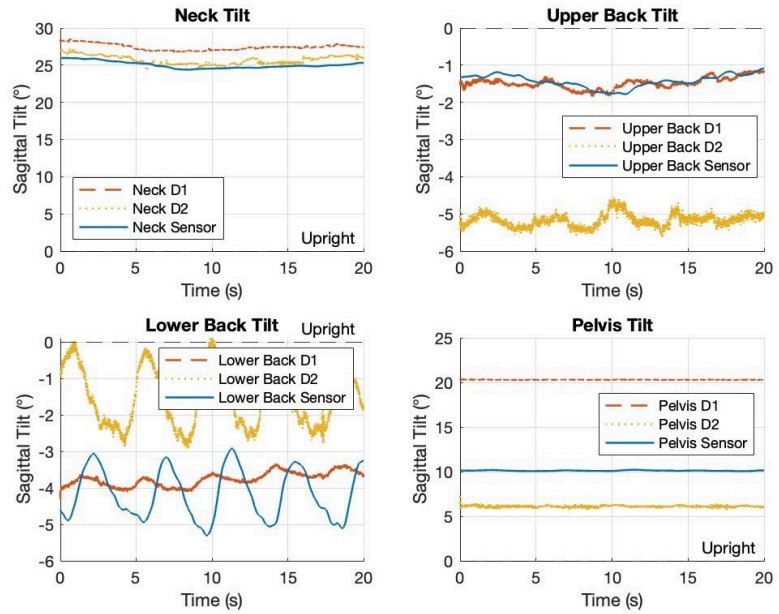

Figure C.8: Plots for Sitting Q3.

Segment	Sensor Mean [°]	Marker D1 Mean [°]	Marker Difference D1 [°]	Marker D2 Mean [°]	Marker Difference D2 [°]
Experiment 1					
Neck	21.309 ± 0.69585	24.318 ± 0.74267	-3.0086	22.118 ± 0.63408	-0.80848
Upper Back	-6.2436 ± 0.61076	-6.1373 ± 0.54107	-0.10634	-9.2556 ± 0.4815	3.012
Lower Back	-11.64 ± 0.91113	11.233 ± 0.18551	-0.4066	-17.637 ± 0.66741	5.9973
Pelvis	10.106 ± 0.086883	19.298 ± 0.08208	-9.1921	5.4546 ± 0.17041	4.6514
Experiment 2					
Neck	30.393 ± 0.47805	32.772 ± 0.48618	-2.379	30.485 ± 0.5997	-0.091256
Upper Back	0.36663 ± 0.15423	-0.053435 ± 0.13456	0.42006	-2.6923 ± 0.28941	3.0589
Lower Back	-12.541 ± 0.91299	-4.7726 ± 0.12806	-7.7682	-9.4272 ± 1.1183	-3.1136
Pelvis	8.9602 ± 0.073269	19.098 ± 0.063932	-10.138	5.2097 ± 0.22566	3.7505
Experiment 3					
Neck	25.025 ± 0.45734	27.429 ± 0.42642	-2.4042	25.672 ± 0.59629	-0.64705
Upper Back	-1.4268 ± 0.173	-1.4849 ± 0.14865	0.05807	-5.1692 ± 0.17359	3.7424
Lower Back	-4.177 ± 0.6988	-3.7612 ± 0.19028	-0.41578	-1.4894 ± 0.819	-2.6876
Pelvis	10.109 ± 0.038982	20.297 ± 0.019474	-10.187	6.1011 ± 0.12143	4.0084

Table C.7: Mean values for Sitting Quaternions.

Segment	Bias D1 [°]	RMSD D1 [°]	Bias D2 [°]	RMSD D2 [°]
Experiment 1				
Neck	-3.0086	3.0206	-0.80848	0.85638
Upper Back	-0.10634	0.20878	3.012	3.0412
Lower Back	-0.4066	0.98703	5.9973	6.1314
Pelvis	-9.1921	9.1925	4.6514	4.6528
Experiment 2				
Neck	-2.379	2.3803	-0.091256	0.25802
Upper Back	0.42006	0.42582	3.0589	3.0696
Lower Back	-7.7682	7.8273	-3.1136	3.1266
Pelvis	-10.138	10.138	3.7505	3.7562
Experiment 3				
Neck	-2.4042	2.4146	-0.64705	0.73574
Upper Back	0.05807	0.15248	3.7424	3.7519
Lower Back	-0.41578	0.85589	-2.6876	2.9561
Pelvis	-10.187	10.187	4.0084	4.0106

Table C.8: Bias and RMSD values for Sitting Quaternions.

C.5 Walking Euler

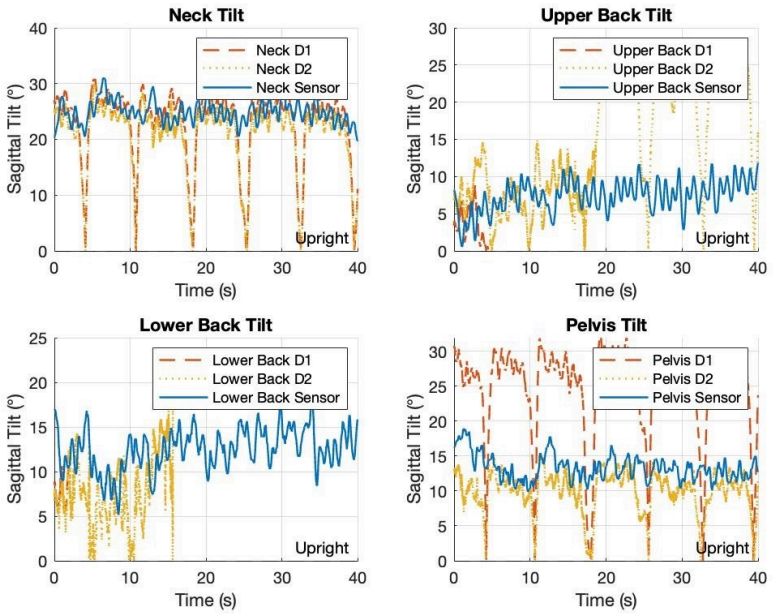

Figure C.9: Plots for Walking E2.

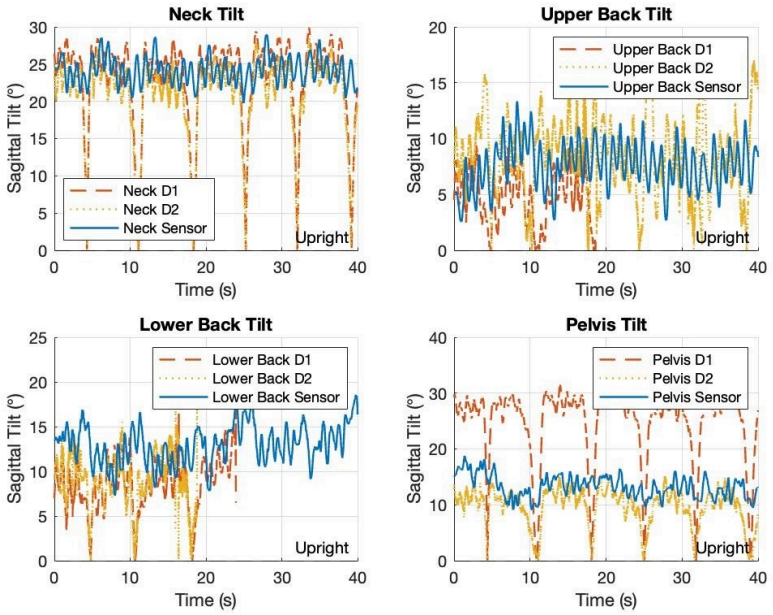

Figure C.10: Plots for Walking E3.

Segment	Bias D1[°]	RMSD D1[°]	Bias D2[°]	RMSD D2[°]
Experiment 1				
Neck	2.1153	6.0655	4.1653	6.6808
Upper Back	3.1941	4.9579	-1.7868[b]	4.4063[b]
Lower Back	4.8885[a]	5.6169[a]	3.3764	4.0263
Pelvis	-10.832	12.573	3.8711	4.948
Experiment 2				
Neck	2.0412	6.9715	3.9385	7.3082
Upper Back	0.94751[c]	3.9106[c]	-4.4487	5.5062
Lower Back	4.5165[d]	5.654[d]	5.1646[e]	6.2858[e]
Pelvis	-11.509	13.359	3.4238	4.7963
Experiment 3				
Neck	1.3364	6.2635	3.41	6.6173
Upper Back	2.8226[f]	4.489[f]	-1.0808	4.3458
Lower Back	4.1782[g]	5.865[g]	3.212[h]	5.1956[h]
Pelvis	-11.374	13.149	3.5955	4.8494

Table C.10: Bias and RMSD values for Walking Euler.
[a] missing 95.10% of data; [b] missing 44.70% of data; [c] missing 88.48% of data; [d] missing 95.25% of data; [e] missing 60.90% of data; [f] missing 53.42% of data; [g] missing 40.32% of data; [h] missing 52.89% of data.

Segment	Sensor Mean [°]	Marker D1 Mean [°]	Marker Difference D1 [°]	Marker D2 Mean [°]	Marker Difference D2[°]
Experiment 1					
Neck	24.033 ± 1.8589	21.918 ± 6.0492	2.1153	19.868 ± 5.569	4.1653
Upper Back	7.8257 ± 2.2901	4.6316 ± 2.426	3.1941	9.6124 ± 3.3127[b]	-1.7868[b]
Lower Back	11.738 ± 1.6157	6.8495 ± 1.9624[a]	4.8885[a]	8.3615 ± 2.2559	3.3764
Pelvis	13.611 ± 1.9551	24.443 ± 6.5621	-10.832	9.7399 ± 2.8621	3.8711
Experiment 2					
Neck	24.864 ± 2.0327	22.823 ± 6.9654	2.0412	20.926 ± 6.4466	3.9385
Upper Back	4.5522 ± 2.0411	3.6047 ± 2.248[c]	0.94751[c]	9.001 ± 2.8403	-4.4487
Lower Back	12.159 ± 2.6875	7.643 ± 1.4972[d]	4.5165[d]	6.9948 ± 1.7981[e]	5.1646[e]
Pelvis	13.306 ± 1.8337	24.814 ± 6.8742	-11.509	9.8818 ± 3.0987	3.4238
Experiment 3					
Neck	24.128 ± 1.8085	22.792 ± 6.1345	1.3364	20.718 ± 5.6899	3.41
Upper Back	7.5749 ± 2.3253	4.7523 ± 2.3516[f]	2.8226[f]	8.6556 ± 3.1274	-1.0808
Lower Back	12.202 ± 1.9808	8.0234 ± 2.8739[g]	4.1782[g]	8.9896 ± 3.1259[h]	3.212[h]
Pelvis	13.241 ± 2.0067	24.615 ± 7.009	-11.374	9.6456 ± 3.4681	3.5955

Table C.9: Mean values for Walking Euler.
[a] missing 95.10% of data; [b] missing 44.70% of data; [c] missing 88.48% of data; [d] missing 95.25% of data; [e] missing 60.90% of data; [f] missing 53.42% of data; [g] missing 40.32% of data; [h] missing 52.89% of data.

C.6 Walking Quaternions

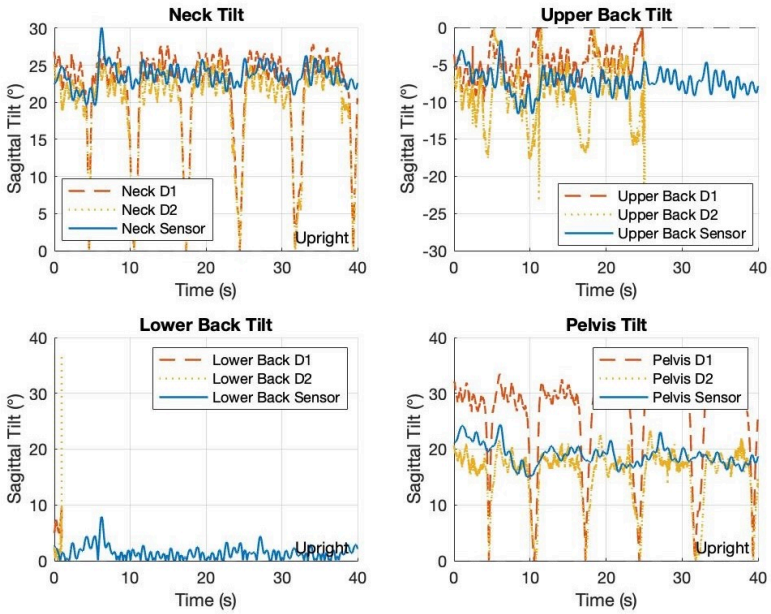

Figure C.11: Plots for Walking Q2.

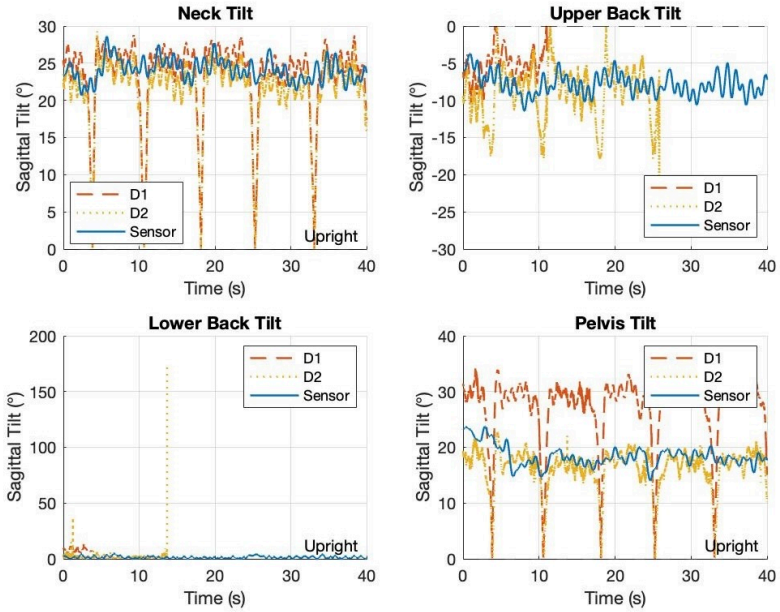

Figure C.12: Plots for Walking Q3.

Segment	Sensor Mean[°]	Marker D1 Mean[°]	Marker Difference D1[°]	Marker D2 Mean[°]	Marker Difference D2[°]
Experiment 1					
Neck	23.3 ± 1.2151	23.248 ± 5.5862	0.051765	21.055 ± 5.1521	2.2443
Upper Back	-6.415 ± 1.3271	-5.6572 ± 2.0092	-0.75774	-8.9931 ± 3.1579	2.5781
Lower Back	-14.474 ± 1.9409	-7.9277 ± 2.6544[i]	-6.5459[i]	-10.866 ± 3.7933[j]	-3.6078[j]
Pelvis	15.312 ± 1.1864	24.856 ± 6.916	-9.5436	10.599 ± 3.3725	4.7134
Experiment 2					
Neck	23.52 ± 0.92888	25.287 ± 0.96483	-1.7669	23.211 ± 4.0064	0.30856
Upper Back	-4.4061 ± 0.95151	-4.99 ± 1.0164[k]	0.58388[k]	-7.2331 ± 1.0981[l]	2.827[l]
Lower Back	1.6735 ± 0.87616	-6.3856 ± 1.0392[m]	8.0591[m]	-0.84365 ± 1.929[n]	2.5172[n]
Pelvis	22.268 ± 1.1716	30.133 ± 1.0457	-7.8659	18.974 ± 0.66396	3.2941
Experiment 3					
Neck	22.917 ± 1.5718	22.187 ± 6.4542	0.72975	19.985 ± 5.5696	2.9323
Upper Back	-5.9024 ± 1.6274	-6.4816 ± 1.7173[o]	0.57924[o]	-11.366 ± 2.928[p]	5.4634[p]
Lower Back	1.5678 ± 1.4126	-7.7609 ± 1.6076[q]	9.3287[q]	0.18629 ± 2.5834[r]	1.3815[r]
Pelvis	22.519 ± 0.99288	26.084 ± 7.9549	-3.5655	16.582 ± 4.2644	5.937

Table C.11: Mean values for Walking Quaternions.
[i] missing 78.29% of data; [j] missing 89.48% of data; [k] missing 38.02% of data; [l] missing 37.27% of data; [m] missing 97.58% of data; [n] missing 97.60% of data; [o] missing 72.39% of data; [p] missing 35.39% of data; [q] missing 90.17% of data; [r] missing 65.78% of data.

Segment	Bias D1 [°]	RMSD D1[°]	Bias D2[°]	RMSD D2[°]
Experiment 1				
Neck	0.051765	5.4474	2.2443	5.5354
Upper Back	-0.75774	3.0344	2.5781	4.4173
Lower Back	-6.5459[i]	7.2634[i]	-3.6078[j]	5.3697[j]
Pelvis	-9.5436	12.025	4.7134	6.1006
Experiment 2				
Neck	-1.7669	2.4229	0.30856	1.9818
Upper Back	0.58388[k]	1.7807[k]	2.827[l]	3.2559[l]
Lower Back	8.0591[m]	8.1546[m]	2.5172[n]	3.0876[n]
Pelvis	-7.8659	8.0374	3.2941	3.6323
Experiment 3				
Neck	0.72975	6.5195	2.9323	6.3706
Upper Back	0.57924[o]	2.838[o]	5.4634[p]	6.4394[p]
Lower Back	9.3287[q]	9.4737[q]	1.3815[r]	2.8486[r]
Pelvis	-3.5655	8.7671	5.937	7.4264

Table C.12: Bias and RMSD values for Walking Quaternions.
[i] missing 78.29% of data; [j] missing 89.48% of data; [k] missing 38.02% of data; [l] missing 37.27% of data; [m] missing 97.58% of data; [n] missing 97.60% of data; [o] missing 72.39% of data; [p] missing 35.39% of data; [q] missing 90.17% of data; [r] missing 65.78% of data.

DEPARTMENT OF ELECTRICAL ENGINEERING
CHALMERS UNIVERSITY OF TECHNOLOGY
Gothenburg, Sweden
www.chalmers.se

CHALMERS
UNIVERSITY OF TECHNOLOGY